ULTRASOUND-GUIDED TRANSGENE EXPRESSION OF KLK10 TO INHIBIT ATHEROSCLEROSIS

A Dissertation
Presented to
The Academic Faculty

by

Renfa Liu

In Partial Fulfillment
of the Requirements for the Degree
Philosophy in the
Department of Biomedical Engineering

Peking University & Georgia Institute of Technology & Emory University
May 2020

ULTRASOUND-GUIDED TRANSGENE EXPRESSION OF KLK10 TO INHIBIT ATHEROSCLEROSIS

Approved by:

Dr. Zhifei Dai, Advisor
Department of Biomedical Engineering
Peking University

Dr. Jinrui Wang
Third Hospital
Peking University

Dr. Hanjoong Jo, Co-Advisor
Department of Biomedical Engineering
Georgia Institute of Technology & Emory University

Dr. Xiaolong Liang
Third Hospital
Peking University

Dr. Brooks Lindsey
Department of Biomedical Engineering
Georgia Institute of Technology & Emory University

Date Approved: [November 1, 2019]

ACKNOWLEDGEMENTS

Six years of doctoral life flies. Looking back to the years passed, I feel full of gratitude when the thesis is about to be completed. First, I sincerely thank my advisor, Pro. Zhifei Dai, for guiding me the direction for the past six years, and supporting me like a family. Thanks to all the laboratory mates in MIMIT lab, Dr Xiaolong Liang, Yunxue Xu, Xiaoting Zhang, Yiming Zhou, Nisi Zhang, Jie Tang, Mengxuan Wang, Shuai Qu, Xinpeng Jiang, Wenlong Zeng,Yijia Liu, Hong Chen, and Miaomiao Zhang. I am very appreciative to all previous lab members, Chuang Gao, Min Chen, Yanyan Li, Lijia Jing, Yunhui Zhao, Chen Shen, Li Lin, Shanshan Feng, Zhengbao Zha, Yan Ma, Hengte Ke, Guanglei Fu, Yushen Jin, Liujiang Song, Ranran Zhao, Sujuan Sun, Yujia You, Yufan Lian, and Xiaona Lin.

I would like to express my sincerest thanks to my co-advisor, Pro. Hanjoong Jo at Emory University for his full support to me, providing me with the conditions for all the experiments, from ideas, funds, to experimental instruments. I would also thank all the members in Jo lab, Dr. Sandeep Kumar, Don Won Kang, Sunkum Kang, Joan Fernandez Esmerats, Rachel Simmons, Catherine Demos, Darian Williams, Junyao Zhang, Chunyan Li and Jiahui Zhang. I learnt a lot and had a really nice experience in Jo lab.

Thanks to the Dr. Brooks Lindsey from Georgia Tech, Maodong Sang and Xiaowei Zhang from Mindray for providing me a lot of supports especially in respect to ultrasound imaging. Thanks to Dr. Daniel Lipinski for providing me AAV. I am very grateful to Jinrui Wang and Shumin Wang from the third hospital of PKU for providing me vast assistance.

Finally, I would like to thank my family, especially my parents, grandparents and sisiters for encouraging and supporting me for everything. Importantly, I would not have

been able to complete this venture without the infinite support of my lover, Yunxue Xu. Their support is the driving force for me to move forward.

TABLE OF CONTENTS

LIST OF FIGURES

LIST OF SYMBOLS AND ABBREVIATIONS

LCA	Left common carotid artery
RCA	Right common cartid artery
US	Ultrasound
MB	Microbubbles
qPCR	Quantitative Polymerase Chain Reaction
LFA	Left femoral artery
RFA	Right femoral artery
KLK10	Kallikrein-10
18s	18S ribosomal RNA
ICAM1	Intercellular adhesion molecule 1
VCAM1	Vascular cell adhesion molecule 1
EGFP	Enhanced green fluorescent protein
AAV	Adeno-associated virus
CAG	Hybrid CMV enhancer/chicken β-actin promoter
PCL	Partial carotid ligation
DSPC	1,2-distearoyl-sn-glycero-3-phosphocholine
DSPE-PEG2000	1,2-distearoyl-sn-glycero-3-phosphoethanolamine-N-[methoxy(polyethylene glycol)-2000] (ammonium salt)
HDL	High high density lipoproteins
LDL	Low density lipoproteins
LS	Laminar shear stress
OS	Oscillatory shear stress
VSMCs	Vascular smooth muscle cells

IMT	Intima-media thickness
EC	Endothelial cells
M+A	Media and adventitial regions
MI	Mechanical index
AAA	Abdominal aortic aneurysm
ITR	Internal terminal repeats
BBB	Blood-brain barrier
RT	Room temperature
TBS	Tris-based solution
IAA	Infararenal abdominal aorta
SAA	Suprarenal abdominal aorta
PAD	Peripheral artery disease
ITR	Internal terminal repeats
ApoE	Apolipoprotein E
TGF-β1	Transforming growth factor-β1

SUMMARY

Atherosclerosis and its implications are the leading cause of death worldwide. Current treatment options fail to prevent and cure atherosclerosis completely. Therefore, new therapeutic options based on newly-discovered pro- and anti-inflammatory pathways linking lipid and inflammation biology are needed. Atherosclerosis is a chronic inflammatory process of the arterial wall that typically occurs at sites with disturbed blood flow (d-flow), such as curved and branched areas in the vasculature. Unidirectional, laminar shear stress upregulates atheroprotective genes, whereas d-flow, characterized as low and oscillatory shear stress, upregulates a number of pro-atherogenic genes which promotes atherosclerosis. In particular, KLK10 (Kallikrein-10) is one of the most important atheroprotective genes identified recently in our lab. Therefore, targeted delivery of KLK10 gene to dysfunctional endothelial cells might be an effective way to inhibit atherosclerotic development. However, there is still a lack of a method for targeted transgene expression in arterial endothelium in vivo. Ultrasound imaging is one of the most common imaging for the diagnosis of atherosclerosis in clinic. Ultrasound combined with gas-filled microbubbles has been widely reported to enhance transgene expression both in vitro and in vivo. In this thesis, we established two technologies based on the sonoporation effect by microbubble destruction with ultrasound for the transgene expression of KLK10 in vivo to inhibit atherosclerosis.

Besides its traditional functions, skeletal muscle has been discovered to be an endocrine organ, secreting a lot of myokines to act on several organs. The use of highly vascularized muscle as an endocrine organ for the systemic administration of therapeutic proteins is a really interesting application. Therefore, we firstly established a method to induce transgene expression of KLK10 in skeletal muscle to inhibit atherosclerosis. After intramuscular injection of naked plasmid and microbubbles, ultrasound is applied to the

injecting site to induced increased transgene expression in the skeletal muscle. By adding a signal peptide to the N-terminal of coding sequence of KLK10, the expressed KLK10 proteins can be secreted out, enter into the blood, and act on the inflamed area to inhibit atherosclerosis. After optimizing the ultrasound parameters, the ultrasound-enhanced transgene expression in skeletal muscle is increased by over 10 fold compared with naked plasmid injection and can persist for over 3 weeks. The transgene expression of KLK10 in skeletal muscle reduced the atherosclerotic lesions from 64.6% to 18.0% in the partial carotid ligation model. These results demonstrated the ultrasound-enhanced transgene expression of KLK10 in skeletal muscle as a potential therapy for atherosclerosis.

Although the transgene expression of KLK10 in skeletal muscle can inhibit atherosclerosis, the expressed KLK10 proteins can act on the whole body, not the artery endothelium alone, which may cause some unexpected side effects. Therefore, we sought to establish a method for targeted gene delivery to arterial endothelium. Adeno-associated virus (AAV) is currently among the most frequently-used gene vectors for gene therapy characterized with lack of pathogenicity, persistence of transgene expression, and the many available serotypes. However, AAV alone is not able to transfect arterial endothelial cells in vivo after system administration. Therefore, we established a simple but highly effective technology for imaging-guided gene delivery to mouse artery combining ultrasound imaging, microbubbles and AAV gene vector.

With color Doppler imaging, the anatomical structure of artery can be visualized and the area of interest can be selected so that ultrasound only irradiate the selected area. After microbubbles injection, the ultrasound can destroy the microbubbles only in the selected areas, resulting increased permeability of the artery. Following system administration, AAV gene vector can preferentially accumulate in the ultrasound-treated area, resulting in highly enhanced transgene expression. The transgene expression in carotid endothelium induced by this ultrasound-guided method is positively related to

ultrasound power and dose of microbubbles. The mechanical index of ultrasound at 0.4 and dose of microbubbles at 5×10^9/kg was selected for further experiments. The time interval between microbubbles and AAV injection is also optimized. No significant differences in transgene expression was found when the time interval was shorter than 3 h, but the expression was much reduced when the time interval was longer than 12 h. The ultrasound-guided method also induced highly enhanced transgene expression in media and adventitia layer, but ~5 days later than that in endothelium. The gene expression in both endothelium and media and adventitia could persist for at least 8 weeks. At 4^{th} week, the ultrasound treatment increased transgene expression by ~18 times in endothelium, while ~85 times in media and adventitia. By labelling AAV with fluorescent dyes, the distribution of AAV in artery wall was determined. Without ultrasound treatment, AAV could only temporally bind to arterial endothelium in big aggregates and was flushed away very soon. However, when the artery is permeabilized by ultrasound in combination with microbubbles, large amounts of AAV could be well dispersed in both intima and media layer and persist for a longer time. This explained the reason why ultrasound in combination with microbubbles could highly increase transgene expression in arteries by AAV. The ultrasound-guided method can also be used for targeted transgene expression in both abdominal aorta and femoral artery. After selectively treating the suprarenal abdominal aorta or infararenal aorta with ultrasound combining with microbubbles and AAV, the gene was only expressed in the ultrasound-treated areas. Similarly, the ultrasound treatment also increased transgene expression in femoral artery by ~58 times. These results demonstrated the novel technique for targeted gene delivery to artery wall in a noninvasive image-guided way.

Finally, the ultrasound imaging-targeted method was used for targeted delivery of KLK10 to inhibit atherosclerosis. After partial carotid ligation surgery, the KLK10 expression in the left common carotid artery (LCA) is reduced compared with the right common carotid artery (RCA). After treating LCA with ultrasound combining with

microbubbles, KLK10-encoding AAV9 at a dose of 2.5×10^{13}vg/kg could increase the expression of KLK10 in LCA to a level comparable to that in RCA. In the atherosclerotic studies, the targeted delivery of KLK10 gene with this technology could significantly reduce the plaque size, CD45, and VCAM1 expression without inducing any significant changes in the plasma lipid profile. This demonstrated that ultrasound imaging-guided delivery of KLK10 can inhibit atherosclerosis.

In summary, this thesis established two technologies for transgene expression of KLK10 in vivo to inhibit atherosclerosis. This research not only highlights the potential of KLK10 for the gene therapy of atherosclerosis, but also provides two important methods of gene delivery, which may find their broad applications in fundamental studies and clinical translation in respect to artery diseases, such as atherosclerosis, AAA, and PAD.

CHAPTER 1. INTRODUCTION

This thesis aims at establishing an ultrasound-guided method for gene delivery to inhibit atherosclerosis. In this chapter, a brief introduction of background knowledge was given, including the biology of atherosclerosis, KLK10 as a novel mechanosensitive gene, current targeting strategies for atherosclerosis, ultrasound for the therapy and diagnosis of atherosclerosis, skeletal muscular gene delivery, and AAV as a gene vector. After that, the significance and innovations of this research is summarized. Finally, the overall organization of this thesis is summarized.

1.1 Background

1.1.1 Biology of atherosclerosis

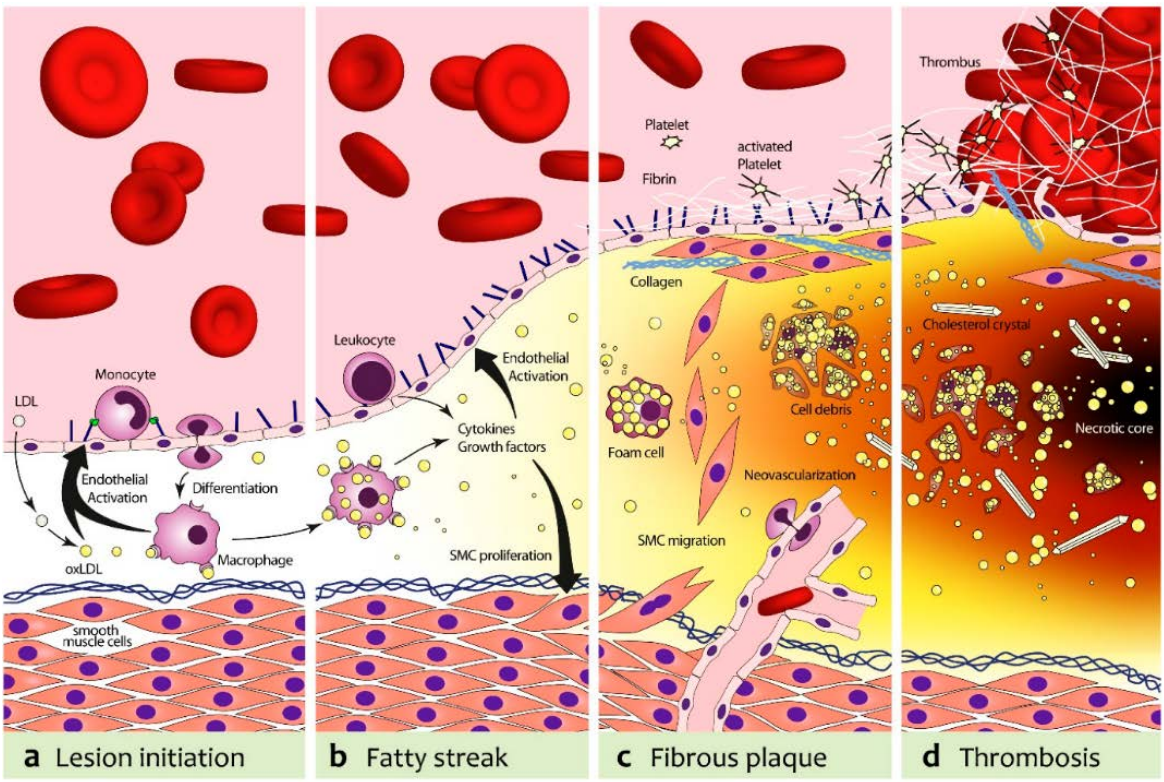

Figure 1.1 Stages in the development of atherosclerosis. [22]

Atherosclerosis is implicated as the key pathogenesis of cardiovascular disease, and a leading cause of death worldwide[1]. Current treatment options of atherosclerosis include lifestyle modifications (diet, exercise, etc.), statins, and surgical procedures [2-8]. However, these methods fail to prevent and cure atherosclerosis completely. Therefore, new therapeutic options based on newly-discovered pro- and anti-inflammatory pathways linking lipid and inflammation biology are needed [9-16].

Atherosclerosis is a chronic inflammatory process of the arterial wall that typically occurs at sites with disturbed blood flow (d-flow), such as curves and branches in the vasculature. Blood flow generates shear stress on mechano-sensors, which transduce sheer stress into cell signaling events and ultimately changes gene expression in vascular endothelial cells. Unidirectional, laminar shear stress (LS, or s-flow) upregulates atheroprotective genes such as Klf2, Klf4 and eNOS, whereas d-flow, characterized as low and oscillatory shear stress (OS), upregulates a number of pro-atherogenic genes including matrix metalloproteinase (MMP), and vascular cell adhesion molecule-1 (VCAM-1), which promotes atherosclerosis[17-19]. The dysfunctional endothelial cells initiates and perpetuates the plaque by recruiting monocytes from circulating blood. The atherosclerotic plaque is characterized by accumulation of lipids in the artery wall, together with infiltration of immunocytes, such as macrophages, and the formation of a fibrous cap by vascular smooth muscle cells[20]. Plaque growth can cause flow-limiting stenosis that may lead to tissue ischemia. Plaque ruptures trigger thrombosis, leading to exposure of thrombogenic materials in the core, followed by platelet aggregation, humoral coagulation and formation of a thrombus that may either interrupt blood flow locally or embolize and lodge in distal arteries [21]. Endothelial cells play a key role in the initializing and development of atherosclerosis, and thus normalizing dysfunctional endothelial cells by upregulating atheroprotective genes and downregulating pro-atherogenic genes can be an effective way to prevent and cure atherosclerosis.

1.1.2 KLK10 as a novel mechanosensitive gene

In response to s-flow or d-flow, hundreds of mechanosensitive genes in endothelial cell were down- or up-regulated. Therefore, to discover novel mechanosensitive genes and uncover their roles in the development of atherosclerosis is a hotpot in atherosclerotic studies and may provide novel therapeutic and diagnostic targets of atherosclerosis. Investigators have conducted DNA microarray studies with cultured endothelial cells exposed to different shear conditions [22-31] and have identified numerous mechanosensitive genes, including Klf2, Klf4 , eNOS, bone morphogenic protein 4 (BMP4), angiopoietin-2 (Angpt2) , VCAM1, ICAM1, and cathepsins. The following functional studies also uncovered the important role of these mechanosensitive genes in the development of inflammation, thrombosis, angiogenesis, and atherosclerosis [32-39].

However, the in vitro shear conditions cannot exactly simulate in vivo conditions. Our group previously established an accurate atherosclerotic model by partial carotid ligation (Figure 1.2)[17]. Three of four caudal branches of left common carotid artery (LCA) are ligated, leaving superior thyroid artery intact. The contralateral right common carotid artery (RCA) serves as internal control. The partial carotid ligation surgery causes d-flow in LCA, which rapidly induce atherosclerosis. Furthermore, we also developed a simple method to isolate endothelial cells-enriched RNA samples that are free of contamination of smooth muscle cells and leukocytes. With these two technologies, we conducted microarray studies using carotid endothelium exposed to d-flow[40]. More than 500 mechanosensitive genes that change in response to disturbed flow within 2 days were identified. Several important novel mechanosensitive genes were found, such as Lmo4, Fosl2, Id1, Jam2, Klk10, and Dhh.

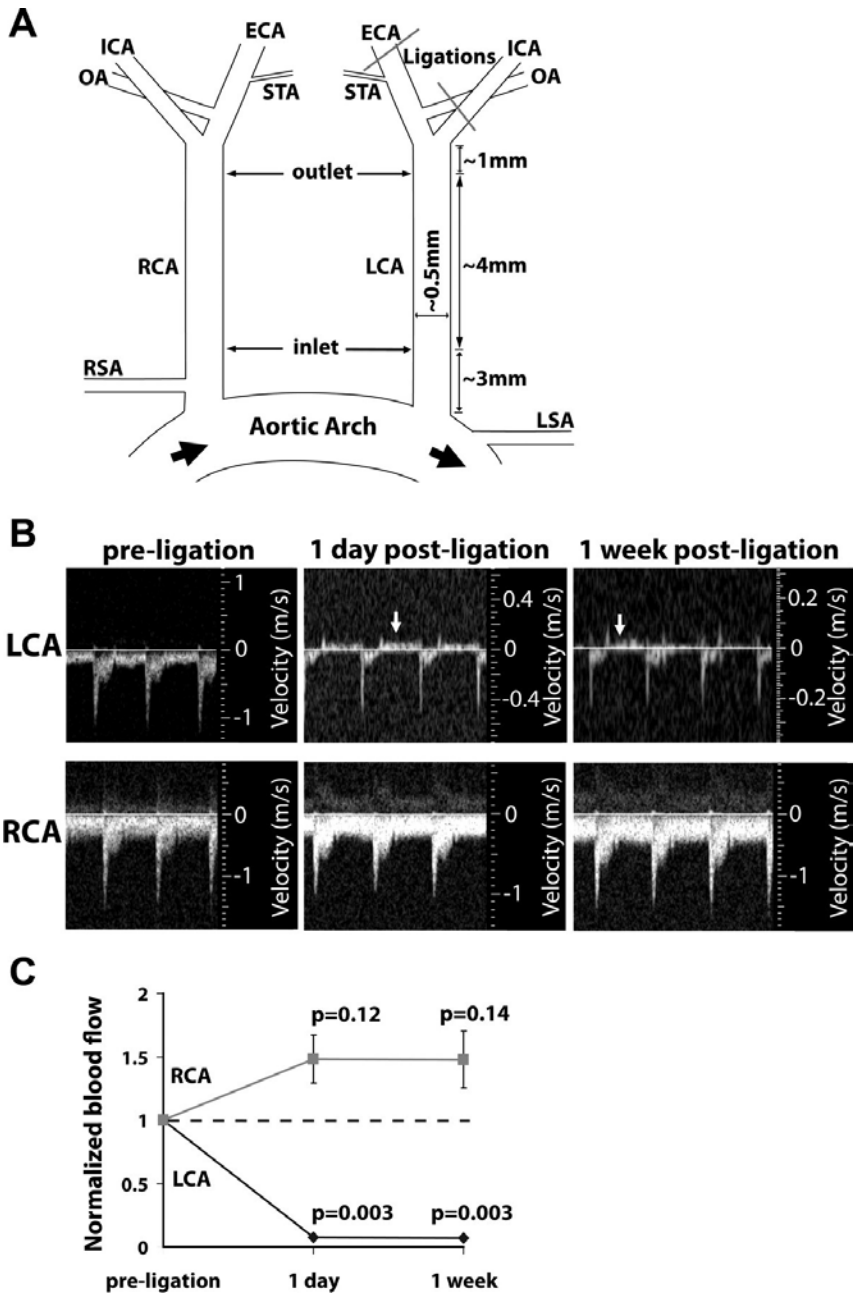

Figure 1.2 Partial carotid ligation surgery induces disturbed flow. (A) Paradigm illustrates the partial carotid ligation surgery. Three branches of the LCA [occipital artery (OA), internal carotid artery (ICA), and external carotid artery (ECA)] were ligated, while the superior thyroid artery (STA) is left intact. (B) Ultrasound shows the flow profiles of the carotid artery after the surgery. (C) Quantification of the blood flow post the surgery. Shown are means ± SE, n = 4 experiments.[17]

Based on our microarrays studies, KLK10 (Kallikrein-10) is one of the genes that are most sensitive to blood flow changes[41]. KLK10 is one of the fifteen kallikrein

subfamily members located in a cluster on chromosome 19. The KLK10 is a secreted serine protease and have been implicated to plays a key role in suppressing the tumorigenesis of breast, ovarian, colorectal, and prostate cancers [42-44]. Our recent studies found that KLK10 is a very important atheroprotective gene, which is down-regulated significantly by d-flow both in vitro and in vivo. Therefore, locally increasing the gene expression of KLK10 in the areas influenced by d-flow might be an efficient way for the therapy of atherosclerosis. However, there is still no effective way for targeted delivery of KLK10 in vivo.

1.1.3 Targeted-delivery strategies for atherosclerosis

The atherosclerotic plaque is primarily made of fatty substances and leukocytes, especially the blood monocytes and tissues macrophages. The predominant cell type is macrophage. Due to its involvement in atherosclerosis and intrinsic nature of engulfing external substances, macrophage is the most common target cell type used for targeted-delivery of therapeutic agents for atherosclerosis. Lipoproteins, such as high density lipoproteins (HDL) and low density lipoproteins (LDL), are nature nanoparticles targeting to macrophages. The primary function of lipoproteins in the body is transporting cholesterol and other lipids. The lipoproteins are composed of a hydrophobic core of triglycerides and cholesterol esters encapsulated with a phospholipid/cholesterol mixed layer, into which apolipoproteins are embedded. Its natural targeting capability and the option to incorporate lipophilic payloads, such as imaging and therapeutic agents, in both the hydrophobic core and the phospholipid shell make the lipoproteins an attractive nanocarrier[45]. Willem J. M. Mulder et al. demonstrated statin-loaded HDL nanoparticles could specifically deliver statins to plaque macrophages, thereby inhibiting their proliferation and reducing inflammation (Figure 1.3)[46]. These therapeutic anti-inflammatory benefits can be maintained by a subsequent 8-week oral statin treatment[47].

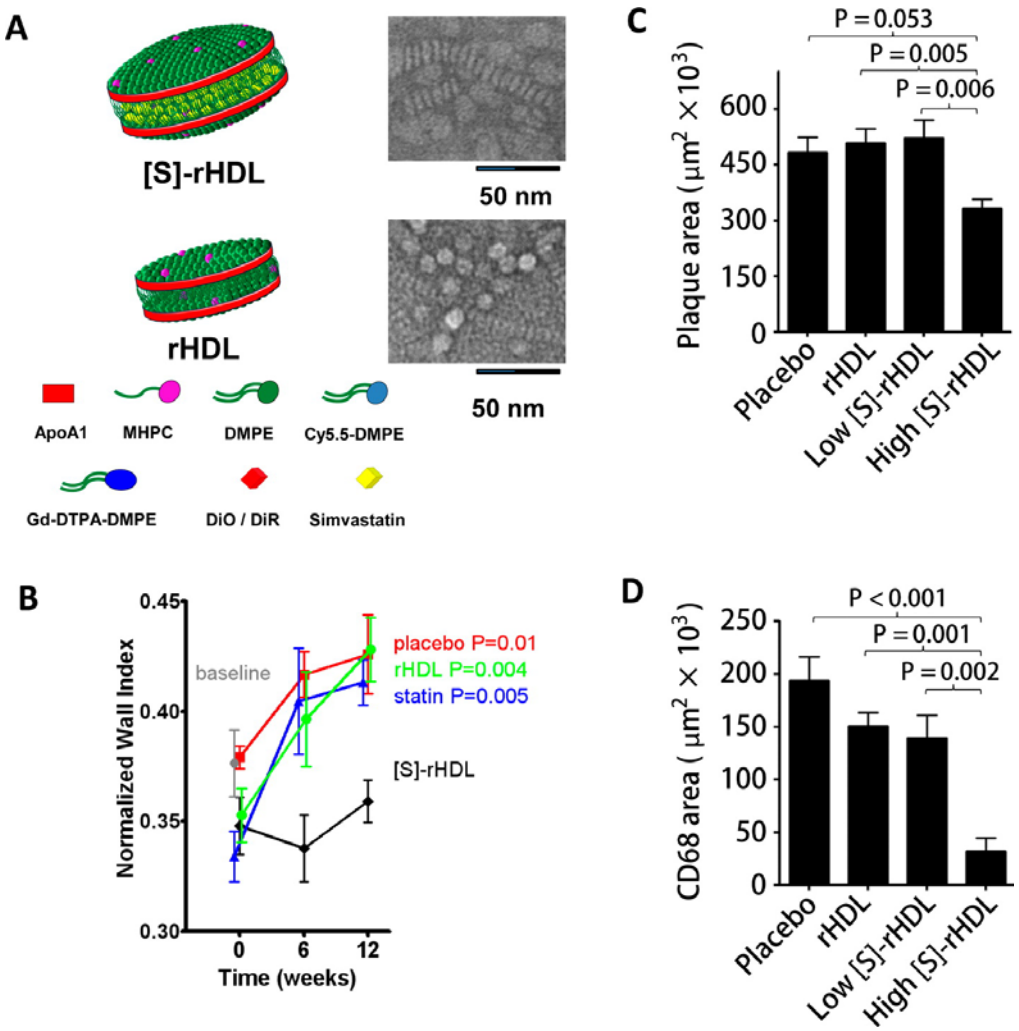

Figure 1.3 Deliver statin to the plaque macrophages with HDL. (A) Schematic illustration of HDL nanoparticles with or without statin ([S]-rHDL and rHDL). (B) Thickness of the vessel wall changes after receiving low-dose [S]-rHDL, blank rHDL, statin, and placebo over a period of 12 weeks. (C) Plaque area of mice after receiving different treatments. (D) CD68-positive area in the plaque after receiving different treatments. [48]

Although lipid transport primarily occurs in macrophages and other phagocytic cells, vascular smooth muscle cells (VSMCs) also play a key role in lipid accumulation[11]. A recent study by *Bo Tang et al.* developed a VSMC-targeted copper sulfate nanoparticles as a photothermal switch (Figure 1.4)[49]. The nanoparticles could specifically accumulate in VSMCs by coating the nanoparticles with an antibody against TRPV1, a cation channel, which is highly expressed in plaque VSMCs. Local temperature increase can be induced

by NIR laser irradiation. The heat-activation of TRPV1 could activate autophagy and reduce lipid accumulation. Injection of the NPs in vivo in ApoE$^{-/-}$ mice followed by laser irradiation greatly reduced plaque formation. This research demonstrated a simple yet highly effective strategy for precise in vivo targeting and controlling of lipid-processing process, which is important for the atherosclerosis.

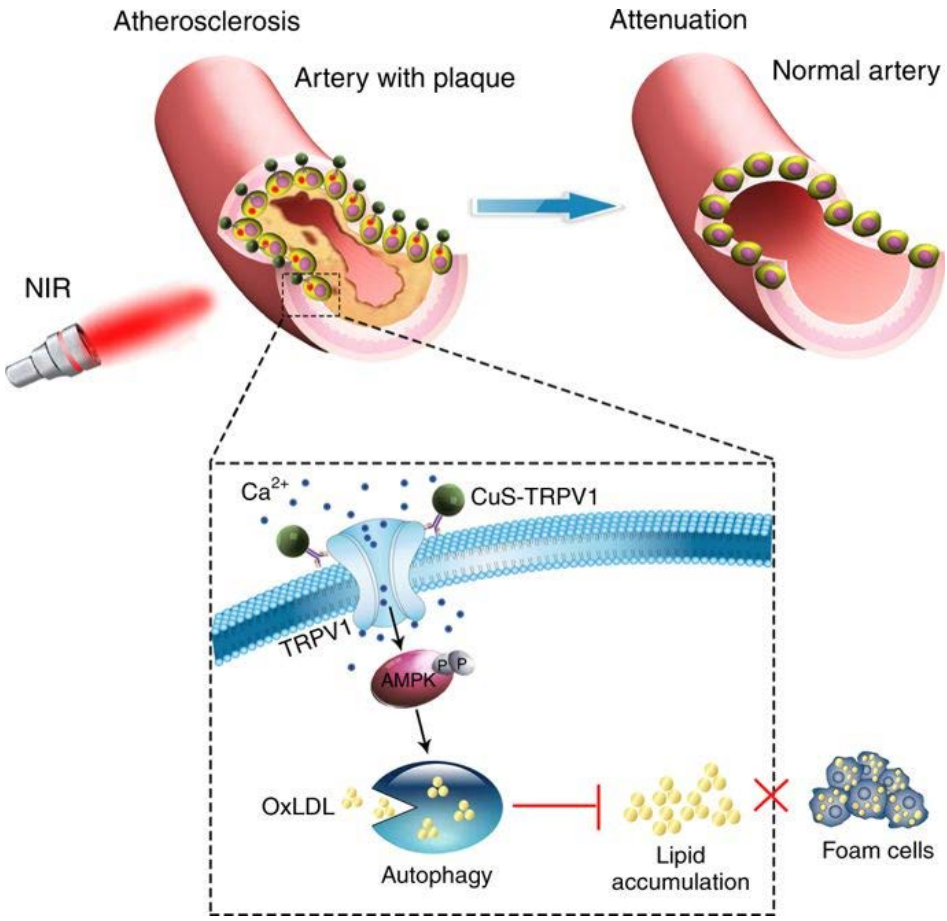

Figure 1.4 Schematic illustration of CuS-TRPV1 as a photothermal switch for activation of TRPV1 signaling to inhibit atherosclerosis.[49]

Endothelial cells form the outlayer of atherosclerosis plaque and play a key role in the initiation and progression of atherosclerosis. Therefore, normalizing the dysfunctional endothelial cells is another promising therapy of atherosclerosis. Our group devised a liposome formulation for targeted delivery of anti-miR-712 to the plaques of ApoE$^{-/-}$ mice (Figure 1.5)[50]. The liposome is decorated with VHPK peptide, a VCAM1-internalizing

peptide, which helps the liposome not only bind to VCAM1 but also internalized by inflamed endothelial cells. The encapsulation allowed for potent in vivo downregulation of miR-712 at a dose 80% lower than if given freely without lipid encapsulation.

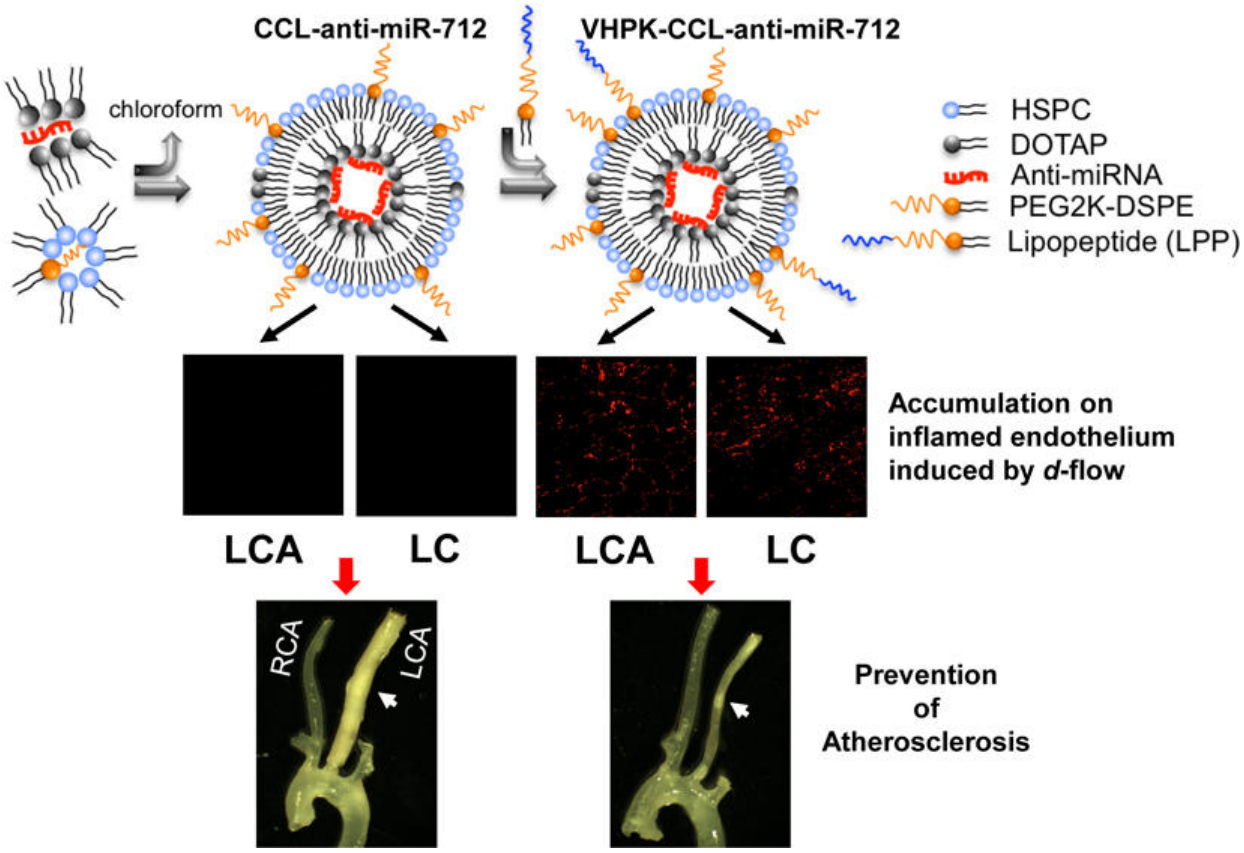

Figure 1.5 Multifunctional liposome formulation for targeted delivery of anti-miR-712 to the plaques of ApoE$^{-/-}$ mice.[50]

Although several strategies are developed for the targeted-delivery of various therapeutic agents, including chemical drugs, RNA and proteins, targeted-delivery of DNA gained very limited success[51]. DNA-based gene therapy holds several advantages compared with protein- and RNA- based therapy. DNA plasmids are easier and cheaper and if delivered properly the therapeutic effect can last for a much longer time than proteins and RNA.

1.1.4 Ultrasound for imaging and therapy of atherosclerosis

Ultrasound is sound waves with a frequency higher than those audible to humans. Ultrasound imaging utilizes the interaction of sound waves with living tissue to produce an image of the tissue or determine the velocity of blood in Doppler-based modes. Quantitative structural and functional information of the target organ can be obtained by analyzing these dynamic, real-time images[52]. This versatile, noninvasive diagnostic tool is widely used in clinic as one of the four most common imaging methods (ultrasound imaging, CT, MRI and PET). Ultrasound imaging is also widely used for diagnosis and risk assessment of atherosclerosis. In addition to imaging, ultrasound can also be used for therapy. Ultrasound, when combined with some specific ultrasound-responsive materials, can produce effects on selected cells or tissues, and thus has been developed for the therapy of a lot of diseases, including cancer[53], neurodegenerative diseases[54, 55] and atherosclerosis[56].

1.1.4.1 Ultrasound imaging of atherosclerosis

Ultrasound as a cheap, noninvasive, non-ionizing and real-time imaging technique is an ideal tool for progress monitoring of atherosclerosis [57-62]. Intima-media thickness (IMT), the distance between the lumen-intima interface and the media-adventitia interface of the arterial wall (Figure 1.6), is widely studied as a surrogate marker for detecting subclinical atherosclerosis for risk assessment and monitoring the progress of atherosclerosis for medical intervention[63-65]. High-frequency ultrasound produce the high spatial resolution required to measure IMT in vessel walls. However, higher frequency also limits tissue penetration of ultrasound. Therefore, this kind of ultrasound examination is limited to vessels close to skin, such as carotid artery. In addition to IMT, ultrasound imaging can also be used to quantify the carotid plaque burden, which has been developed as a promising alternative to carotid IMT (CIMT) measurements. Carotid plaque burden can be measured as total plaque area or total plaque volume. Compared with CIMT, plaque burden has been demonstrated as a better risk predictor of cardiovascular diseases[66].

Besides the anatomical information, addition information can be obtained from ultrasound images. Plaques containing a large lipid core appear echolucent, while plaque fibrosis and calcification tend to appear echogenic. Based on the echolucency, carotid plaques can be classified into four categories as echolucent, predominantly echolucent, predominantly echogenic, and echogenic[67]. In patients with carotid stenosis, the degree of plaque echolucency is correlated with increased risk for cerebral ischemic symptoms[68].

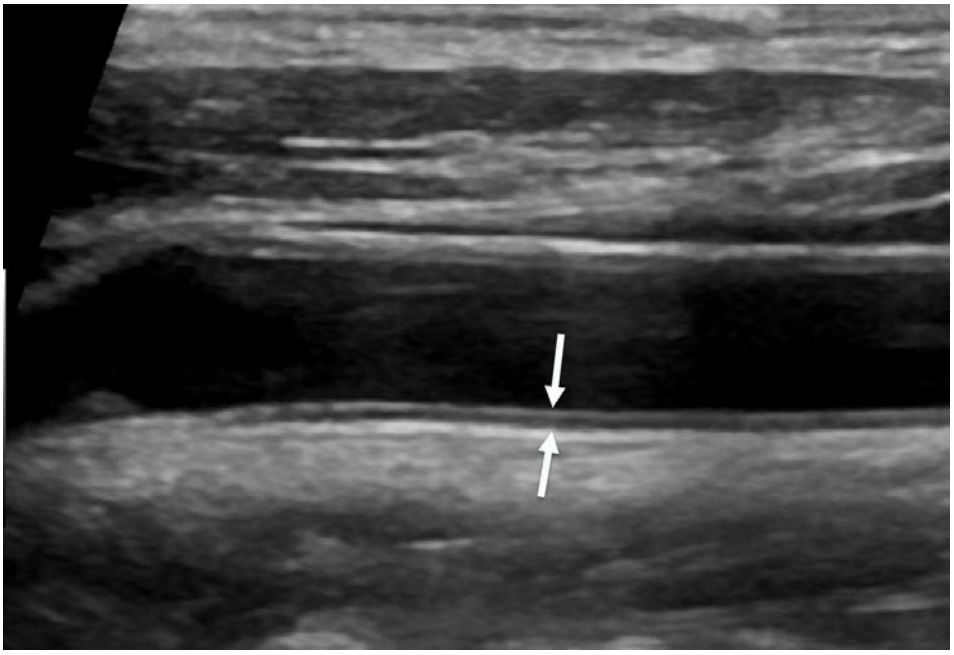

Figure 1.6 Longitudinal view of carotid artery shows IMT. The IMT is the distance between two echogenic lines at the far wall representing the lumen-intima interface and media-adventitia interface (arrows).[66]

Ultrasound contrast agents were developed in the early 1990s with the goal of better delineation of the left ventricular endocardial border[69]. With technique advances, the most popular contrast agents used in clinic nowadays are microbubble-based contrast agents composed of large-molecular-weight hydrophobic gases such as sulfur hexafluoride or perfluorocarbons encapsulated with a thin phospholipid shell. These microbubbles measure on average 1–2 μm in diameter and thus can circulate freely throughout the blood. Microbubbles undergo volumetric oscillations with compression during the pressure peaks, and expansion during the pressure nadirs of an incident ultrasound wave. These volumetric

oscillations result in a strong backscattered acoustic signal that can be detected by ultrasound systems. With the aid of this kind of contrast-enhanced ultrasound imaging, the sensitivity and specificity for plaque ulceration and neovascularization is increased[70, 71]. The distribution of ulceration and neovascularization provides additional information for assessment of plaque vulnerability..

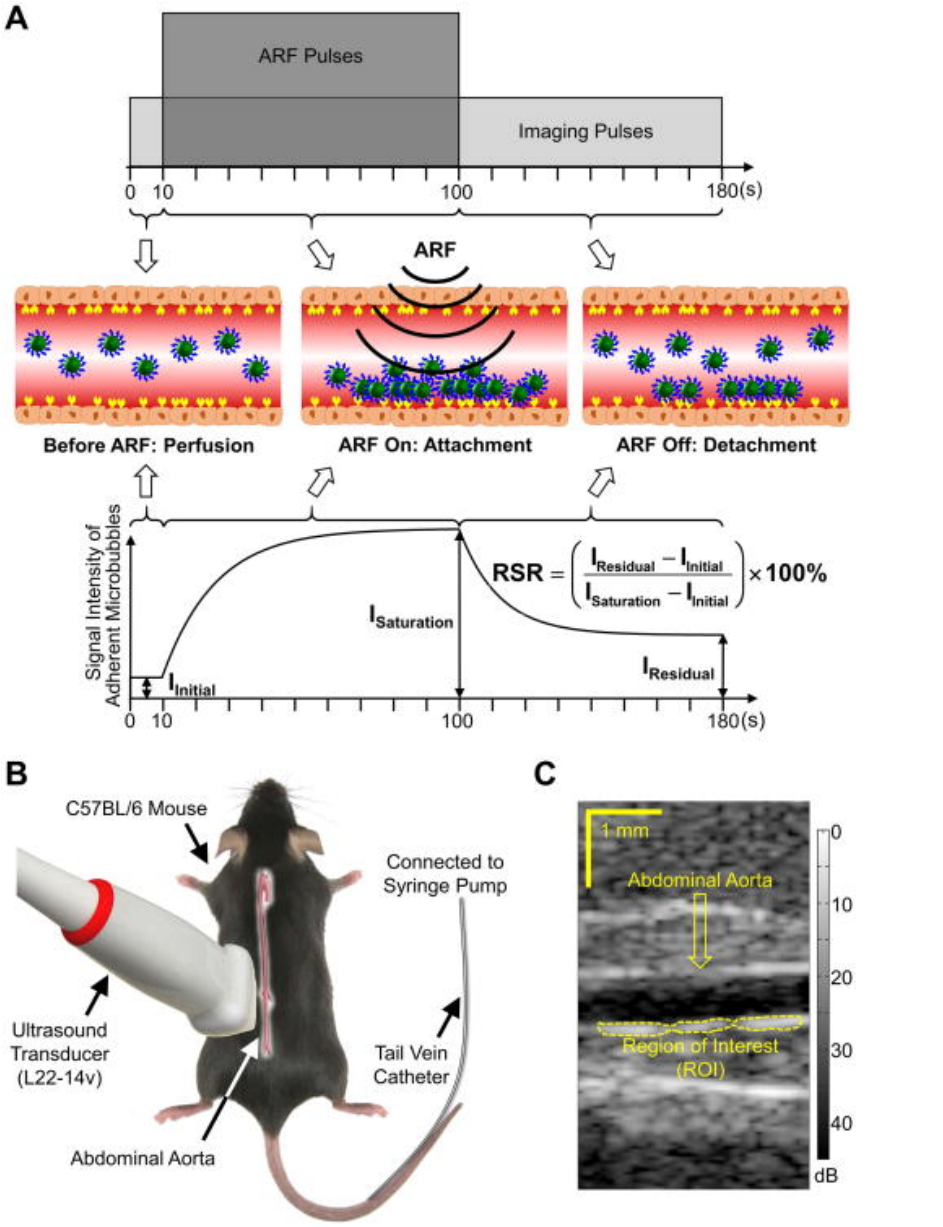

Figure 1.7 Ultrasound molecular imaging with acoustic radiation force (ARF). (A) Schematic diagram illustrating the modulated ARF-based imaging. (B) The experimental setup of mice and probe for ARF imaging. (C) A representative image of the mouse abdominal aorta. [75]

Another promising application of contrast imaging is the specific attachment of microbubbles to a target of interest. For example, the ligands targeting activated endothelial cells or leukocytes can be coupled to the surface of microbubbles via a polyethylene glycol (PEG) spacer[72]. Protocols for this kind of ultrasound molecular imaging usually involve intravenous bolus injections of targeting microbubbles[73]. Over several minutes, some microbubbles will adhere to a target of interest within tissue, while other un-attached microbubbles are cleared from the circulation. After destruction of the microbubbles with high-power ultrasound pulses, the presence of attached microbubbles can be derived by comparing images before and after microbubbles destruction. An ultrasound image of these attached microbubbles provide information about the level of expression of the target in tissues. Although promising, molecular ultrasound imaging at current status is still far away from clinical adoption for two main reasons. On one hand, the targeting microbubbles with high specificity is still not applicable in clinic due to the complex fabrication procedure and low stability of microbubbles. On the other hand, the length (30-40 min) and complexity of the existing molecular imaging protocols could delay clinical adoption and increase procedure costs[74]. Recently, *Shiying Wang* et.al. reported a novel molecular imaging method, referred to as modulated acoustic radiation force (ARF)-based imaging, for rapid assessment of P-selectin and VCAM-1 in the abdominal aorta of mice in just 180 seconds (Figure 1.7)[75]. This method might have the potential for clinical translation with considerable further improvement and validation.

1.1.4.2 Ultrasound for the therapy of cardiovascular disease

While low and intermediate acoustic pressure results in linear and non-linear oscillations of microbubbles, at high acoustic powers, microbubbles can be destroyed by either outward diffusion of the gas during the compression phase, diffusion from large shell defects, or from complete fragmentation of microbubbles. Microbubble destruction during

high-power ultrasound can lead to increased permeability of cell membranes, which may facilitate gene or drug delivery.

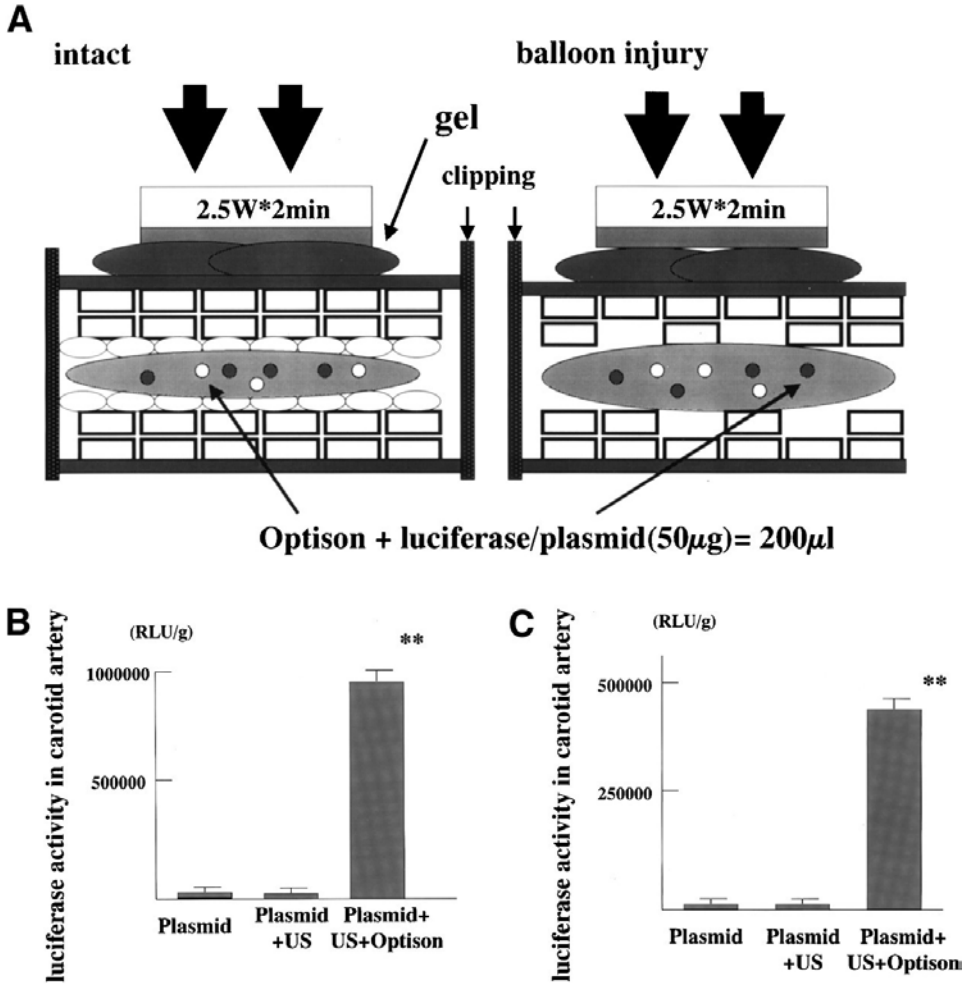

Figure 1.8 Local delivery of plasmid DNA into rat carotid artery using ultrasound in a restenosis model induced by balloon injury. (A) Schematic illustration of transfection of naked plasmid DNA using ultrasound with Optison into intact or balloon-injured blood vessels in vivo. Comparison of luciferase activity is shown after in vivo transfection into intact blood vessels (B) and ballooninjured blood vessels (C).[76]

Yoshiaki et al. reported an ultrasound transfection method with enhanced transfection efficiency of naked plasmid DNA into blood vessels (Figure 1.8)[76]. Plasmid mixed with Optison, a commercial microbubble agent, could significantly increase transfection efficacy in cultured human VSMC and ECs in vitro. Furthermore, they tested the method to transfect the artery in vivo. They induced the vascular injury of the common carotid with a balloon catheter. The injured segment was transiently isolated by temporary

ligatures. Then the isolated vessel was incubated with Optison and plasmid within the lumen, and then treated with ultrasound. With this method, significantly higher luciferase activity was detected in carotid artery transfected with Optison and ultrasound than with plasmid alone. In addition, transfecting the carotid artery with p53 gene utilizing this method could significantly reduce the intimal-to-medial area ratio in rats two weeks after balloon injury. This research highlighted the high efficacy of the sonoporation in enhancing gene delivery. However, this method requires complicated surgery procedures and cause a lot of pain to animals, thus limiting its wide applications.

Recently, *Xiaowei Wang et al.* developed a VCAM-1-targeted miR-126-loaded microbubble as a theranostic agent for early diagnosis and long-sought-after medical therapy of AAA (Figure 1.9) [77]. In this research, microbubbles are linked with VCAM1-targeted single-chain antibody, while miR-126 is tagged with cholesterol to insert in the lipid membrane of microbubbles. After intravenous injection, this microbubbles can selectively bind to inflamed endothelial cell, in which VCAM-1 is highly expressed. The ultrasound is then applied to destroy the microbubbles and the released miR-126 will enter adjacent cells. With this method, the development of AAA in an angiotensin-II-induced mouse model can be prevented.

Hong Jin et al. also reported ultrasound-targeted microbubbles could deliver miR-21 into carotid plaques rescued the vulnerable plaque rupture phenotype without off-target effects[78]. The miR-21 is electrostatically bind to the charged microbubbles. This ultrasound-targeted local delivery of miR-21 could enhance the accumulation of miR-21 in plaque, and thereby stabilizes fibrous caps in vulnerable atherosclerotic lesions. Compared with systemic forms of injection without ultrasound and microbubbles, this ultrasound-targeted delivery show reduced off-target effects in liver and brain.

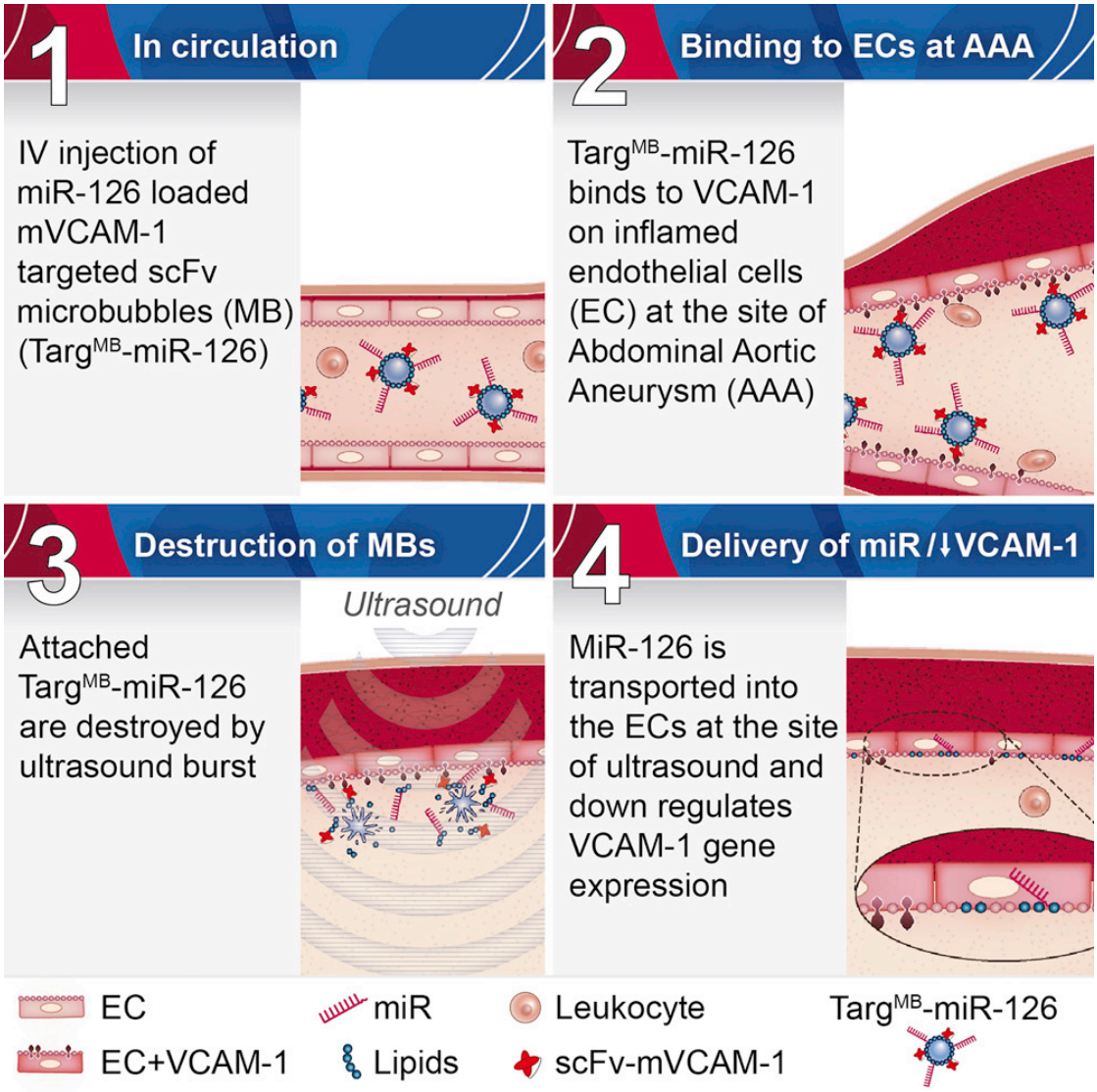

Figure 1.9 Schematic illustration of dual-targeted delivery of miR-126 to inflamed endothelial cells.[77]

In addition of enhancing gene of drug delivery, another promising therapy of atherosclerosis with ultrasound is sonodynamic therapy (SDT), which utilizes ultrasound to locally activate sonosensitizers to induce cell death. Low-intensity SDT stabilized early atherosclerotic plaques by inducing macrophage apoptosis and apoptotic cell clearance[56]. A recent study by *Ye Tian et al.* shows that SDT efficiently decreased the atherosclerotic burden within 1 week in atherosclerotic rabbit and ApoE-deficient mouse models[79]. Compared with atorvastatin, the standard of care for atherosclerosis, SDT showed more significant plaque shrinkage and lumen enlargement during 1 week treatment. In a pilot

clinical trial recruiting the patients suffering atherosclerotic peripheral artery disease, combination therapy of SDT with atorvastatin efficiently reduced progression of atherosclerotic plaque within 4 weeks, and its efficacy was able to last for at least 40 weeks.

1.1.5 Skeletal muscular gene delivery

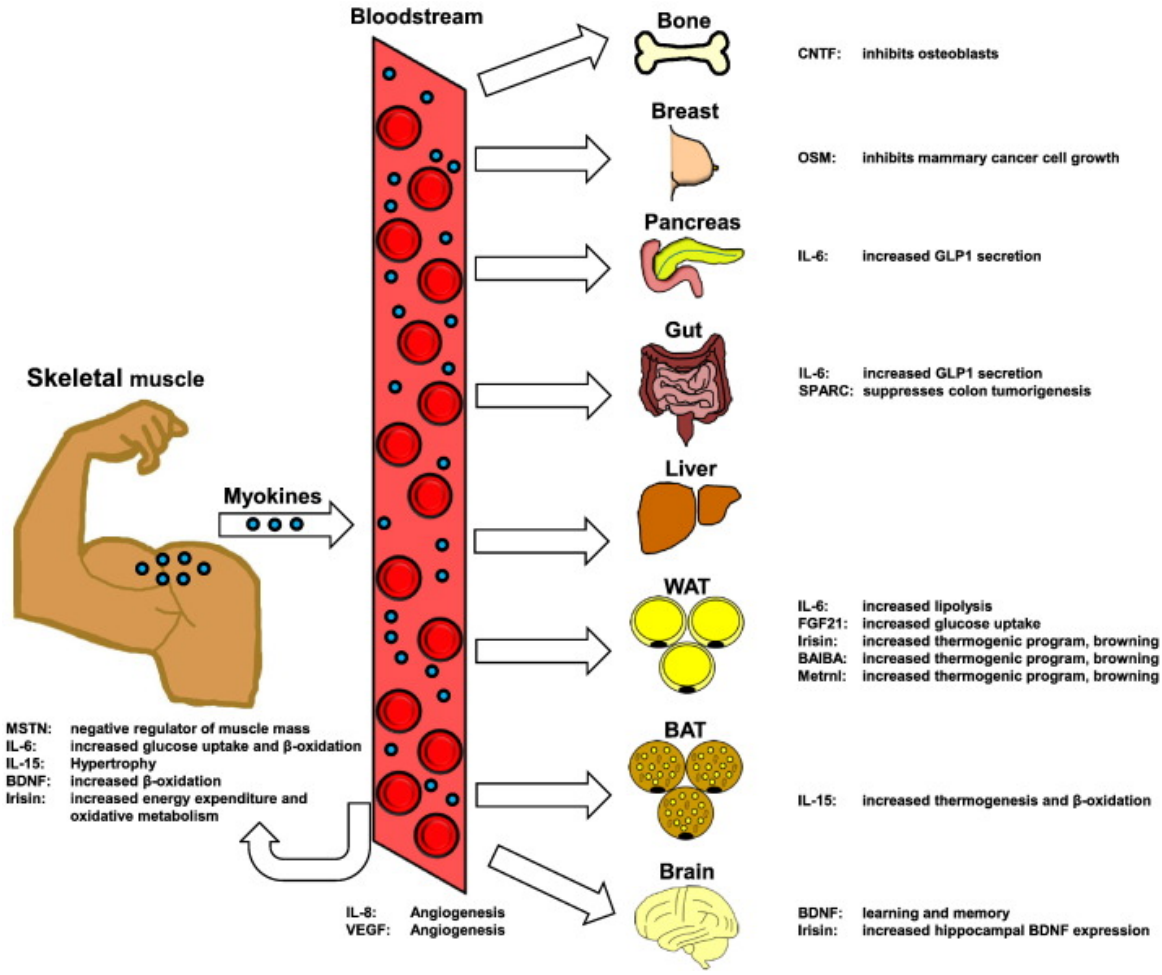

Figure 1.10 Physiological consequences of the production and release of myokines on skeletal muscle and other organs.[86]

Gene transfer for gene therapy is a rapidly expanding field. Tissues with high transgene efficacy is sought including tumors, and organs such as the liver, heart, or brain [80-82]. Special interest has been devoted to gene delivery to skeletal muscle fibers, for the correction of myopathies, local secretion of angiogenic or neurotrophic factors, and vaccination [83-85]. Besides its traditional functions, skeletal muscle has been discovered to

be an endocrine organ, secreting a lot of myokines to act on several organs(Figure 1.10)[86]. Therefore, the use of highly vascularized muscle as an endocrine organ for the systemic secretion of therapeutic proteins is a really interesting application.

Deposition of extracellular matrix is the major cause of fibrosis, which may destroy the function of tissues involved, such as kidney, liver, heart, etc. Overproduction of transforming growth factor-β1 (TGF-β1), induced by injury or disease, is thought to be the underlying reason for extracellular matrix deposition. Therefore, inhibiting TGF-β1is an effective way for the therapy of fibrosis. *Yoshitaka Isaka et al.* found that skeletal muscle expression of decorin, an inhibitor of TGF-β1, could prevent fibrotic disease in rat model of glomerulonephriti [87]. The gene transfer into skeletal muscle is achieved with the method of combining plasmid with a mixture of hemagglutinating virus of Japan and liposome. The gene transfer into rat skeletal muscle increases the amount of decorin expression in skeletal muscle and decorin present in kidney. This resulted in a significant reduction in levels of glomerular TGF-β1 expression, extracellular matrix accumulation and proteinuria. This research highlights the transgene expression in skeletal muscle as a potential therapy for fibrosis induced by TGF-β1.

Human apolipoprotein E (ApoE) is a secreted plasma protein playing an important role in removing remnant lipoproteins and in transporting cholesterol from peripheral tissues to liver. Therefore, deficiency of ApoE causes severe hypercholesterolemia and atherosclerotic development. *Takis Athanasopoulos et al.* found that intramuscular injection of a plasmid vector expressing human apolipoprotein E (ApoE) in ApoE deficient mouse could limit atherosclerosis in aorta[88]. *Emanuela Signori et al.* reported that intramuscular injection of naked plasmid vector encoding human ApoE could reduce severe hypercholesterolemia in newborn mice and when the DNA is injected early, no immune response is generated, allowing repeated injections[89]. These researches indicate the potential applications of intramuscular gene transfer for the therapy of atherosclerosis.

Although intramuscularly injecting naked plasmid can transfer a foreign gene into muscle fibers, this method holds several major limitations, such as low efficiency, lack of reproducibility. Thus, alternative strategies aiming at the level and reliabilities of skeletal muscular gene expression are needed. Several physical method such as electroporation, sonoporation, and magnetofection have been developed with enhanced efficacy.

Galina Shapiro et al. used nonlinear ultrasound and bioluminescence imaging to optimize the acoustic pressure, microbubble concentration, treatment duration, DNA dosage, and number of treatments required for in vivo luciferase gene expression in a mouse thigh muscle model[90]. Mice injected with 50 μg luciferase plasmid DNA and 5×10^5 microbubbles followed by ultrasound treatment at 1.4 MHz, 200 kPa, 100-cycle pulse length, and 540 Hz pulse repetition frequency (PRF) for 2 min exhibited superior transgene expression compared to all other treatment groups. They found that localized ultrasound-mediated, microbubble-enhanced gene delivery to endogenous mesenchymal progenitor cells could effectively induce efficient bone regeneration and fracture repair in mini-pigs, thereby addressing a major orthopedic unmet need and offering new possibilities for clinical translation[91].

1.1.6 Adeno-associated virus (AAV) as an gene vector for gene therapy

AAV is currently among the most frequently used gene vectors for gene therapy characterized with lack of pathogenicity, persistence of transgene expression, and the many available serotypes. Up to now, AAV vectors have been used in over 238 clinical trials worldwide, approximately 8.1% of gene therapy clinical trials[92]. In 2017, the United States Food and Drug Administration (FDA) approved the LUXTURNA™ from Spark Therapeutics as the first gene therapy product for the eye.

AAV was originally found as a contaminant of adenovirus preparations. AAV is about 20 nm in diameter made of a protein shell surrounding a sing-stranded DNA genome

of about 4.8 kb. The viral genome contains three genes, *Rep*, *Cap*, and *aap*, flanked by two internal terminal repeats (ITR). *Rep* is essential for viral genome replication and packaging, while *Cap* encodes viral capsid proteins (VP1/VP2/VP3). The *aap* gene expresses the assembly-activating protein, which is thought to assist in capsid assembly. The viral capsid is composed of 60 proteins assembled in a molar ratio of 1:1:10 (VP1:VP2:VP3) to form an icosahedral structure. For gene delivery applications, the coding sequences of viral genome is replaced by a promoter and the gene of interest. It is believed that the ITR-flanked transgene can form non-integrated non-replicating episomes that persists in nucleus of cells. Several clinical trials for hemophilia, heart failure, and lipoprotein lipase deficiency and so on have demonstrated that AAV gene transfer can result in sustained therapeutic effects for several years.[93-95]

Local delivery of AAV can maximize concentration and residence time of the gene vector in close to the target cells, avoiding wide biodistribution. This is useful for several tissues, including eye, cardiac muscle, skeletal muscle, and central neural system. However, there are also many diseases or applications requiring system delivery, as the target sites are not accessible with local delivery, for example, atherosclerosis. Systemic administration of AAV of results in a significant accumulation in the liver and also other cells and tissues types. To restrict expression to only the liver, a common method is to use the liver-specific promoter [96-100]. Our group has previously reported to deliver PCSK9 gene driven by a liver-specific promoter with AAV, which could induce hyperlipidemia. By combining this technology with partial carotid ligation surgery, an accelerated model of atherosclerosis was developed in C57 mice[81]. Compared with the control, PCSK9

delivery could result in increased serum PCSK9, hypercholesterolemia, and accelerated atherosclerosis development in three weeks.

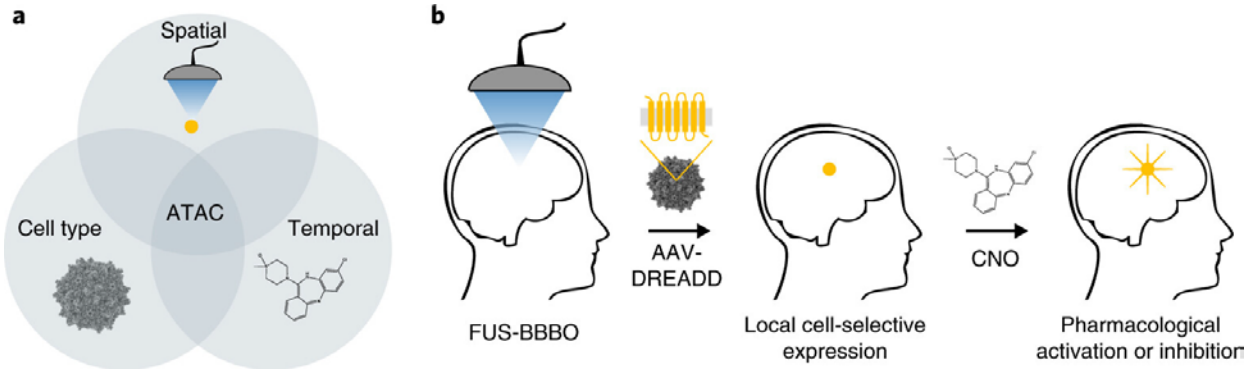

Figure 1.11 The paradigm of Acoustically Targeted Chemogenetics (ATAC). [80]

To deliver gene to specific cells or tissues with AAV often requires specially designed promoters or modified capsid protein. Despite some success, these methods are usually limited by low efficacy, lack of highly specific promoters or targeting ligands, and off-target effects. *Jerzy O. Szablowski et al.* reported a concept named as Acoustically Targeted Chemogenetics (ATAC) to spatially control gene expression in brain for the non-invasive modulation of neural circuits (Figure 1.11)[80]. In this method, the blood-brain barrier (BBB) can be temporally opened with focused ultrasound, and systemically injected AAV encoding a cell-specific-promoter-driven designer receptor accumulate in the treated area. After several weeks, the receptor is expressed in specific cells of the targeted area and targeted cells can be excited or inhibited by the designer chemogenetic drugs of the receptor. In a mouse model of memory formation, they show the ATAC could activate or inhibit neurons within the hippocampus, with selective control over individual brain regions.

1.2 Significances and Innovations of the Thesis

1.2.1 Significances

The thesis study of ultrasound-guided gene delivery is of great significances in the following aspects:

(A) Meet unmet need for the gene therapy of atherosclerosis

Cardiovascular disease is one of the leading causes of death globally, among which 68% is attributed to atherosclerosis[101]. Atherosclerosis a chronic inflammatory process of the arterial wall that typically occurs at sites with disturbed blood flow (d-flow), such as curved and branched in in the vasculature. Disturbed blood flow generates shear stress on vascular endothelial cells, upregulating proatherogenic genes and downregulating atheroprotective genes. The dysfunctional endothelial cells initiates and perpetuates the plaque by recruiting monocytes from circulating blood. Therefore, normalizing dysfunctional endothelial cells by durable transgene expression of atheroprotective genes is a promising strategy for preventing and therapy of atherosclerosis. However, primary arterial endothelial cell is one of the most hard-to-transfect cell types that only a few attempts succeeded via invasive surgeries [102-104]. Therefore, this thesis meets the critical unmet need for the gene therapy of atherosclerosis by providing two methods for the gene therapy of atherosclerosis.

(B) Providing an alternative method for the atherosclerotic therapy based on secreted protein

Proteins have been developed as drugs for decades. However, proteins are intrinsically unstable and their circulating time is very short after system injection. To produce durable effect, repeated injection is needed. This thesis provided an alternative method for the delivery of secreted protein for the atherosclerotic therapy. After intramuscular injection of microbubbles and naked plasmid, the ultrasound is applied to the injecting site. The gene expression of the plasmid in skeletal muscle can be increased by over 10 fold compared with the naked plasmid injection. By manipulating the encoding sequence of the plasmid, proteins expressed in skeletal muscle can be secreted into blood and act on the targeted tissue for the atherosclerotic therapy. With this method, the transgene expression in skeletal muscle can persist for over 3 weeks after just one injection.

This method might also be applicable for other secreted proteins, such as ApoE[88, 89], IL-12[105], etc.

(C) Providing a method for manipulating transgene expression in artery wall

Blood vessels controls the blood supply to the body. Problems in any part of this big networks can cause disability or death. The most common vascular diseases include carotid artery disease (CAD), peripheral artery disease (PAD), abdominal aortic aneurysm (AAA), deep vein thrombosis (DVT) , arteriovenous malformation (AVM), etc. In the process of these disease, several cells (endothelial cells, smooth muscle cells, immunocytes, etc.) are involved through several complicated signal pathways. Although in vitro models are important for clarifying the underlying mechanisms of these diseases, in vitro conditions cannot replicate the in vivo conditions. Therefore, selectively increasing or inhibiting the expression of the gene of interested in the diseased vessels in vivo would be provide a strong evidence to demonstrate the role of the genes in the development of the vascular diseases. In this thesis, a simple but effected method for non-invasive image-guided gene delivery to artery cells was established. Although the applicability of this technique is only demonstrated in carotid artery, abdominal aorta, and femoral artery, in theory, this technique might also be applicable for targeted gene delivery of almost all the vessels that can be visualized by ultrasound imaging. With considerable further improvement and validation, this technique will find its broad applications in the fundamental research and clinical translation in respect to vascular diseases.

1.2.2 Innovations

(A) For the first time, the transgene expression of KLK10 in skeletal muscle is achieved to inhibit atherosclerosis

KLK10 is newly-discovered mechano-sensitive gene. KLK10 expression in endothelial cells is reduced by d-flow, resulting in reduction of endothelial inflammation, barrier disruption and atherogenesis. Our previous results also show that systematic

administration of recombinant KLK10 protein could inhibit atherosclerosis. However, recombinant protein have a very short circulation time and repeated injection is needed. In this research, ultrasound-enhanced transgene expression of KLK10 can be induced in skeletal muscle and thereby continuously produce KLK10 protein, which can be secreted into blood and act on the endothelium that is prone to atherosclerosis. With this method, the transgene expression of KLK10 in the skeletal muscle can last for over 3 weeks.

(B) For the first time, the transgene expression in artery way can be manipulated in a noninvasive image-guided way

By far, expressing external gene in selected arterial endothelial cell is a very hard task, while a few invasive methods can make it. In this research, we established a noninvasive image-guided method using ultrasound combined with microbubbles to selectively induce transgene expression in arterial endothelium, which has not been achieved before. The method established here utilizes the sonoporation effect by ultrasound and microbubbles to specifically express external genes in arterial endothelium. The gene expression in ultrasound-treated areas is as high as 86-fold higher than that in areas without ultrasound treatment, which is hard-to-achieve with conventional method. In addition, this method of gene delivery is image-guided. So genes can be delivered with this technology to almost all the area that can be in visualized by ultrasound imaging, including carotid, aorta, femoral artery, *etc.*

(C) For the first time, targeted transgene expression of KLK10 in the arterial endothelium is achieved to inhibit atherosclerosis

Although our previous research have demonstrated that the KLK10 expression is reduced by d-flow in vivo and might be an atheroprotective gene according to the in vitro experiments, there is still no direct evidence to confirm if local enhancement of KLK10 expression in artery endothelium affected by d-flow in vivo can inhibit atherosclerosis. With the technique established here, targeted transgene expression of KLK10 in the artery

endothelium was induced in a noninvasive image-guided way. The transgene expression of KLK10 was demonstrated to significantly inhibit atherosclerotic development in the partial carotid ligation animal model. These results not only confirm the atheroprotective function of KLK10, but also provide an effective way to gene delivery of KLK10 in vivo for gene therapy of atherosclerosis.

1.3 Thesis Organization

This thesis contains 5 chapters in total. Chapter 1 and Chapter 5 are the introduction and conclusion, respectively. Chapter 2 to 4 are the main parts of this research and each part is organized by four sections: introduction, methods, results and discussions, and summary. The thesis is organized as follows: (1) In Chapter 1, a brief introduction of background knowledge was given, including the biology of atherosclerosis, KLK10 as a novel mechanosensitive gene, current targeting strategies for atherosclerosis, ultrasound for the therapy and diagnosis of atherosclerosis, skeletal muscular gene delivery, and AAV as an gene vector. After that, the significance and innovations of this research is summarized. (2) In the Chapter 2, the ultrasound-enhance transgene expression of KLK10 in skeletal muscle was established to inhibited atherosclerosis. Firstly, the parameters involved in the ultrasound treatment is optimized. Then an atherosclerotic study is conducted to determine if the transgene expression of KLK10 skeletal muscle can inhibit atherosclerosis in the partial carotid ligation model. (3) In Chapter 3, the ultrasound-imaging-guided method for targeted gene delivery to mouse artery was established. The parameters involved in this procedure is optimized, including ultrasound power, dose of microbubbles, and the time interval between microbubbles and AAV injection. The persistence of gene expression in both endothelium and media and adventitia layer were also characterized. The mechanism of enhanced gene expression by ultrasound was then studied. The permeability changes of carotid artery after ultrasound treatment was evaluated with Evans blue staining. The distribution of AAV in the artery wall was then

evaluated by labelling AAV with fluorescent dyes. This ultrasound-guided method of gene delivery was further expanded to other arteries besides carotid artery. Two important arteries were selected: abdominal aorta and femoral artery. (4) In Chapter 4, the ultrasound-guided method of gene delivery was used for targeted gene delivery of KLK10. Firstly, the dose of KLK10-encoding AAV was optimized. Then the role of ultrasound, microbubbles and AAV were demonstrated. Finally, the transgene expression of KLK10 by the ultrasound-guided method were demonstrated to be able to inhibit atherosclerotic development in the partial carotid ligation model.

CHAPTER 2. ULTRASOUND-ENHANCED TRANSGENGE EXPRESSION IN SKELETAL MUSCLE

2.1 Introduction

KLK10 is novel atheroprotective gene identified recently in our lab. Our previous results have shown that intravenous injection of recombinant KLK10 protein could inhibit atherosclerosis. However, recombinant protein has a very short circulation time and repeated injection is needed to get prolonged efficacy. Besides its traditional functions, skeletal muscle has been discovered to be an endocrine organ, secreting a lot of myokines to act on several organs[86]. Therefore, the use of highly vascularized muscle as an endocrine organ for the systemic administration of therapeutic proteins is a really interesting application. However, the efficacy of gene transfer in skeletal muscle through direct intramuscular injection of naked plasmid is very limited. The sonoporation effect generated by microbubble destruction with ultrasound have been demonstrated to be able to increase transgene expression in skeletal muscle[90]. Therefore, we hypothesized that ultrasound in combination with microbubbles could increase the transgene expression of KLK10 in skeletal muscle and thus inhibit atherosclerotic development.

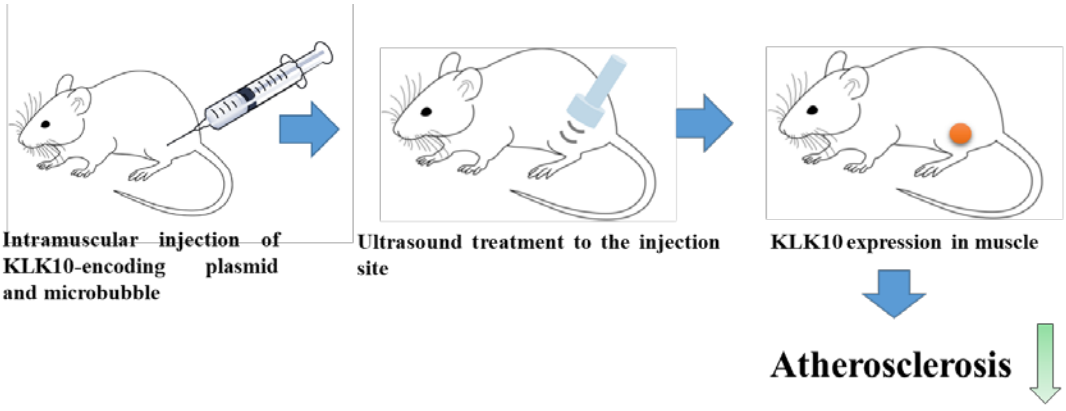

Figure 2.1 Ultrasound-enhanced transgene expression of KLK10 in skeletal muscle to inhibit atherosclerosis.

In this chapter, we will firstly optimize the parameters of ultrasound treatment, including duty, burst rate, power, time, etc. The optimized parameters will then be used for transgene expression of KLK10 in skeletal muscle to determine if the atherosclerosis can be inhibited in the partial carotid ligation model.

2.2 Methods

2.2.1 Microbubble preparation

The microbubbles are prepared with a modified mechanical agitation method established in our lab. The method is described as followings:

a) Dissolve DSPC and DSPE-PEG2000 in ethanol at the concentration of 10 mM.

b) Add 1800 μL DSPC and 200 μL DSPE-PEG2000 solution into a 20 mL glass vial and mix.

c) Heat the glass vial at 80 ℃ and evaporate the ethanol completely under nitrogen gas flow.

d) Add 1 mL (1.036g) propylene glycol and heat at 60 ℃ to fully dissolve the lipids.

e) Add 1.26 g glycerol to the solution.

f) Place a magnetic stir bar into the glass vial. Heat the vial at 60 ℃ and make sure the solution is clear and no precipitates exist.

g) Under vigorous stirring, add 8 mL PBS (pre-warmed at 60 ℃) to the lipid solution.

h) Filter the solution with a 0.45 μm syringe filter and then 0.22 μm syringe filter to sterilize the solution.

i) Sub-pack the solution into 2-mL glass vials (1 ml/vial). The headspace of the vial is filled with perfluoropropane gas. The solution can be stably stored at 4 ℃ for several months.

j) Before use, the vial is shaken with the Vialmix for 45s to get the microbubbles.

k) The concentration of microbubbles can be quantified with cytometry. The concentration of microbubbles is around 1.2×10^{10}/mL.

2.2.2 Plasmid construction

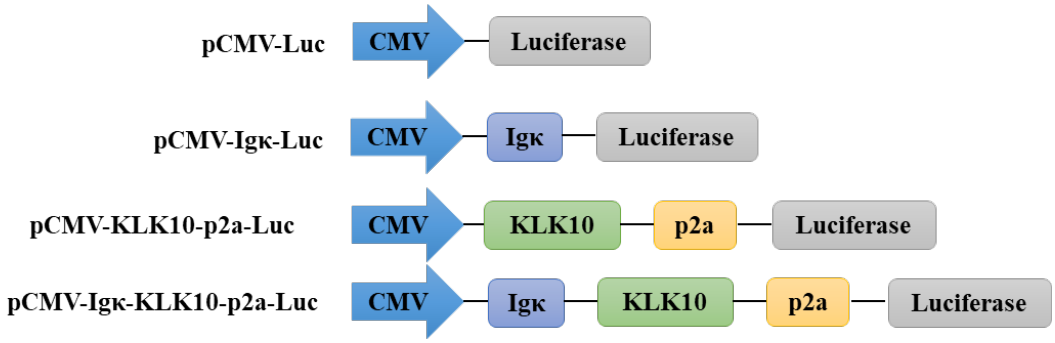

Figure 2.2 Structure of the plasmids.

The plasmid was constructed by GENEWIZ (Suzhou, China) and confirmed with DNA sequencing. Four plasmids were involved in this research (Figure 2.2). The plasmid pCMV-Luc was obtained from Ambion. The plasmid was constructed by adding an Igκ signal peptide sequence to the N-terminal of the sequence of luciferase. The pCMV-KLK10-T2A-Luci was constructed by adding cDNA sequence of KLK10 and T2A peptide sequence to the N-terminal of the sequence of luciferase. The pCMV- Igκ-KLK10-T2A-Luci was further constructed by adding the Igκ signal peptide sequence to the N-terminal of the sequence of KLK10.

2.2.3 Protocols for gene transfer in skeletal muscle

The equipment used for the ultrasound treatment is the Sonopore KTAC-4000 sonoporator equipped with an S-PW-1.0-20mm probe (Plane Wave Transducer, 20mm diameter tip, 1MHz).

1) Anesthetize the mice with isoflurane in oxygen in an anesthesia chamber. Maintain body temperature using the heating pad. Ensure complete anesthetization by assessing for a reaction to a toe pinch, and then maintain anesthesia at 1.5 - 2% isoflurane.

2) The animal was shaved to remove any fur from both thighs. Wipe the site of hair removal and surrounding area down with an alcohol prep pad.

3) Dilute the microbubbles with pure water to a concentration of 5×10^8/mL.

NOTE： Microbubbles are not very stable after dilution. Do not leave microbubbles exposed to the air for longer than 30 min. It's better to dilute the microbubbles every time before use.

4) Add 2 μL 9% sodium chloride solution, 1μL diluted microbubble solution and 50 μg plasmid to 200-μL conical tube. Then add some water to make the total volume to be 20 μL.

5) Mix the solution well and inject the solution intramuscularly into the thigh muscle with a 30G syringe.

6) Place the probe on the top of the inject site and use some ultrasound gel to couple the probe with the mouse thigh.

7) Turn on the sonoporator to apply the ultrasound (Frequency: 1MHz, Duty cycle: 25%, Burst rate: 50Hz, Intensity: 1.5W/cm^2, Wave Pattern Type: sine, Time: 4 min,)

2.2.4 Protocols for bioluminescence imaging

1) Thaw D-Luciferin Potassium Salt at room temperature and dissolve in PBS (no calcium or magnesium) to a final concentration of 15mg/mL.

2) Sterilize the Luciferin solution through a 0.22μm syringe filter.

3) Once prepared, the solution need to be used immediately or stored in -20℃ after sub-packed.

4) For bioluminescence imaging in vivo, anesthetize the mice with isoflurane in oxygen. The animal is then shaved to remove any fur on the hind leg.

5) Intraperitoneally inject with 10μL of Luciferin stock solution per gram of body weight (~200 μL/mouse).

6) The bioluminescence images are then collected at 12 min post injection with an exposure time of 2 minutes.

2.2.5 Mouse partial carotid ligation surgery

All animal experiments were approved by the Animal Care and Use Committee at Peking University. The partial carotid ligation surgery was conducted as previously reported[17]. Male C57BL/6 and ApoE$^{-/-}$ mice (Charles River Laboratories, Beijing) were allowed ad libitum to standard chow diet and water until surgery at 8–9 weeks of age. Mice were anaesthetized with 3.5% isoflurane initially and then ~2% during the entire procedure. Before surgery, analgesic carprofen (5mg/kg) was administrated subcutaneously. The LCA bifurcation was exposed by blunt dissection and three caudal branches of LCA (left external carotid, internal carotid and occipital arteries) were ligated with 6-0 silk sutures while leaving the superior thyroid artery intact. For atherosclerotic studies, the ApoE$^{-/-}$ mice were fed with a Paigen's high fat diet (Research diets) following the surgery until killed. C57BL/6 mice were continued with a chow diet.

2.2.6 Plaque lesion analysis

Carotid arteries were isolated *en bloc* from ligated ApoE$^{-/-}$ mice fed with a high fat diet for 3 weeks. The artery trees were photographed using a dissection microscope and the

opaque area covered by plaque and total area of LCA were quantified using NIH ImageJ software

2.2.7 Immunohistochemistry

Arteries were embedded in optimal cutting temperature compound (Tissue-Tek), frozen on dry ice and stored at -80 ℃ until used. To visualize atherosclerosis development, Oil-red-O staining was carried out. Frozen sections were fixed in formalin for 10 min, rinsed with water and 60% propylene glycol, and then stained with Oil Red O staining solution (Solarbio). Slides were then differentiated in 60% propylene glycol, rinsed with distilled water, and counterstaining was done using Mayer's haematoxylin (Beijing Leagene Biotechnology Co., Ltd.) for 5 min.

2.3 Results and discussions

2.3.1 Multi-parameter optimization of transgene expression in skeletal muscle

Gene transfer for gene therapy is a rapidly expanding field. Tissues with high transgene efficacy is sought including tumors, and organs such as the liver, heart, or brain. Special interest has been devoted to gene delivery to skeletal muscle fibers, for the correction of myopathies, local secretion of angiogenic or neurotrophic factors, and vaccination. Although transgene expression in skeletal muscle can be achieved by intramuscular injection of naked plasmid, the expression is usually very weak and inconsistent. Therefore, a lot of researches have been done to increase the level and reliabilities of skeletal muscular gene expression. Ultrasound destruction by high power ultrasound can increase the permeability of cells and thereby enhance the transgene expression. Therefore, we focused on enhancing gene transfer to skeletal muscle utilizing the sonoporation effect.

Galina Shapiro et al. used nonlinear ultrasound and bioluminescence imaging to optimize the acoustic pressure, microbubble concentration, treatment duration, DNA dosage, and number of treatments required for in vivo luciferase gene expression in a mouse thigh muscle model[90]. Mice injected with 50 μg luciferase plasmid DNA and 5×10^5 microbubbles followed by ultrasound treatment at 1.4 MHz, 200 kPa, 100-cycle pulse length, and 540 Hz pulse repetition frequency (PRF) for 2 min exhibited superior transgene expression compared to all other treatment groups.

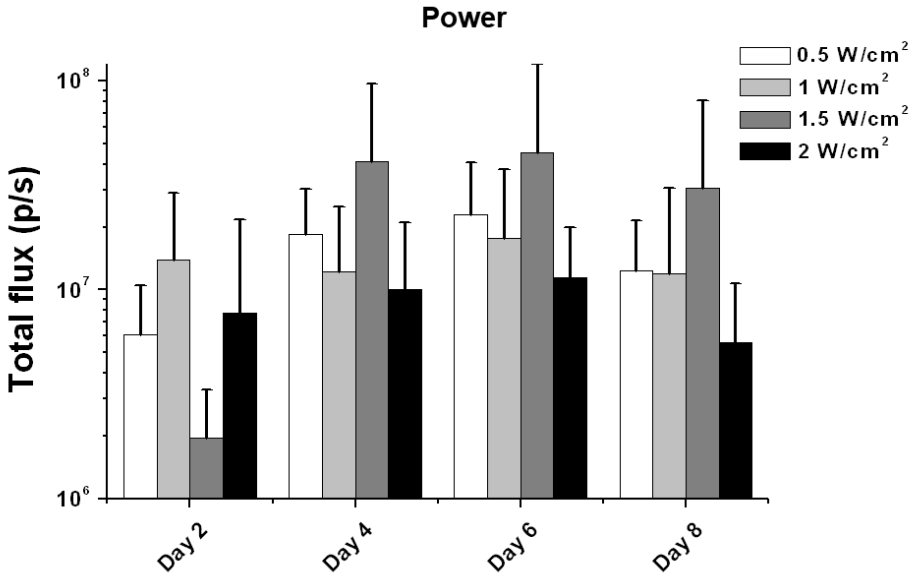

Figure 2.3 Luciferase expression profile in mice treated with microbubble-enhanced sonoporation at various ultrasound power. n=4, data are shown as mean ±SD.

In this research, we modified the protocol used by Galina Shapiro et al. The Sonopore KTAC-4000 sonoporator equipped with an S-PW-1.0-20mm probe (Plane Wave Transducer, 20mm diameter tip, 1MHz) was used in our research. 50 μg luciferase plasmid DNA (pCMV-Luc) and 5×10^5 microbubbles were dispersed in saline and intramuscularly injected into thigh muscle of the mice followed by ultrasound treatment. The parameters of the ultrasound treatment were firstly optimized

The power of ultrasound was firstly optimized. Mice were injected with 50 μg plasmid DNA premixed with 5×10^5 microbubbles and then treated with a duty of 50%, a burst rate

of 50 Hz, and a power of 0.5 W/cm^2, 1 W/cm^2, 1.5 W/cm^2, and 2 W/cm^2 for 4 min. Gene expression of luciferase was monitored using the bioluminescence imaging for 8days after treatment. As shown in Figure 2.3, at day 4, day 6, and day 8, the highest gene expression was found at the power of 1.5 W/cm^2. Therefore, the power of 1.5 W/cm^2 was selected for further experiments.

The duty is defined as the fraction of time the *ultrasound* field is "on". Mice were injected with 50 μg plasmid DNA premixed with 5 × 10^5 microbubbles and then treated with a burst rate of 50 Hz, a power of 1 W/cm^2, and with a duty of 25%, 50%, 75%, and 100%for 4 min Gene expression of luciferase was monitored using the bioluminescence imaging for 8days after treatment. As shown in Figure 2.4, the transgene expression is negatively related to the duty. The highest transgene expression is found with a duty of 25%.

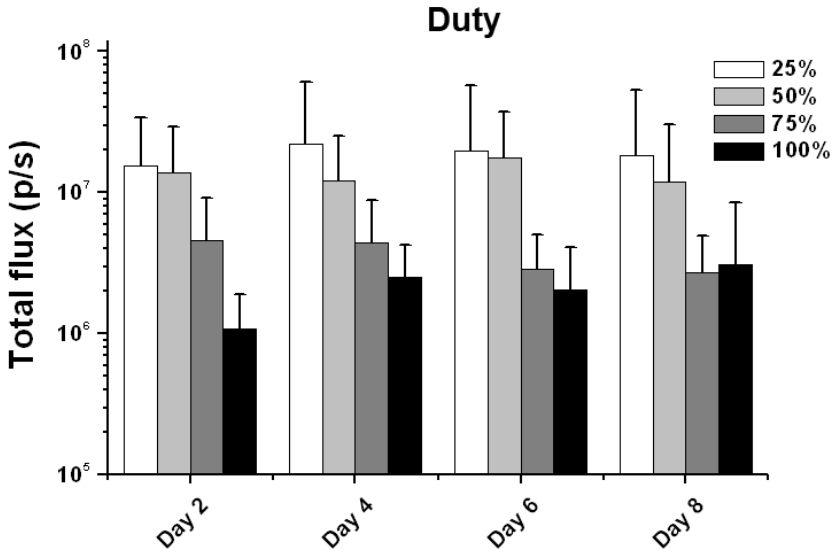

Figure 2.4 Luciferase expression profile in mice treated with microbubble-enhanced sonoporation at various duties. n=4, data are shown as mean ±SD.

Burst rate is the frequency with which the pulses are repeated. Mice were injected with 50 μg plasmid DNA premixed with 5 × 10^5 microbubbles and then treated, a duty of 50%, a power of 1 W/cm^2, and with a burst rate of 25 Hz, 50 Hz, 75 Hz, and 100 Hz for 4

min Gene expression of luciferase was monitored using the bioluminescence imaging for 8 days after treatment. As shown in Figure 2.5, the transgene expression of luciferase is not significant changed with the burst rate.

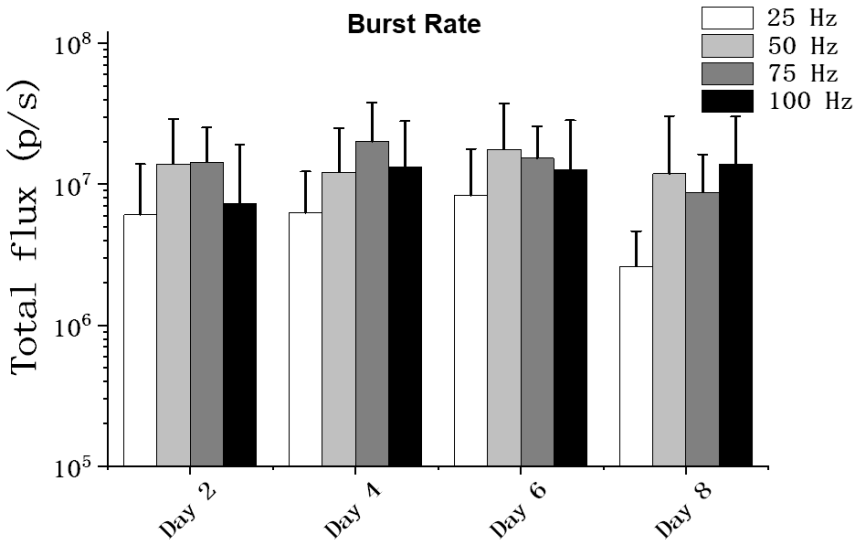

Figure 2.5 Luciferase expression profile in mice treated with microbubble-enhanced sonoporation at various burst rates. n=4, data are shown as mean ±SD.

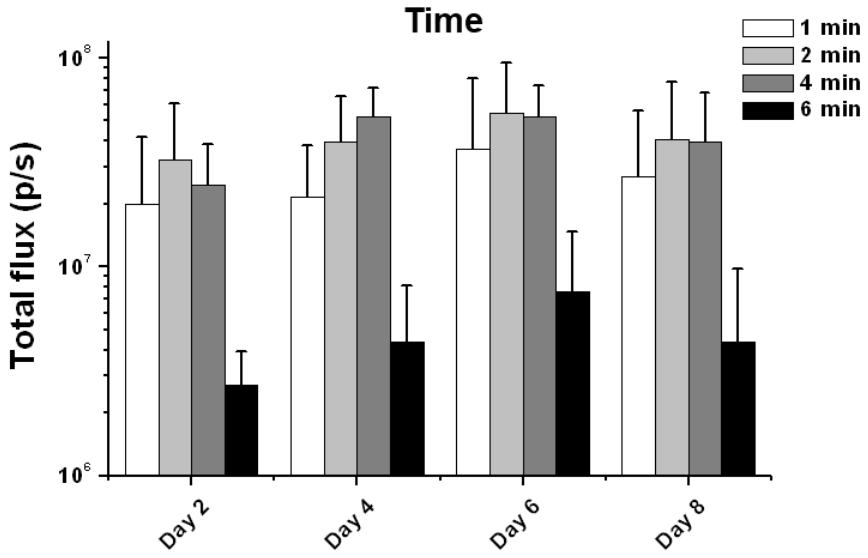

Figure 2.6 Luciferase expression profile in mice treated with microbubble-enhanced sonoporation at various treatment time. n=4, data are shown as mean ±SD.

Finally, the total treatment times is optimized. Mice were injected with 50 μg plasmid DNA premixed with 5×10^5 microbubbles and then treated, a duty of 50%, a power of 1 W/cm^2, and with a burst rate of 50 Hz for 4 min Gene expression of luciferase was monitored using the bioluminescence imaging for 8days after treatment. As shown in Figure 2.6, the transgene expression with a treatment time of 1 min, 2min and 4 min are not significantly different, while the expressing is much reduced when the treatment time is as high as 6 min.

2.3.2 Combining effect of ultrasound and microbubbles for gene delivery

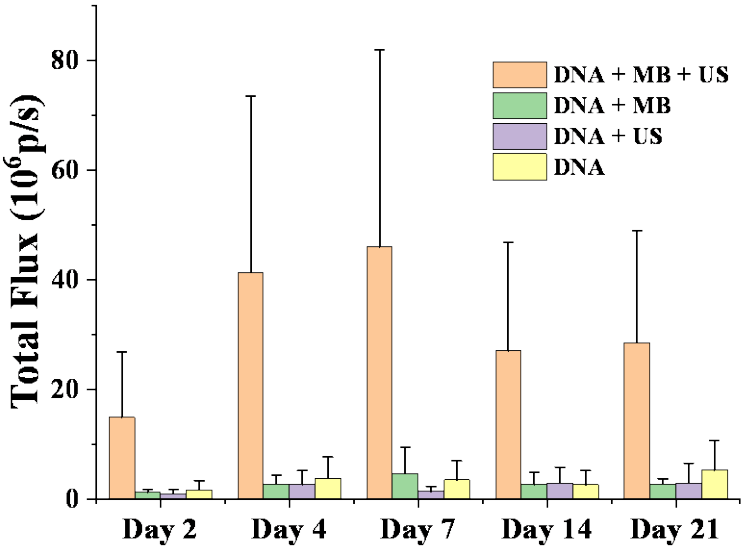

Figure 2.7 Luciferase expression profile in mice with different treatments. n=4, data are shown as mean ±SD.

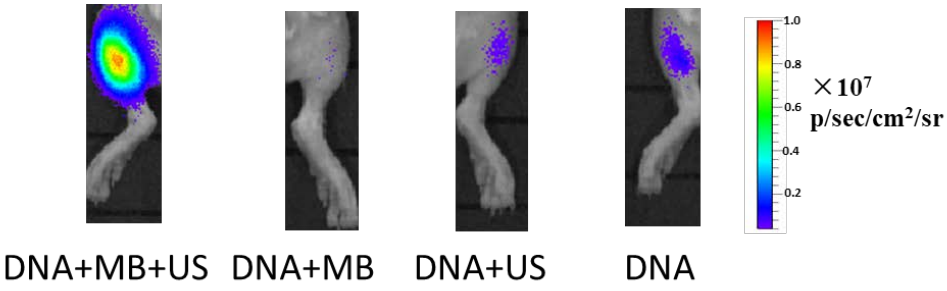

Figure 2.8 Representative bioluminescence images of the thigh leg of mice with different treatments at the 21st day.

Based on the previous results, the ultrasound with a duty of 25%, a power of 1.5 W/cm^2, and with a burst rate of 50 Hz for 2 min was selected for further experiments. To clarify the combining effect of ultrasound and microbubbles in enhancing transgene expression in skeletal muscle, the mice were divided into four groups for four different treatments: DNA+MB+US (plasmid and microbubbles injection followed by ultrasound treatment), DNA+MB (plasmid and microbubbles injection only), DNA+US (plasmid injection followed by ultrasound treatment), and DNA (plasmid injection only).The gene expression were determined by bioluminescence imaging for 21 days post treatment. As shown in Figure 2.7&2.8, microbubble or ultrasound alone did not induce any significant changes of transgene expression as compared with naked plasmid injection. However, ultrasound in combination with microbubbles can induce over 10-fold increase in transgene expression compared with all the other groups. This demonstrated that the microbubble-enhanced sonoporation can significantly enhance transgene expression in skeletal muscle.

Transgene expression induced by the combining treatment of microbubbles and ultrasound could persist as long as 3 weeks (longer time was not determined). This is one of biggest advantages of gene delivery as compared with protein delivery. Since the circulation time of proteins is very short, repeated injection is needed. With the method established here, transgene expression in skeletal muscle can persist for a long time with just one injection.

2.3.3 KLK10 expression in skeletal muscle to inhibit atherosclerosis

The ultrasound-enhanced transgene expression in skeletal muscle was further applied for KLK10 delivery to determine if this method can be used to inhibit atherosclerosis. KLK10 is novel atheroprotective gene identified recently in our lab. Our previous results have shown that intravenous injection of recombinant KLK10 protein could inhibit atherosclerosis. However, recombinant protein has a very short circulation time and repeated injection is needed to get prolonged efficacy. The ultrasound-enhanced

transgene expression of KLK10 is expect to continuously produce KLK10 protein in skeletal muscle, which can be secreted into blood and inhibit atherosclerosis.

Figure 2.9 Experimental design to determine if KLK10 expression in skeletal muscle can inhibit atherosclerosis.

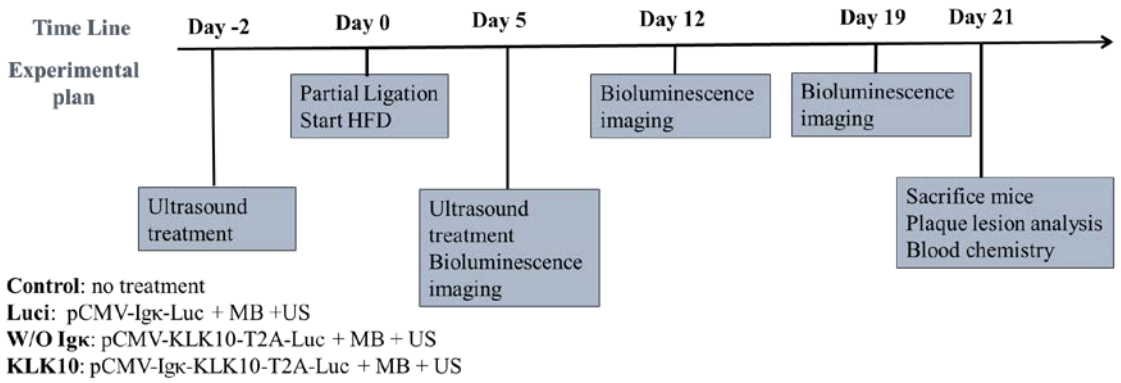

To monitor the expression of KLK10 in the skeletal muscle, the KLK10 sequence is linked with the luciferase sequence through a T2A pepetide. The T2A peptide is a "self-cleaving" peptide, which undergoes self-cleavage to generate mature proteins by a translational effect that is known as "stop-go" or "stop-carry"[106-108]. The cleavage site is located between the last glycine of its C-terminal and the first praline of the downstream protein. The incorporation of T2A makes the genes co-expressed while their function are not affected. Therefore, the level of luciferase expression should reflect how much KLK10 is the result of exogenous expression. In this way, the KLK10 expression can be determined by the bioluminescence imaging. In addition, to make the KLK10 secreted out of the cells, an Igκ signal peptide is also added to the N-terminal of the KLK10 sequence. The Igκ signal peptide mediates targeting of KLK10 to the endoplasmic reticulum (ER), so that KLK10 can be efficiently secreted. Therefore, the resultant pCMV- Igκ-KLK10-T2A-Luci plasmid is used for the in vivo delivery of KLK10. In addition, the plasmid pCMV-Igκ-

Luci which lacks of KLK10 sequence and plasmid pCMV-KLK10-T2A-Luci whick lacks of Igκ signal peptide were also constructed as control.

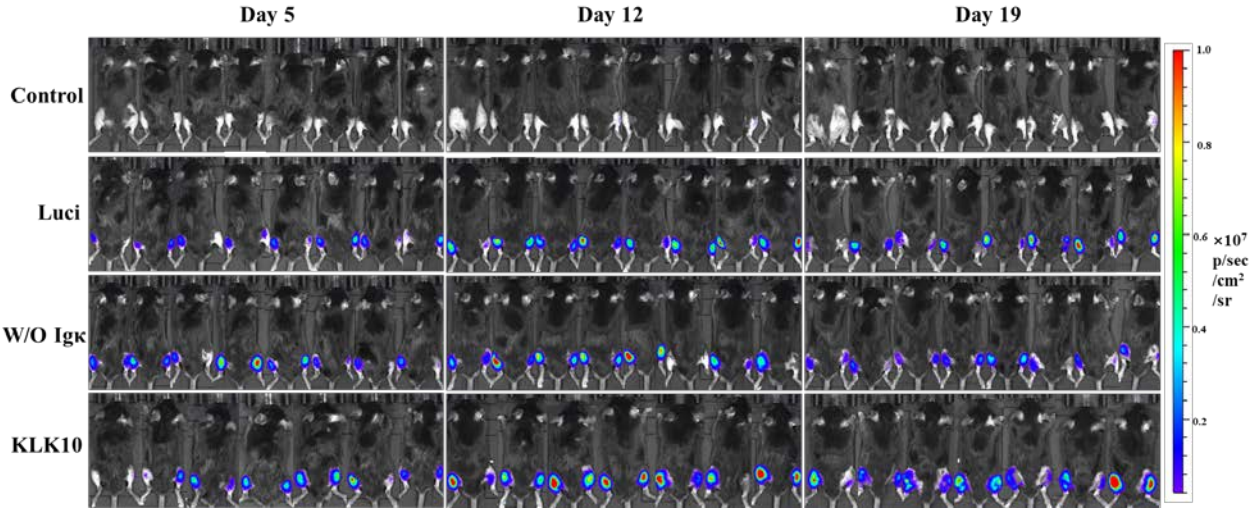

Figure 2.10 Bioluminescence images of the mice at different time points.

The mice were divided into four groups (Figure 2.9). The Control group was the group without any treatment at Day -2 and Day 5. The Luci group, W/O Igκ group, and KLK10 group were intramuscularly injected with pCMV-Igκ-Luci, pCMV-KLK10-T2A-Luci, and pCMV- Igκ-KLK10-T2A-Luci premixed with microbubbles followed by ultrasound treatment in both legs, at Day -2 and Day 5, respectively. The mice were subjected to partial carotid ligation at Day 0 and then fed with high fat diet for three weeks.

Utilizing the sequence of luciferase inserted in the plasmids, the transgene expression can be monitored noninvasively with the bioluminescence imaging. As shown in Figure 2.10, no signal is detected in the Control group owing to lack of luciferase expression. The luciferase are expressed in both legs of the other three groups, indicating that the transgenes encoded by the plasmids were expressed in the skeletal muscle.

Although there are some variations in the gene expression， there are no significant difference between these three groups.

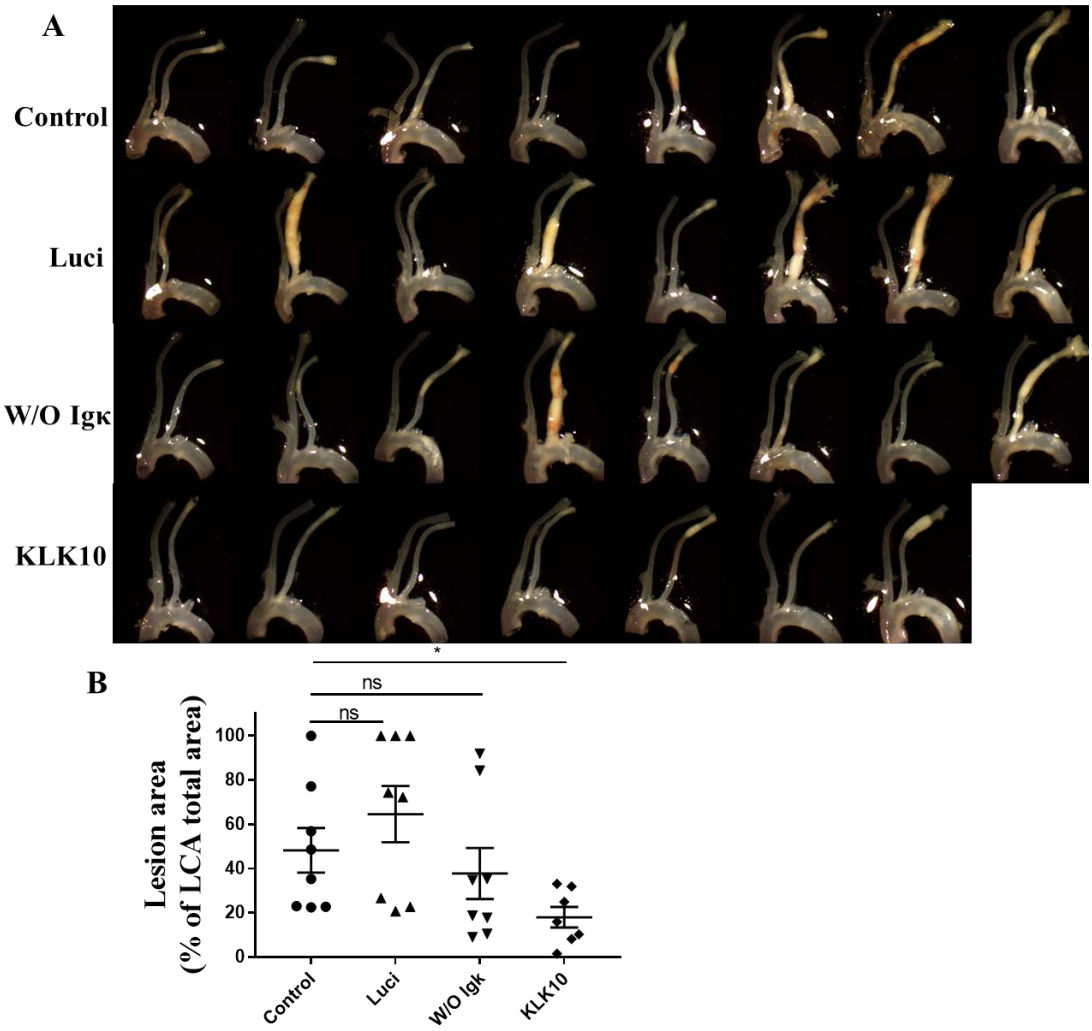

Figure 2.11 Atherosclerotic plaque analysis. (A) Three weeks post the partial carotid ligation surgery, the mice were sacrificed and the artery trees were dissected out for bright field imaging. (A) The percentage of atherosclerotic lesion in LCA is quantified with Image J. Data shown as mean ± s.e.m.; *$p<0.05$, ns $p>0.05$ as determined by student's t-test.

The mice were sacrificed at the 21st day for atherosclerotic plaque analysis. As shown in Figure 2.11, the plaque lesions in the Luci group and W/O Igκ group were not significantly different from that in the Control group, while the plaque lesions in the KLK10 group were significantly different from that in the Control group. Compared with the Luci group, the plaque lesion area in KLK10 group is decreased from 64.6% to 18.0%.

The carotid arteries in the Luci and KLK10 group were also sectioned and stained with Oil-Red-O (Figure 2.12). The plaque size in KLK10 group is reduce by 77.4%. These results demonstrated that the transgene expression of KLK10 in skeletal muscle could inhibit atherosclerosis.

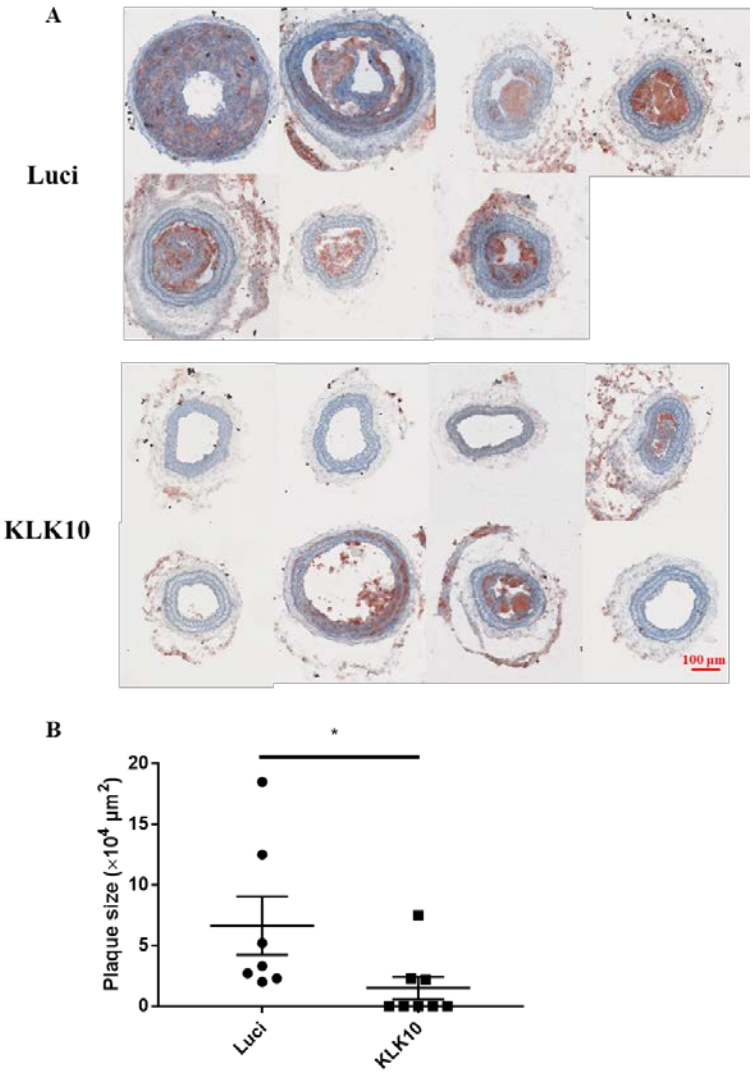

Figure 2.12 Oil-Red-O staining. (A) The carotid arteries in the Luci and KLK10 group were further sectioned and stained with Oil-Red-O. (B) The plaque size indicated by the Oil-Red-O staining were quantified. Data shown as mean ± s.e.m.; *$p<0.05$, as determined by student's t-test. Note: The mice used for the Oil-Red-O staining is different from the mice in Figure 2.12. This atherosclerotic experiments were repeated in two batches of mice.

2.4 Summary

In this chapter, we established a method to induce transgene expression of KLK10 in skeletal muscle to inhibit atherosclerosis. After intramuscular injection of naked plasmid and microbubbles, ultrasound is applied to the injection site to induced increased transgene expression in the skeletal muscle. After optimizing the ultrasound parameters, the ultrasound-enhanced transgene expression in skeletal muscle is increased by over 10 fold compared with naked plasmid injection and can persist for over 3 weeks. By adding a signal peptide to the N-terminal of coding sequence of KLK10, the expressed KLK10 proteins can be secreted out, enter into the blood, and act on the inflamed area to inhibit atherosclerosis. The transgene expression of KLK10 in skeletal muscle reduced the atherosclerotic lesions from 64.6% to 18.0% in the partial carotid ligation model. These results demonstrated the ultrasound-enhanced transgene expression of KLK10 in skeletal muscle as a potential therapy for atherosclerosis.

CHAPTER 3. ULTRASOUND IMAGING-GUIDED GENE DELIVERY TO MOUSE ARTERY

3.1 Introduction

In the previous chapter, ultrasound combined with microbubbles was demonstrated to be able to increase transgene expression in skeletal muscle. The ultrasound-enhanced transgene expression of KLK10 in skeletal muscle could significantly inhibit atherosclerosis in the partial carotid ligation model. However, this kind of technology is only suitable for the gene delivery of secreted proteins and proteins expressed in skeletal muscle will also act on all the major organs in addition to artery. Therefore, there is a need to establish a new method for targeted delivery exogenous genes to artery endothelium.

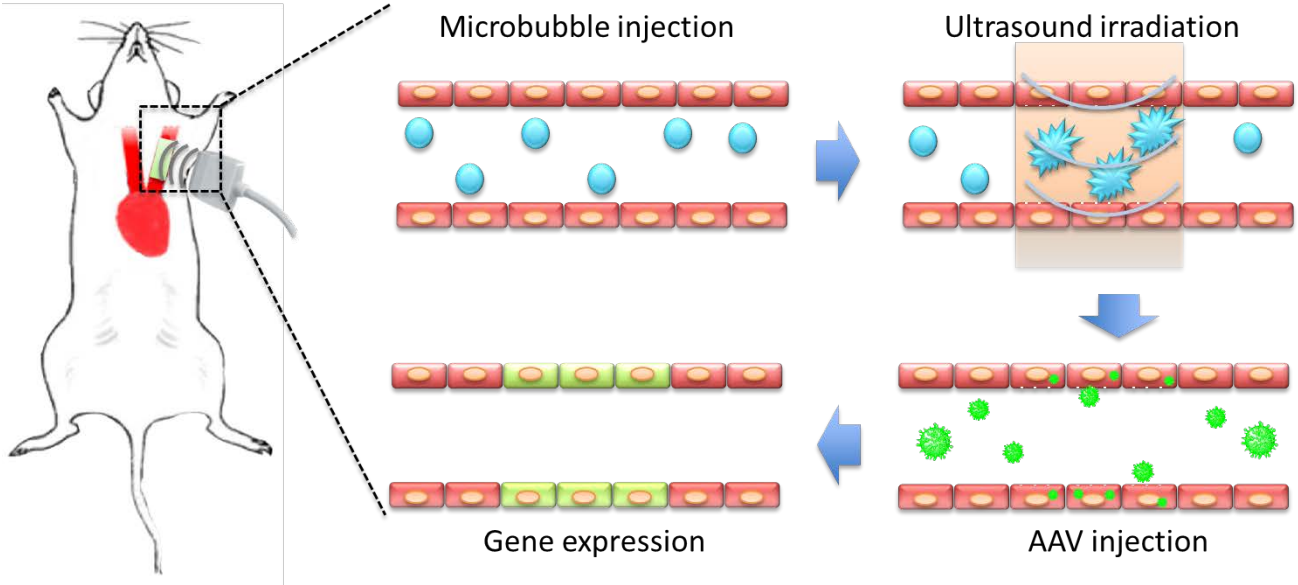

Figure 3.1 Schematic illustration the proposed rationale of ultrasound imaging-guided gene delivery.

In this chapter, a simple but effective method for image-guided targeted gene delivery to is established based on the sonoporation effect by ultrasound and microbubbles (Figure 3.1). Under the ultrasound imaging, the carotid artery can be clearly visualized. The area of interest can be selected from the ultrasound image. Then microbubbles can be injected intravenously. After that, ultrasound will be applied with the imaging probe to the

selected area. Hopefully, the permeability of arterial endothelium will increase and then AAV gene vectors encoding genes of interest will be injected. The gene is expected to be selectively expressed in the ultrasound-treated area. In this chapter, various parameters involved in this procedure will be optimized, including, microbubble concentration, ultrasound power, the time interval between microbubble and AAV injection, etc. Some characterization of the procedure will also be conducted, including specificity, durance, safety, etc. To explain the reason why ultrasound in combination with microbubble and AAV can enhance transgene expression in artery, Evans blue staining will be used and then AAV will be labelled with fluorescent dyes to track the distribution of AAV in arterial wall. Finally, the ultrasound-guided method for targeted gene delivery to artery will be further demonstrated for the potential applications in the targeted gene delivery to abdominal aorta and femoral artery.

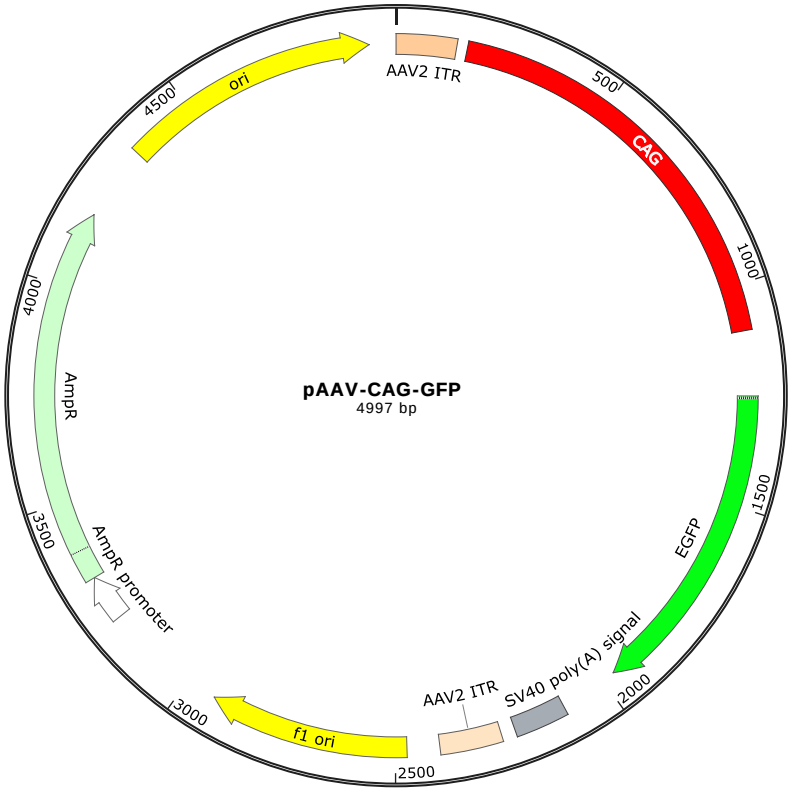

Figure 3.2 Map of plasmid encoding EGFP for AAV packaging.

3.2 Methods

3.2.1 AAV packaging

Recombinant AAV serotype-9 expressing EGFP under the control of CAG promoter, a hybrid construct consisting of the cytomegalovirus (CMV) enhancer fused to the chicken beta-actin promoter are produced by Vigene Biosciences (Jinan, China) (Figure 3.1).

3.2.2 Isolation of Endothelial-Enriched RNA.

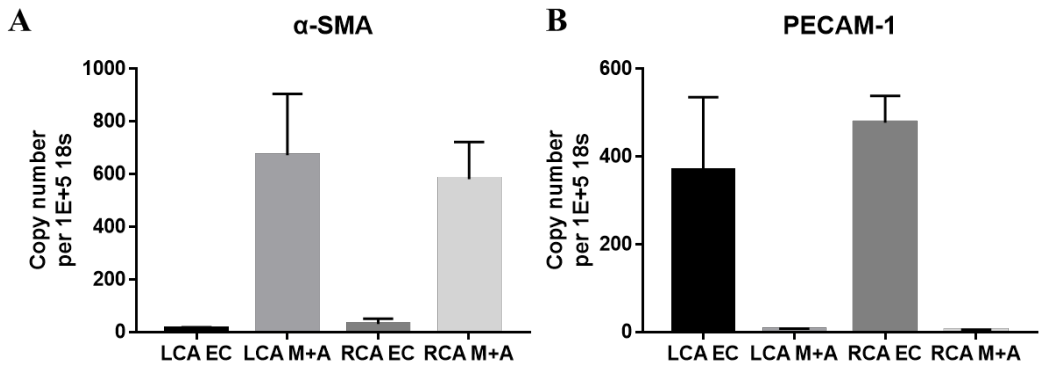

Figure 3.3 Marker genes (PECAM-1 and α-SMA) expression of endothelial-enriched RNA samples from LCA and RCA.

Endothelial-enriched RNA from the carotid arteries was extracted as previously described[17]. Briefly, mice were killed by CO_2 inhalation and perfused with saline via the left ventricle after severing the inferior vena cava. The left common carotid artery (LCA) and the right common carotid artery (RCA) were then isolated and carefully cleaned. The carotid lumen was quickly flushed with 100 µl of QIAzol lysis reagent (QIAGEN) using a 29-gauge insulin syringe in a microfuge tube. The eluate was then used for intimal RNA isolation using an RNA MiniPrep kit (ZYMO research) according to the manufacturer's instructions. The carotid artery leftover after flushing with QIAzol was used to prepare RNA from media and adventitia. Media and adventitia was placed in QIAzol lysis reagent

(350 μl per carotid), and homogenized with a homoginizer. Marker genes (PECAM-1 and α-SMA) was used to determine the purity of endothelial RNA in each prep (Figure 3.3).

3.2.3 Quantitative Real-Time PCR (qPCR).

RNA samples were reverse-transcribed with the PrimeScript RT reagent kit (TAKARA) and qPCR was performed on selected genes using the SYBR Premix Ex Taq (TAKARA) with custom-designed primers using 18S as house-keeping control. The Bio-rad CFX96 Touch qPCR machine was used for qPCR measurements. The PCR conditions were 30 s at 95 ℃, followed by 40 cycles of 95 ℃ for 5 s and 60 ℃ for 30 s. Fold changes between LCA and RCA were determined for all targets using the ΔΔCt method. Sequences for primers used in this studies were as follows:

18s(F)	CGCCGCTAGAGGTGAAATTCT
18s(R)	CGAACCTCCGACTTTCGTTCT
PECAM-1(F)	ACGCTGGTGCTCTATGCAAG
PECAM-1(R)	TCAGTTGCTGCCCATTCATCA
α-SMA(F)	TTTCCAAATCATTCCTGCCC
α-SMA(R)	CGCTCTCAAATACCCCGTTT
EGFP(F)	AAGCTGACCCTGAAGTTCATCTGC
EGFP(R)	CTTGTAGTTGCCGTCGTCCTTGAA
ICAM-1(F)	AGGTGGTTCTTCTGAGCGGC
ICAM-1(R)	AAACAGGAACTTTCCCGCCA
VCAM-1(F)	TCTTGGGAGCCTCAACGGTA
VCAM-1 (R)	CAAGTGAGGGCCATGGAGTC
mCherry(F)	GAACGGCCACGAGTTCGAGA
mCherry(R)	CTTGGAGCCGTACATGAACTGAGG

KLK10(F)	CGCTACTGATGGTGCAACTCT
KLK10(R)	CAGTGGCTTATTTCTCCAGCAA

3.2.4 General procedures for ultrasound-guided gene delivery to carotid

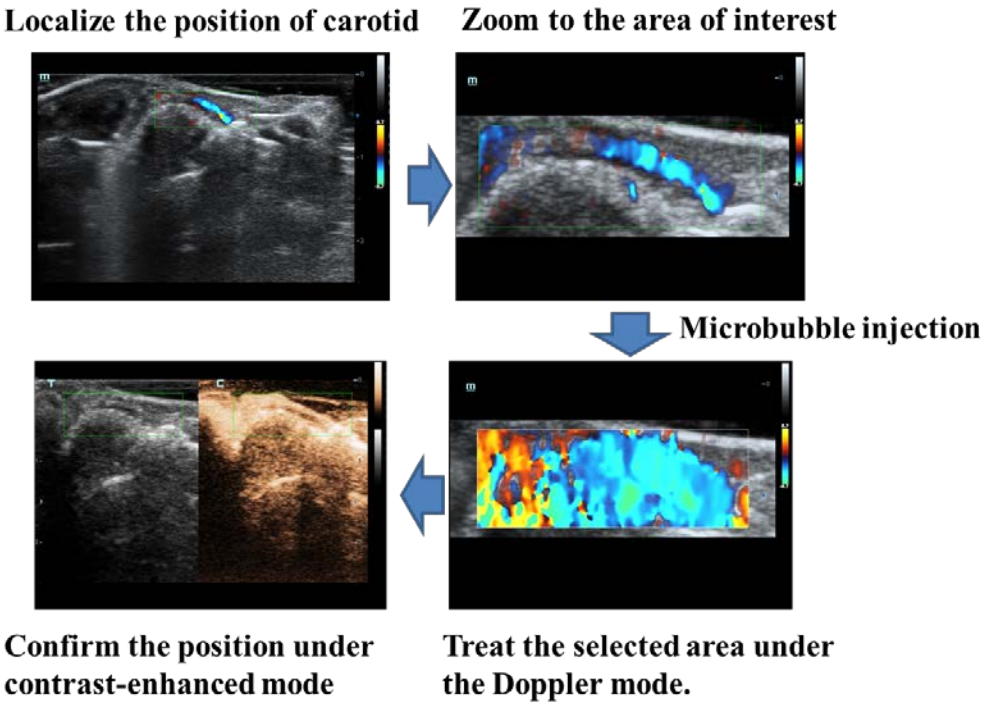

Figure 3.4 General procedures of ultrasound treatment of carotid artery

All ultrasound imaging treatments were conducted using a DC-8 ultrasound system equipped with a L12-3E linear-array probe (Mindray). Mice were anesthetized with inhaled isoflurane, and body temperature was maintained on a heated stage for the duration of studies. The position of left carotid artery can be found under B-mode ultrasound imaging (Figure 3.4). Then switch to colour Doppler-mode. Change the size and position of colour box to the region of interest, zoom to the selected area and then change mechanical index (MI) to desired value (0.2, 0.3, 0.4, and 0.5, respectively). Immediately after microbubbles injection, press the “Freeze” button every 0.5 s so that ultrasound is applied in an ON/OFF mode (0.5s ON followed by 0.5s OFF) for a total time of 30s. After the ultrasound treatment,

the AAV encoding gene of interest will be injected intravenously. At certain time point post the treatment, the mice are sacrifice for further characterization of gene expression.

3.2.5 En face staining of carotid artery

The carotid arteries are excised, fixed in 4% paraformaldehyde, penetrated with 0.025% Triton X-100 for 10 min, blocked with 10% goat serum for 1 h at room temperature, and incubated with primary anti-EGFP antibodies (abcam ab6556) overnight at 4 ℃. To visualize primary antibodies, Alexa Fluor ® 594-conjugated secondary antibody (abcam ab150080) was used for 1 h at room temperature. Nuclei were counterstained with DAPI. Samples were imaged using a Nikon confocal microscope.

3.2.6 Evaluate the permeability changes of carotid artery with Evans blue

The permeability changes of the artery can be determined by Evans blue. At pre-determined time points post ultrasound treatment, inject 100 μL Evans blue (1% in saline) intravenously and sacrifice the mouse 30 min later. The carotid arteries are then dissected and observed under microscope. The level of blue colour in the treated area directly reveals the permeability changes by ultrasound treatment.

3.2.7 Fluorescence labelling of AAV

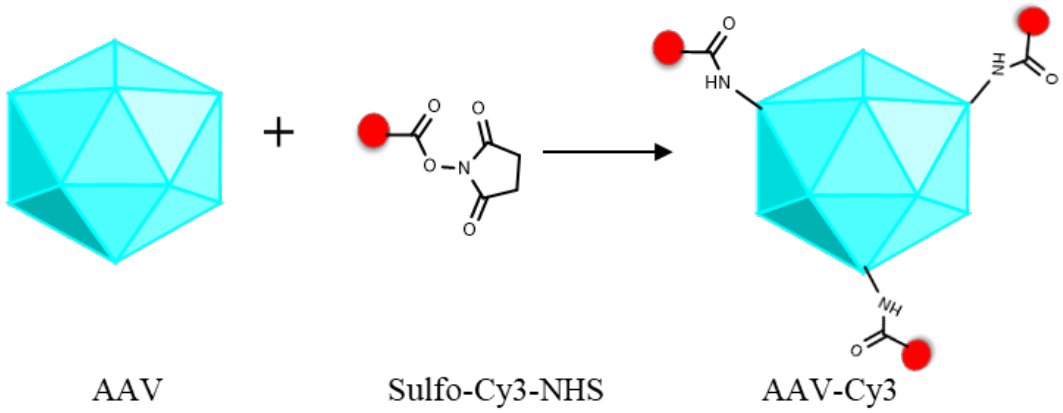

Figure 3.5 Paradigm of fluorescence labelling of AAV.

The AAV was modified with fluorescent dyes following a procedure reported in the literature with some modification (Figure 3.5)[109]. In brief, purified AAV9 was incubated for 1 hour at 4 ℃ in PBS with tenfold excess of Sulfo-Cyanine3 NHS ester over the capsid protein units (each AAV is composed of 60 capsid protein units). Labelled viruses AAV-Cy3 were separated from the free dyes by dialysis against PBS at 4 ℃ and stored at −80 ℃ in small aliquots.

3.2.8 Fluorescence tracking of AAV in carotid artery

Following ultrasound treatment to LCA, 5×10^{11} vg/mouse AAV-Cy3 was injected intravenously. At predetermined time points post injection, the mice were sacrificed. The carotid arteries were dissected, fixed with formalin, and stained with DAPI. Samples were then subjected to *en face* confocal imaging with a Nikon confocal microscope.

3.2.9 General protocols for ultrasound treatment of abdominal aorta

All ultrasound imaging treatments were conducted using a DC-8 ultrasound system equipped with a L12-3E linear-array probe (Mindray). Mice were anesthetized with inhaled isoflurane, and body temperature was maintained on a heated stage for the duration of studies. The mice were placed supine and shaved to expose the abdomen. The ultrasound probe was placed in parallel with the abdominal aorta. The position of abdominal aorta can be found under B-mode ultrasound imaging. Then switch to colour Doppler-mode. Change the size and position of colour box to the region of interest, zoom to the selected area and then change mechanical index (MI) to 0.4. Immediately after microbubbles injection (3×10^7/mouse), press the “Freeze” button every 0.5 s so that ultrasound is applied in an ON/OFF mode (0.5s ON followed by 0.5s OFF) for a total time of 1 min. After the ultrasound treatment, the AAV encoding gene of interest will be injected intravenously. At certain time points post the treatment, the mice are sacrifice for further characterization of gene expression.

3.2.10 General protocols for ultrasound treatment of femoral artery

Mice were anesthetized with inhaled isoflurane, and body temperature was maintained on a heated stage for the duration of studies. The mice were placed prone and shaved to expose the hind leg. The ultrasound probe was placed in parallel with the femoral artery. Switch the ultrasound imaging to the contrast mode. Inject microbubbles (1×10^8/mouse) and find the position of femoral artery under the contrast mode. Change the size and position of box to the region of interest, zoom to the selected area. Switch the ultrasound imaging to the colour Doppler mode and treat the selected area with a MI of 0.4. Press the "Freeze" button every 0.5 s so that ultrasound is applied in an ON/OFF mode (0.5s ON followed by 0.5s OFF) for a total time of 30s. After the ultrasound treatment, the AAV encoding gene of interest will be injected intravenously. At certain time point post the treatment, the mice are sacrificed for further characterization of gene expression.

3.3 Results and Discussion

3.3.1 Optimization of the ultrasound power and microbubble dose

To do the ultrasound imaging-guided gene delivery, a DC-8 ultrasound system equipped with a L12-3E linear-array probe was used. This machine has already been used in clinic. The centre frequency of this probe is 4.4 MHz, which is used in clinic for carotid imaging. With this system, we can clearly see the blood flow in mouse carotid artery under the colour-Doppler mode (Figure 3.4). By changing the position and size of the colour box, the area of interest can be selected. Then zoom the image to the selected area so that ultrasound only irradiated to the selected area. After injecting the microbubbles, the permeability of the artery in selected area is expected to be increased by the ultrasound.

After that, the AAV9 vectors encoding EGFP is injected. Hopefully, the EGFP can be expressed in the area with ultrasound treatment.

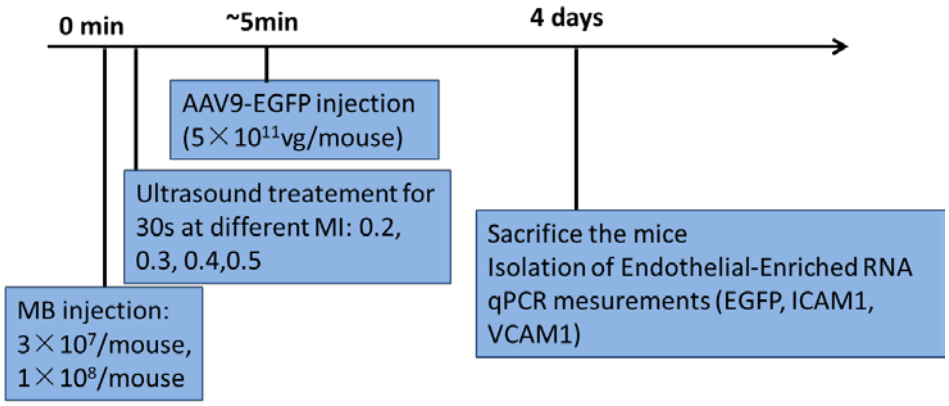

Figure 3.6 Experiment design for optimization of the ultrasound power and microbubble dose.

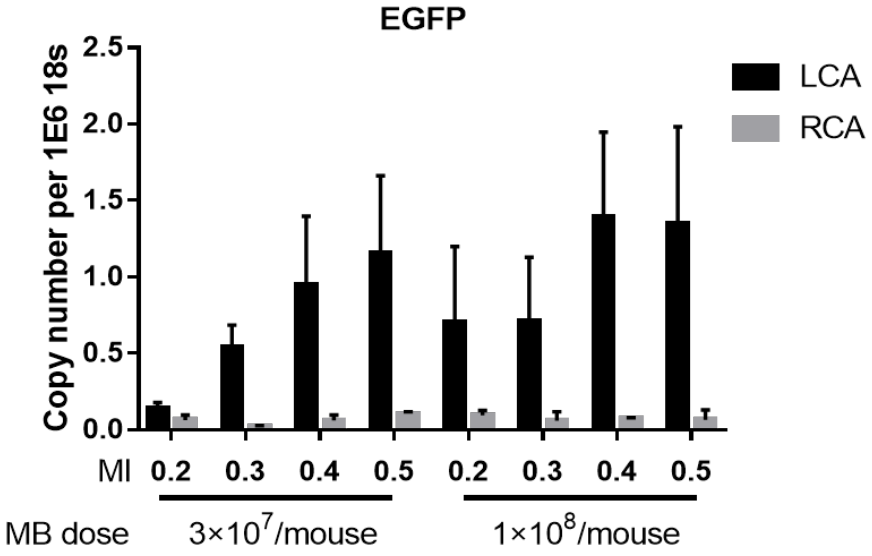

Figure 3.7 EGFP expression in carotid endothelium after different treatments. LCA is treated with ultrasound while RCA is used as control. n = 3 or 4 mice each, data shown as mean ± s.e.m.

During this process, the dose of microbubbles and the power of ultrasound are the two key factors that may affect the transgene expression (Figure 3.6). Two microbubble doses were chosen: 3×10^7/mouse (~1.5×10^9/kg) is the lowest dose that may cause significant artery permeability changes according to our pilot experiments, while $1\times$

10^8/mouse (~5×10^9/kg) is close to the highest dose that will not cause significant shadowing effect when doing ultrasound imaging of mouse carotid. Four ultrasound power were selected with the mechanical index (MI) at 0.2, 0.3, 0.4, and 0.5, respectively.

In this experiment, the ultrasound is applied to left common carotid artery (LCA), while the right common carotid artery (RCA) is used as the control. The mice were sacrificed at day 4 to check gene expression in carotid endothelium with qPCR. As shown in Figure 3.7, the gene expression in the LCA is positively related to the MI used for the treatment. At the same MI, increasing MB dose could increase the gene expression. In all the groups, the gene expression in RCA is very low. At the MB dose of 3×10^7/mouse, the gene expression in LCA is nearly linearly related to the MI. This could be explained by increasingly higher permeability with high ultrasound power. At the MB dose of 3×10^7/mouse, the gene expression of MI=0.4 is not significantly different from that of MI=0.5. So based on this results, the MI=0.4 and MB dose at 1×10^8/mouse were selected for further experiments.

Under the optimized condition, the gene expression in the endothelium of LCA is about 24 times higher than that of RCA at the 4^{th} day post ultrasound treatment. In this experiment, the gene expression in both RCA and LCA was determined by qPCR. However, limited by the amount of RNA that can be obtained from one mouse artery, the sample size is very small, which may result in accurate results obtained with qPCR. When the EGFP expression of RCA is determined with qPCR, the Ct value is close to 40, which is usually thought to be a result of nonspecific PCR reactions. Therefore, the EGFP expression in RCA is probably overestimated. It is reasonable to hypothesis that the gene expression the endothelium of LCA might be more than 24 times higher than that of RCA. With this high enhancement in transgene expression, the technology may have a lot of potential applications.

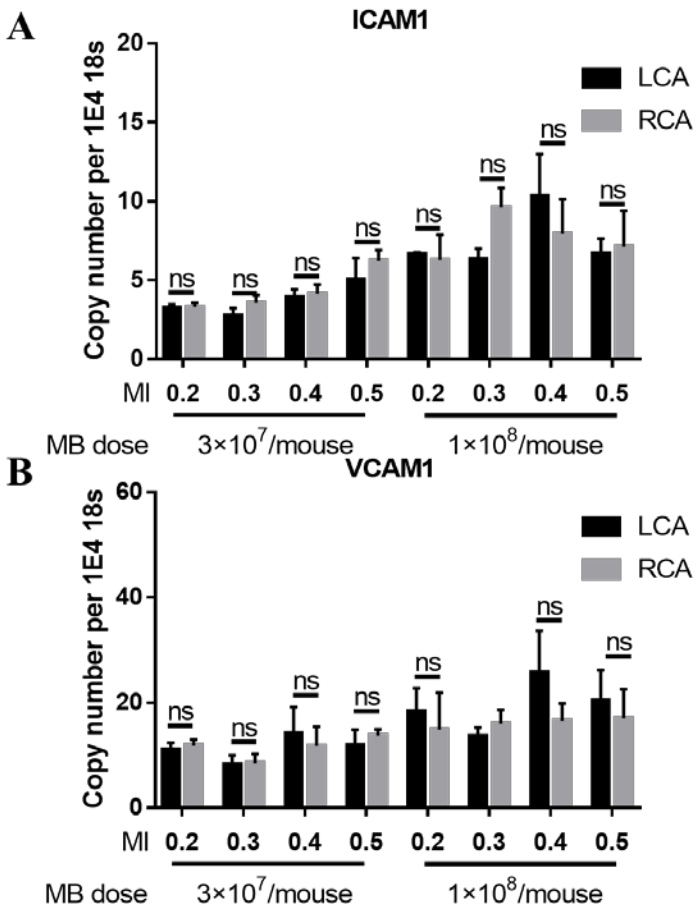

Figure 3.8 ICAM1 and VCAM1 expression in carotid endothelium after different treatments. LCA is treated with ultrasound while RCA is used as control. n = 3 or 4 mice each, data shown as mean ± s.e.m; ns, $p>0.05$ as determined by student's t-test.

The microbubble destruction caused by high-power ultrasound can increase the permeability of the cells in the arterial wall. Although the efficacy of transgene expression is very high, the potential long-term damage to the cells need to be determined. Two key maker genes of inflammation, ICAM1 and VCAM1 were measured with all the samples. As shown in Figure 3.8, no significant difference in VCAM1 and ICAM1 expression were detected in all the groups. Since this result is just from the artery samples obtained from mouse at the 4th day post ultrasound treatment, we cannot rule out the possibility that the ultrasound treatment may cause some inflammation in the first three days. However, we can conclude that the ultrasound treatment does not cause a long-term inflammation in the

arterial endothelial cell. Therefore, this ultrasound-based gene delivery method is a relatively safe technology.

The gene expression in carotid was also characterized with immunofluorescence imaging. As shown in Figure 3.9, the EGFP is significantly highly expressed in the carotid endothelium of ultrasound-treated side, while almost no EGEP expression can be observed in the carotid without ultrasound treatment at the 4th day post ultrasound treatment. This results further confirmed the results of qPCR, since the gene expression in ultrasound-treated area is over 20 times higher than that without ultrasound treatment. In addition, the EGFP expression was predominately in the endothelium, not the media or adventitia layer.

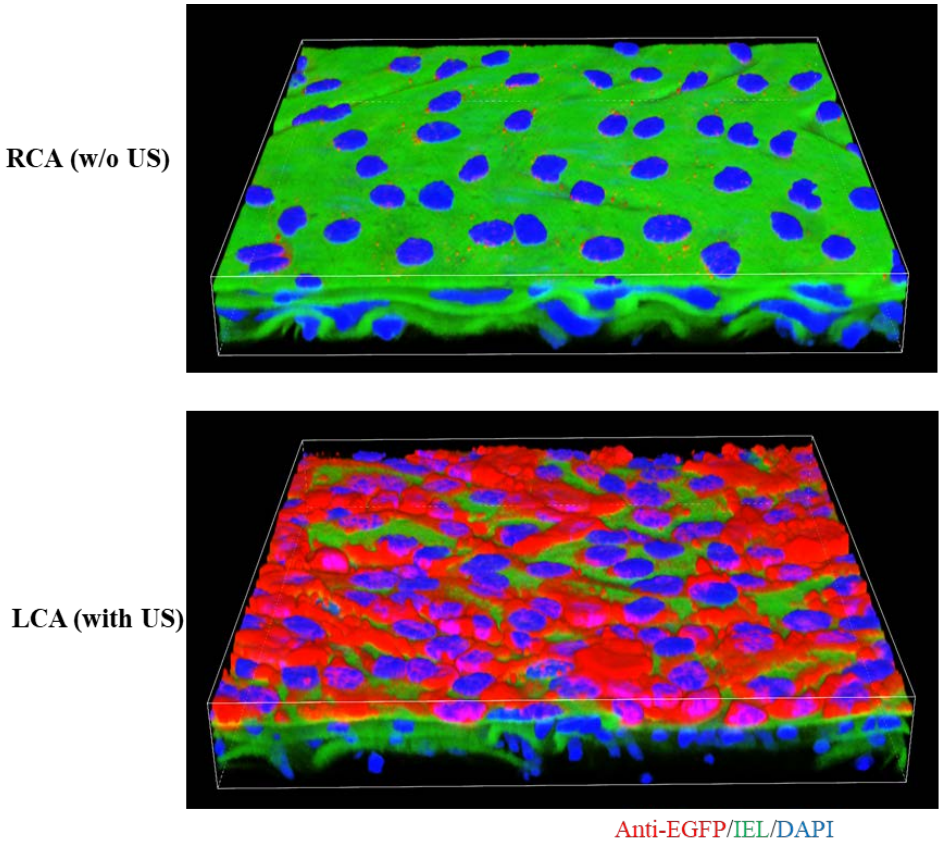

Figure 3.9. Confocal images of *en face* staining of carotid artery. The mouse was sacrificed 4 days post ultrasound treatment. The carotid arteries were dissected and stained with EGFP antibody and analysed by enface confocal imaging. RCA is the control side without ultrasound treatment, while LCA is the ultrasound-treated side. IEL: internal elastic lamina.

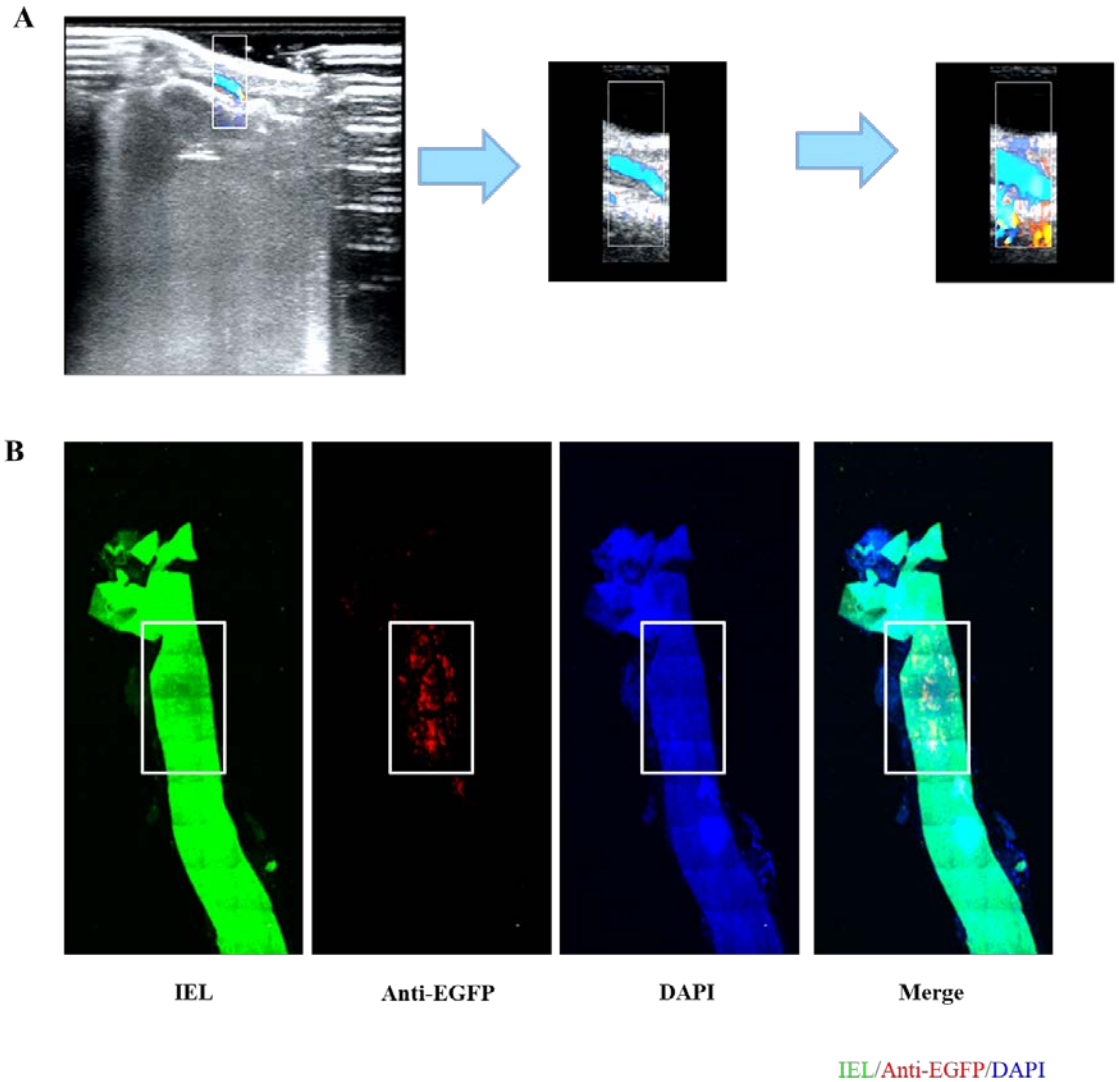

Figure 3.10 The size of ultrasound-treated area can be changed. (A) The color box was changed to the top part of the carotid artery so that ultrasound is only applied to top part. (B) 4 days post ultrasound treatment and AAV9-EGFP injection, the mice were sacrificed, and the carotid arteries were dissected and stained with EGFP antibody for enface confocal imaging. The while box indicate the area with ultrasound treatment.

Since the transgene is only expressed in the ultrasound-treated area, the size of transgene expression is determined by the area of ultrasound treatment. With ultrasound imaging, the size of the color box can be changed from the ultrasound images so that areas with ultrasound treatment can be changed very easily. As shown Figure 3.10, the color box is adjusted to the top half of carotid and then inject the microbubbles to selectively treat the top part of carotid artery. The mouse was then injected with AAV9-EGFP and

sacrificed four days later for en face immunofluorescence imaging. In the fluorescence images, the EGFP expression can only be detected in the top half of carotid, not in the bottom half. This experiment further demonstrated the high specificity of this ultrasound-guided method of gene delivery.

3.3.2 Optimizing the time interval between MB and AAV injection

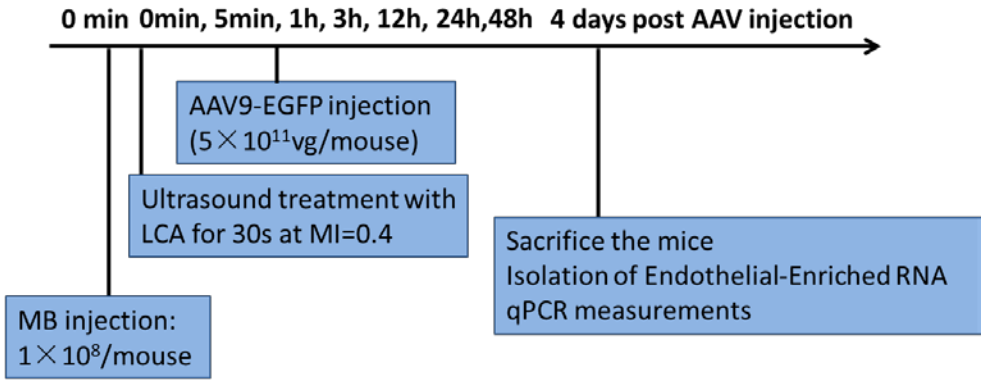

Figure 3.11 Experiment design for optimizing the time interval between MB and AAV injection.

The time interval between MB and AAV injection is another important parameter for the ultrasound imaging-guided gene delivery. Seven different time intervals were selected for this experiment: 0min (AAV co-injected with MB), 5min, 1 h, 3 h, 12 h, 24 h, and 48 h (Figure 3.11). 4 days post the AAV injection, the EGFP expression in the carotid endothelium was determined with qPCR. As shown in Figure 3.12, the gene expression with a time interval between 0min and 3 h didn't shown any statistics difference. This indicates that the permeability changes induced by the sonoporation effect could last for at least 3 h. Gene expression with a time interval at 12 h was significant reduced compared with that at 5 min, indicating that the permeability was mostly recovered at that time.

In the literature, injecting gene vectors together with MB is a very common strategy [80, 82, 110, 111]. There are two proposed mechanisms for enhanced gene expression. On one hand, the enhanced permeability caused by the sonoporation effect between US

and MB can increase the accumulation of gene vectors. On the other hand, the power generated by the destruction of MBs can push the gene vectors into adjacent cells or tissues. Therefore, according to this theory, injecting gene vectors simultaneously with MB will be the optimal choice. However, according to the above experimental results, injecting the gene vectors before or after ultrasound treatment doesn't make significant differences. Therefore, the former mechanism for enhanced gene may make the major contribution. However, injecting gene vectors together with MB is not always that convenient. Once injected, the gene vectors start to be cleared out from blood. If injecting gene vectors is ahead of ultrasound treatment, the time interval between these two steps should be as short as possible. Otherwise, the gene expression will decrease a lot, since the gene vectors can accumulate in the target sites only if the permeability has changed. Therefore, for the sake of experimental convenience, injecting gene vectors post ultrasound treatments is selected for the following experiments.

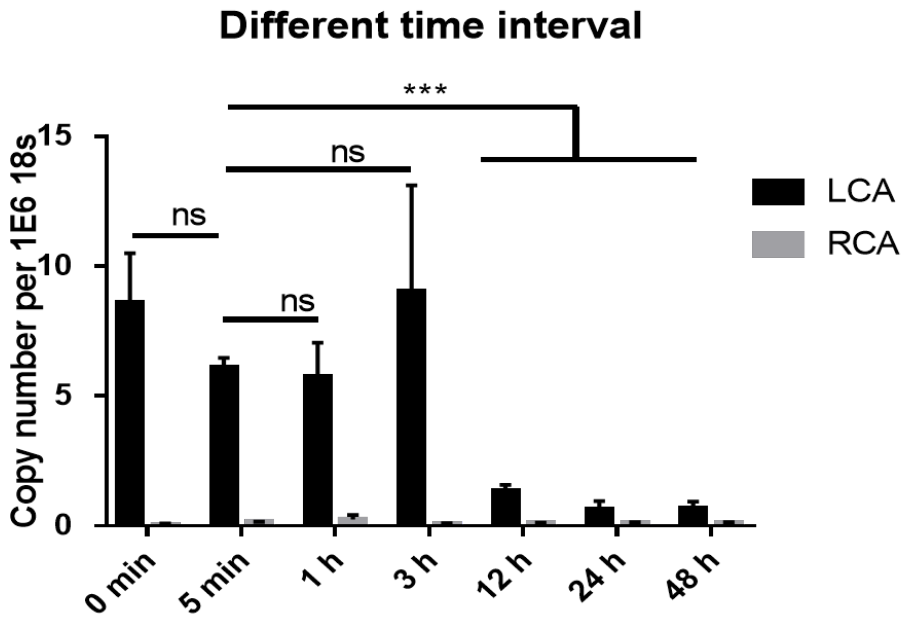

Figure 3.12 EGFP expression in carotid endothelium after ultrasound treatments at different time intervals between MB and AAV injection. LCA is treated with ultrasound while RCA is used as control. n = 3 or 4 mice each, data shown as mean ± s.e.m. ns $p > 0.05$, ***$p < 0.001$ as determined by Student's t-test.

3.3.3 Persistence of the gene expression

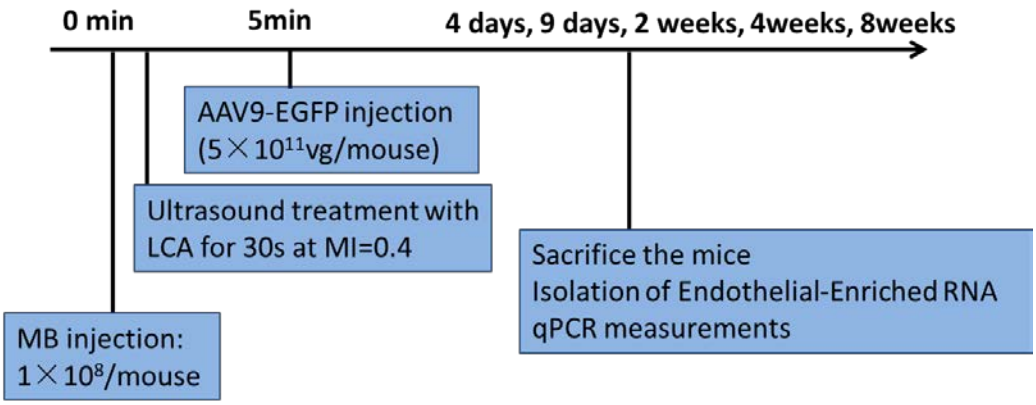

Figure 3.13 Experiment design for evaluation of the persistence of gene expression

Compared with other therapies based on chemical drugs, proteins, RNA and so on, one of the biggest advantages of gene therapy is the durable effect with just one injection. The persistence of the gene expression induced by the ultrasound-based method was evaluated (Figure 3.13). After the ultrasound treatment and AAV9-EGFP injection, the mice were sacrificed at different time points (4 days, 9 days, 2 weeks, 4 weeks, and 8 weeks). The gene expression in both endothelial cells (ECs) and media and adventitia (M+A) layer was determined.

As shown in Figure 3.14, the gene is highly expressed in ECs from 4 days to 8 weeks. The highest gene expression is found at the 4th week. The gene in the ultrasound-treated side is significantly higher than the untreated side. Interestingly, the gene is also expressed in M+A layer. However, the expression in M+A is not synchronized with ECs. The earliest time that gene expression in M+A can be detected is at the 9th day, at least 5 days later than ECs. This is probably related to different rates of capsid uncoating and second strand DNA synthesis of AAV in different cell types[112-115].

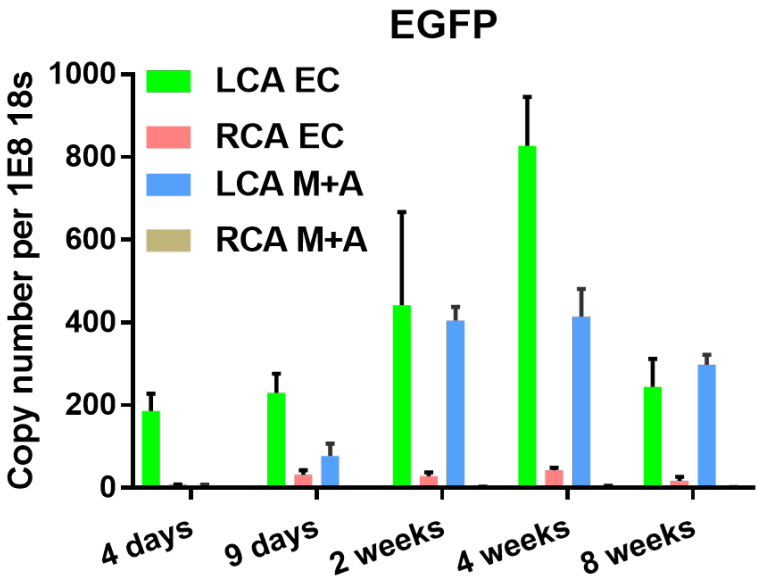

Figure 3.14 Evaluation of transgene expression in carotid artery at different time points. LCA was treated with ultrasound while RCA is used as control. n = 3 or 4 mice each, data shown as mean ± s.e.m. EC, endothelial cells; M + A, media and adventitia.

Another phenomenon is that the response of M+A to ultrasound treatment is higher than that of endothelial cells. At the 4th week, the gene expression of LCA EC is ~19 times higher than that of RCA EC, while the gene expression of LCA M+A is ~86 times higher than that of RCA M+A. Without ultrasound treatment, gene is also expressed in RCA EC at a level significant higher than that in RCA M+A. One possible explanation is that AAV have a higher opportunity to contact with AAV. In normal arteries, EC layer is the layer that directly contact with the blood, while M+A layer is not easy to contact with materials in blood if the EC layer is intact. However, when artery is treated with ultrasound, both EC layer and M+A layer have similar opportunities to contact with AAV.

One of most important aspects of AAV as a gene vector is its ability to induce prolonged gene expression without genome integration. Several studies have shown that gene expression by AAV vector could last for several years in human and non-human primates[116-118]. The AAV genomes are thought to be persistent in host cells as non-integrated non-replicating episomes. The persistence of AAV relies on the rate of cell

turnover and the number of AAV genomes in the cell. In our study, the gene expression in carotid artery could last for over 8 weeks. At the 8th week, the gene expression still remains very high. The long persistence of gene expression makes this ultrasound-guided method a very useful tool for vascular researches and a promising technique for clinical translation.

3.3.4 Evaluate the permeability changes of carotid artery with Evans blue

Evans blue is an azo dye with a very high affinity for serum albumin. Evans blue is often used to evaluate the permeability of BBB to macromolecules. After intravenous injection, almost all the dyes are bound to albumin. Since albumin cannot cross the barrier in normal condition, normal tissue remains unstained. However, when the BBB is damages, albumin-bound Evans blue can enter the tissue. In our previous research, the Evans blue can also be used to assess the permeability of carotid artery based on a similar rationale [18].

In this experiment, the permeability changes caused by ultrasound treatment in carotid artery was also evaluated with Evans blue. As shown in Figure 3.15, Evans blue staining immediately post ultrasound treatment in LCA show dark blue staining in LCA while RCA remains unstained. This indicates that ultrasound treatment could significantly increase the permeability of artery wall. In addition, Evans blue staining at 24 h post ultrasound treatment shows that both LCA and RCA were unstained, indicating the recovery of permeability. This result is in accordance with the previous results that the gene expression reduced significantly when time interval between AAV and MB injection is 24 h. These results further confirmed our hypothesis that ultrasound treatment could increase gene expression by temporally increasing the permeability of carotid artery.

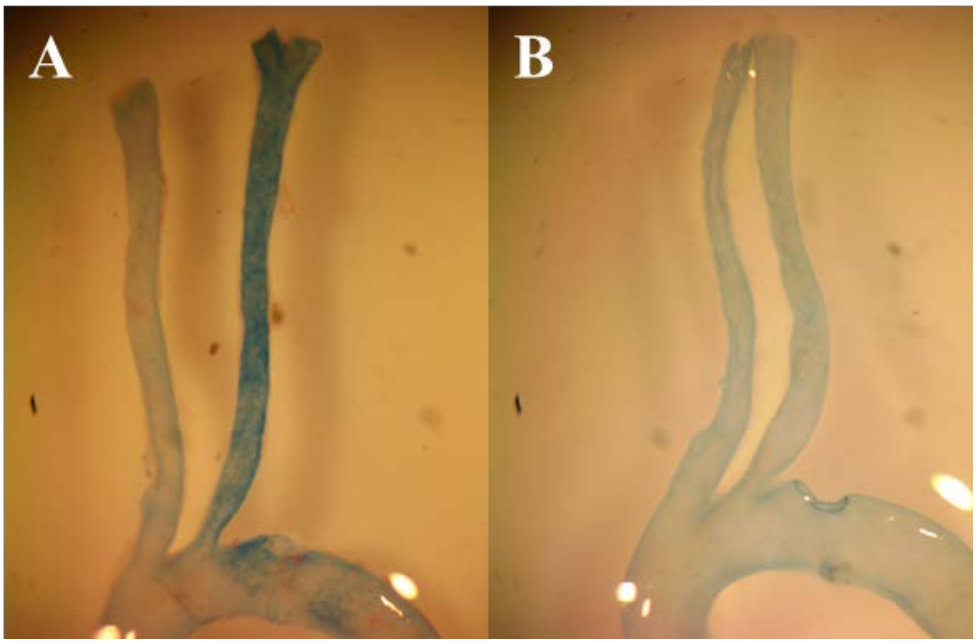

Figure 3.15 Permeability changes of carotid artery determined by Evans blue. Ultrasound treatment was applied to LCA (MI = 0.4, 1×10^8 MB/mouse). Evans blue was injected intravenously immediately (A) or 24 h (B) post ultrasound treatment. The mice were sacrificed 30 min post Evans blue injection and artery trees were dissected out for bright field imaging.

3.3.5 Fluorescence tracking of AAV in carotid artery

To further evaluate the behaviour of AAV in carotid artery after system injection, AAV9 was labelled with a fluorescent dye Sulf-Cy3-NHS to get AAV-Cy3 (Figure 3.5). It has been demonstrated that the fluorescence labelling doesn't affect both morphology and functionality of AAV[109]. After MB injection, the LCA was treated with ultrasound and then AAV-Cy3 was injected intravenously. The mice were sacrifice 1 h or 3 h later and the carotid artery was then dissected for *en face* confocal imaging (Figure 3.16-18).

At 1 h, the signal of AAV-Cy3 in RCA was predominately detected in the intima layer in the form of big bright spots, while the signal in LCA was uniformly dispersed in both endothelium and media layer. At 3h, the signal in LCA remains very high, while no

significant AAV-Cy3 signal could be detected in RCA. The signal in LCA is about 37 times higher than that in RCA at 3 h.

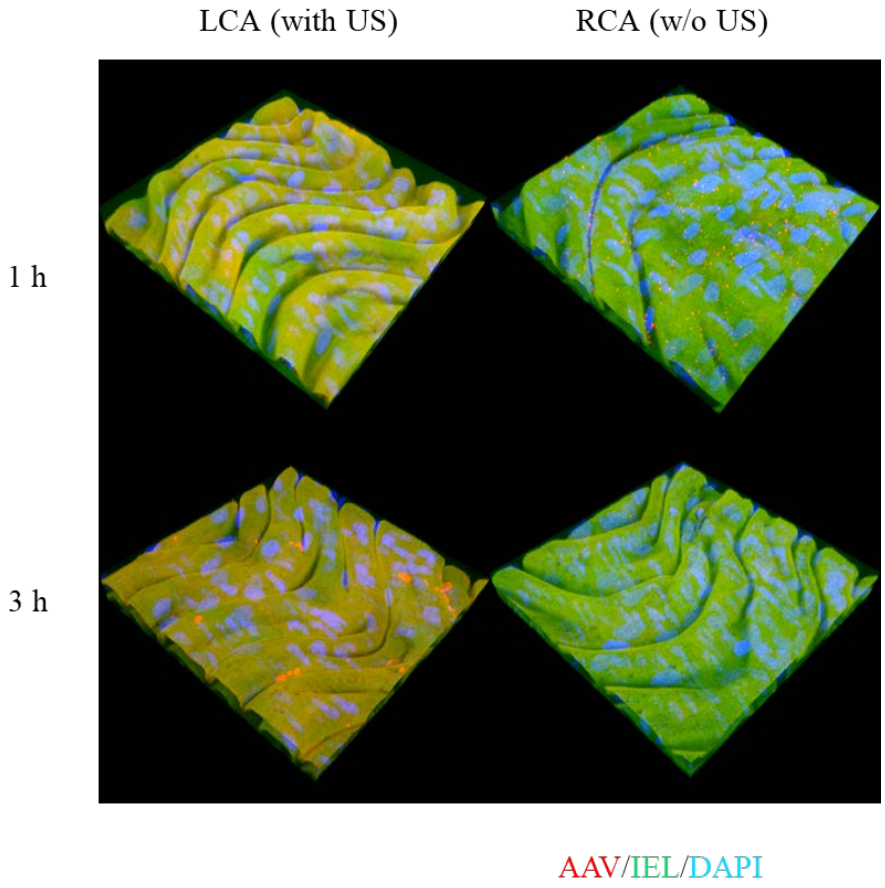

Figure 3.16 Confocal images of mouse carotid artery after ultrasound treatment and AAV-Cy3 injection. After MB injection, LCA was treat with ultrasound while RCA was set as the internal control. Following ultrasound treatment, mice were intravenously injected with AAV-Cy3 and sacrificed at 1 h and 3h later, respectively.

These results provide a robust evidence to explain why gene expression by AAV gene vector is highly enhanced by ultrasound treatment. Without ultrasound treatment, most AAVs are initially bind to the endothelial cells as big aggregates. But this kind of binding is not stable and most of the bound AAV are flushed away by blood flow. Since the endothelium is intact, AAV cannot penetrate the intima layer to enter into media layer. This explained why genes encoded by AAV is slightly expressed in endothelial cells but not in media and adventitia layer, when ultrasound is not applied.

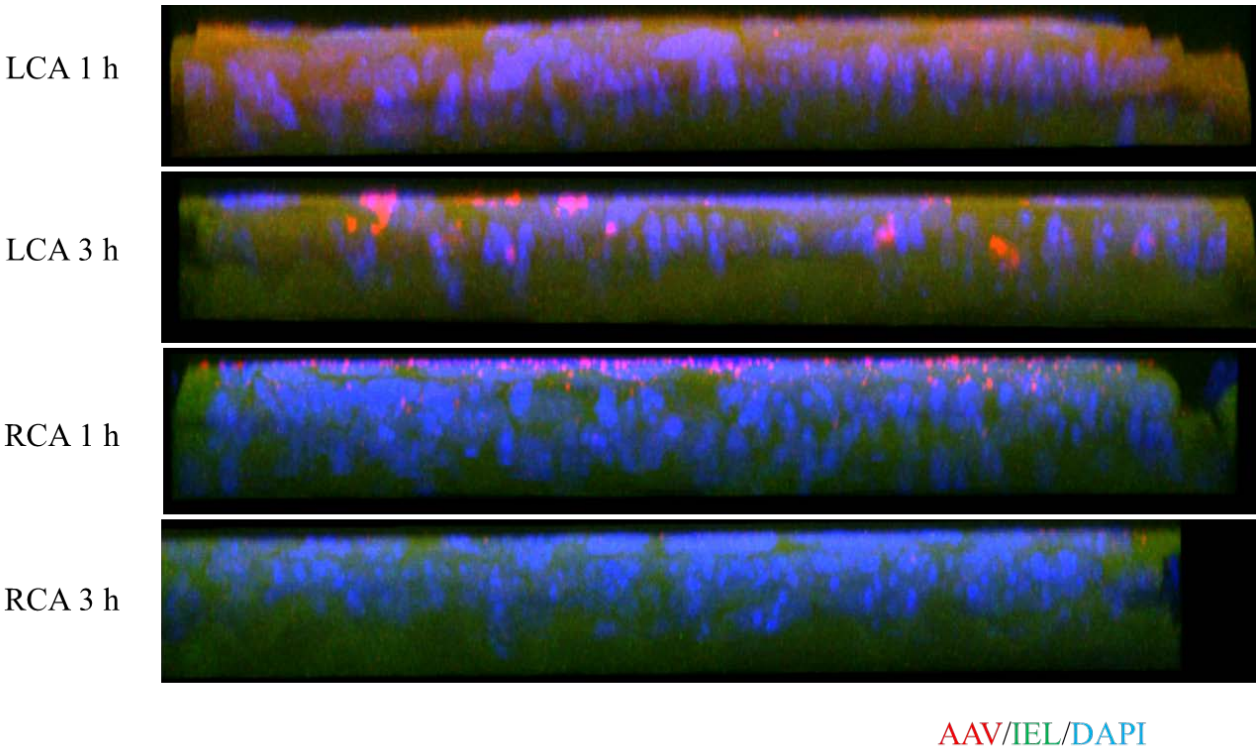

Figure 3.17 Confocal images of carotid artery show the penetration of AAV-Cy3 in carotid artery.

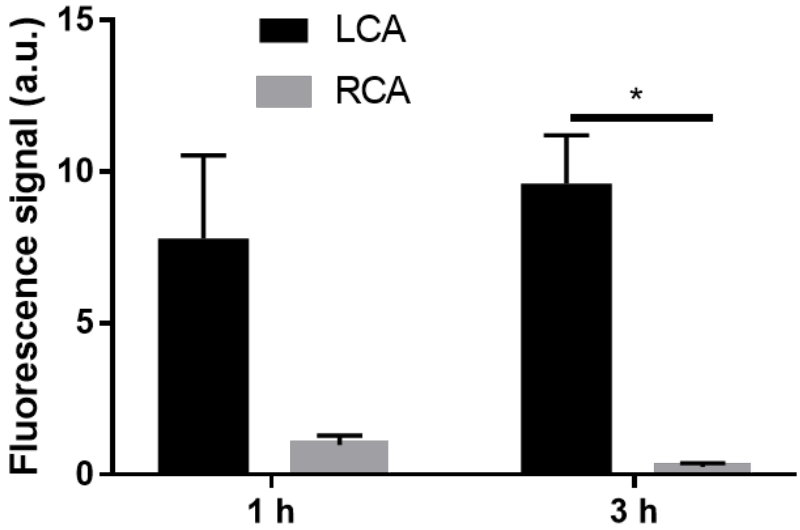

Figure 3.18 Quantification of AAV-Cy3 signals in carotid artery. Data shown as mean ± s.e.m. *p < 0.05 as determined by Student's t-test.

However, when ultrasound is applied, the permeability of artery is increased both in intima and media and adventitia layer. Therefore, AAV can be well dispersed in the intima and media layer. Since the AAV goes deep in the artery, the retained AAV is not easy to be flushed away by blood flow, providing enough time for the AAV to be internalized by cells. Therefore, gene expression in the ultrasound treated area is much higher than that in the untreated area.

3.3.6 Ultrasound-guided gene delivery to abdominal aorta

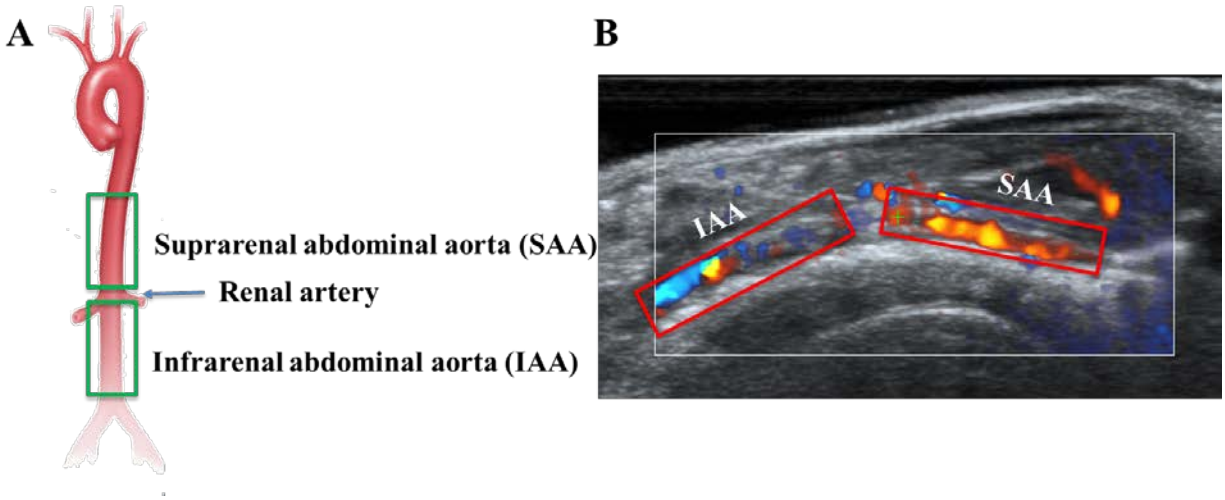

Figure 3.19 Color Doppler ultrasound imaging of abdominal aorta. (A) Paradigm illustrates the abdominal aorta separated by renal artery intro two part, suprarenal abdominal aorta (SAA) and infrarenal abdominal aorta (IAA). (B) Color Doppler ultrasound imaging shows the position of SAA and IAA. The color of Doppler imaging indicates the directions of blood flow.

Abdominal aorta is the largest artery in the abdominal cavity. As part of aorta, it supplies blood to most of the organs in abdomen. With several branch points, abdominal aorta is one of the most commons sites for developing atherosclerotic plaque [119-121]. Another common disease in abdominal aorta is abdominal aortic aneurysm (AAA), which is characterized with localized enlargement of abdominal aorta[122-124]. When the diameter of aorta is larger than 5.5 cm, the only effective treatment is surgery, which is associated with a risk of complication[77, 125]. There are currently no non-invasive treatment options

available. Therefore, targeted gene delivery to abdominal aorta is of great significance for non-invasive treatment of both atherosclerosis and AAA.

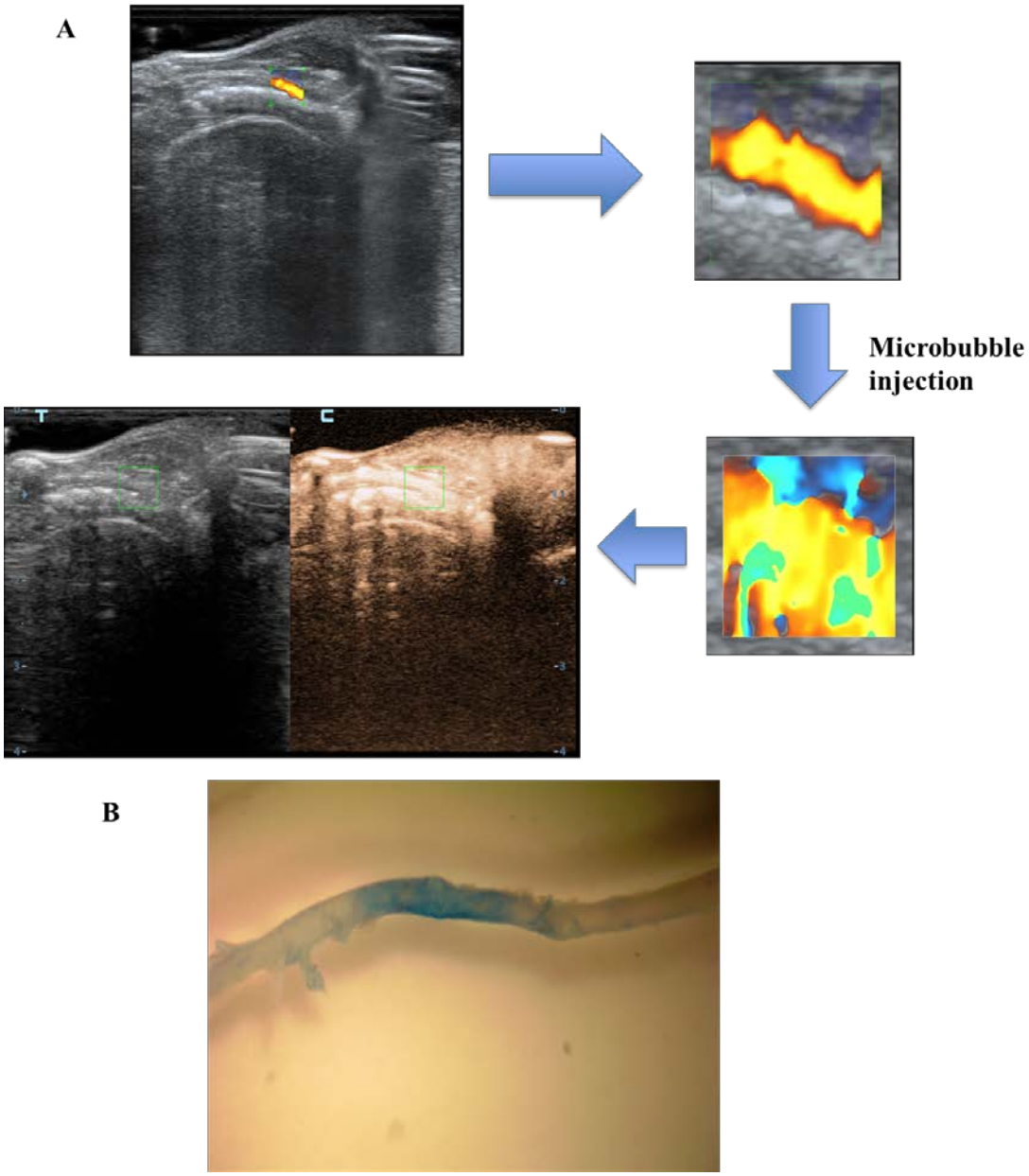

Figure 3.20 Ultrasound treatment to abdominal aorta. (A) Under the color Doppler ultrasound imaging, the structure of the mouse abdominal aorta can be visualized and the region of interest can be selected. Then zoom the area of interest so that ultrasound is only applied to the selected area. After the microbubble injection, a "blooming" effect can be seen in the color Doppler imaging, indicating the destruction of microbubbles. Finally, the ultrasound imaging can be switched to the contrast enhanced mode to confirm position of the area of interest with very high image quality. (B) After ultrasound treatment, the mouse

was injected with Evans blue and sacrificed 30 min later. The blue color in the abdominal aorta indicates the permeability changes of abdominal aorta.

Under colour Doppler imaging, the whole abdominal aorta of mice can be clearly visualized (Figure 3.19). The abdominal can be divided into two part: suprarenal abdominal aorta (SAA) and infrarenal abdominal aorta (IAA). The diameter of SAA is larger than IAA and IAA is located close to inferior vena cava. Therefore, SAA and IAA shows distinct characters in color Doppler images.

Firstly, we evaluated if the ultrasound treatment could induce the permeability changes of abdominal aorta (Figure 3.20). Under the color Doppler ultrasound imaging, a small area in the SAA was selected. After zooming to the selected area, microbubbles were injected and microbubbles were destructed in this area. After ultrasound treatment, the Evans blue staining was applied. As we can see, a small area in the abdominal aorta is stained as blue while other areas are not stained. The size and position of the stained area is same as what we can see from the ultrasound imaging. This demonstrated that ultrasound treatment can increase permeability of the abdominal aorta.

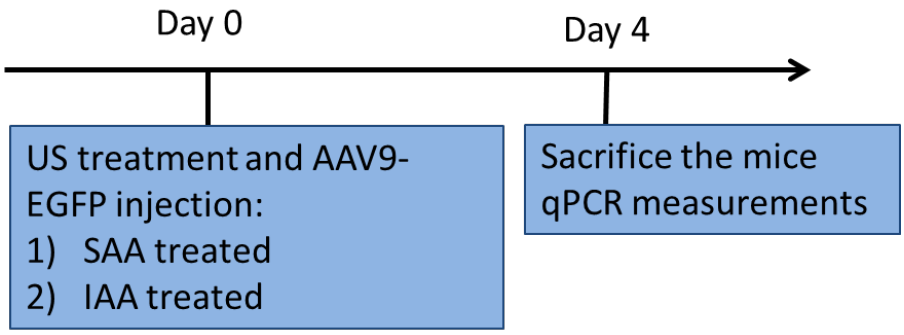

Figure 3.21 Experimental design for targeted gene delivery to abdominal aorta.

The feasibility of targeted gene delivery with the ultrasound-guided method was then evaluated. The mice were divided into two groups (Figure 3.21). After microbubbles injection, SAA or IAA was treated with ultrasound imaging. The mice were then injected with AAV9 encoding EGFP and sacrificed 4 days later to determine gene expression with qPCR. As shown in Figure 3.22, when SAA was treated with ultrasound, the gene

expression in SAA was very high while gene expression in IAA was very low. Similarly, the gene was only highly expressed in IAA when IAA was treated with ultrasound. This result demonstrated the feasibility of using ultrasound-guided method for targeted gene delivery to abdominal aorta.

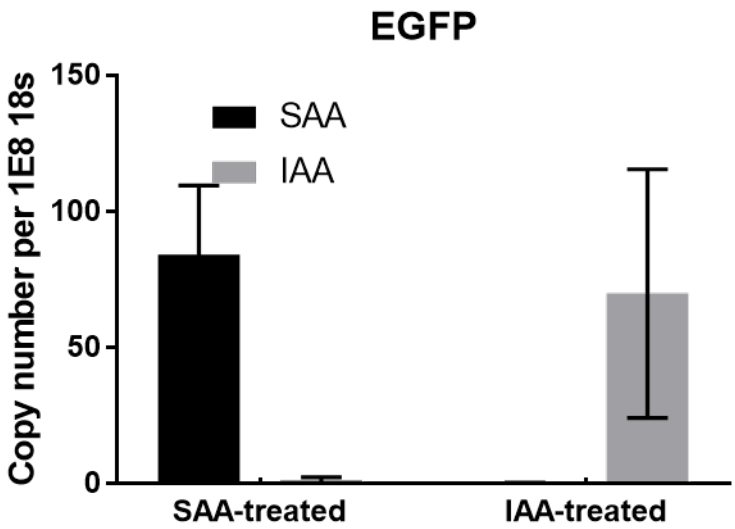

Figure 3.22 Expression of EGFP in abdominal aorta as determined with qPCR. Data shown as mean ± s.e.m, n=4.

3.3.7 Ultrasound-guided gene delivery to femoral artery

Femoral artery is a large artery in the thigh and controls the blood supply to the leg and thigh. The femoral artery gives off several branches, making its susceptible to atherosclerosis. When femoral artery is narrowed or blocked by atherosclerosis, people will get peripheral artery disease (PAD). The symptoms of PAD include leg pain when walking, skin ulcers, bluish skin, and cold skin. The PAD may also cause tissue death which may require amputation, ischemic heart disease, heart attack, or stroke.

The femoral artery of mouse is a very small artery and hence very hard to be found under the colour Doppler mode ultrasound. Therefore, we modified the protocol of ultrasound treatment. Firstly the microbubbles were injected and then the femoral

bifurcation can be found very easily under the contrast-enhanced mode ultrasound imaging (Figure 3.23). The area of interest can be selected from the ultrasound imaging. Then zoom to the selected area, switch to colour Doppler mode, and treat the selected area for 30s. The permeability of the artery was evaluated with Evans blue staining (Figure 3.24). Without ultrasound treatment, the femoral bifurcation is not stained. However, after treating the femoral bifurcation with ultrasound, the artery is stained as blue. This indicates that the ultrasound treatment can increase the permeability of femoral artery.

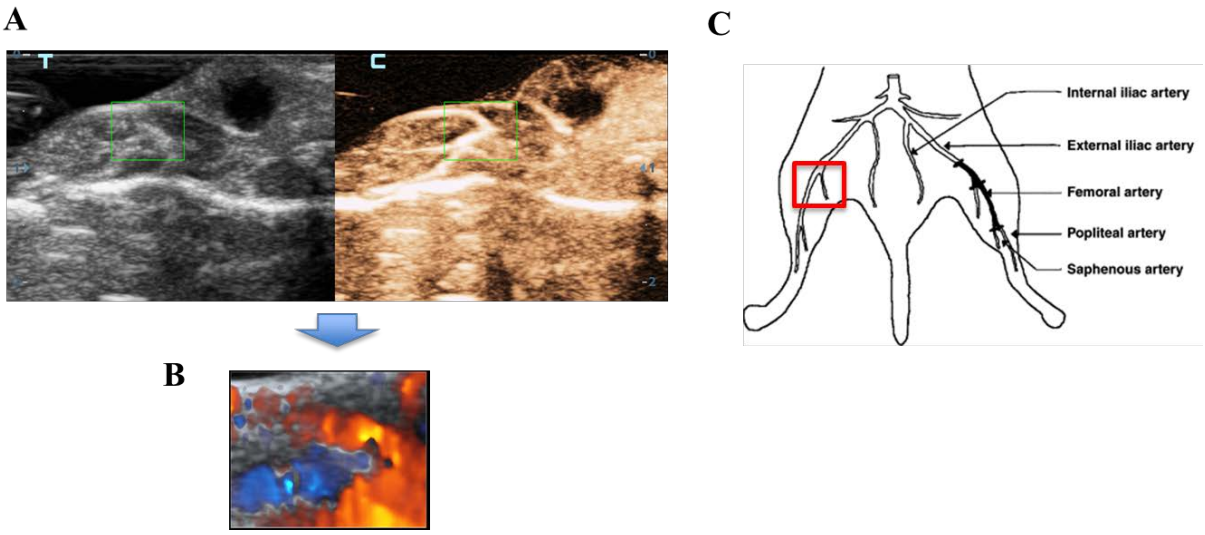

Figure 3.23 Ultrasound imaging of femoral artery. (A) Ultrasound images of the thigh of a mouse under the contrast-enhanced mode. The green box indicates the position of femoral bifurcation. (B) Color Doppler imaging of the femoral bifurcation during ultrasound treatment. (C) Paradigm illustrates the anatomical structure of the artery in the mouse leg. The red box indicates the position of femoral bifurcation.

The feasibility of targeted gene delivery to femoral artery was further evaluated. The right femoral artery (RFA) was treated with ultrasound, while the contralateral left femoral artery (LFA) was the control. Following the ultrasound treatment, AAV9-EGFP was injected intravenously and the mice were sacrificed 4 days later for qPCR measurements. As shown in Figure 3.25, the EGFP expressions in LFA is very low, while the gene expression in RFA is about 59 times higher than that in LFA. This result

demonstrates that this ultrasound-guided method can be used for targeted gene delivery to femoral artery.

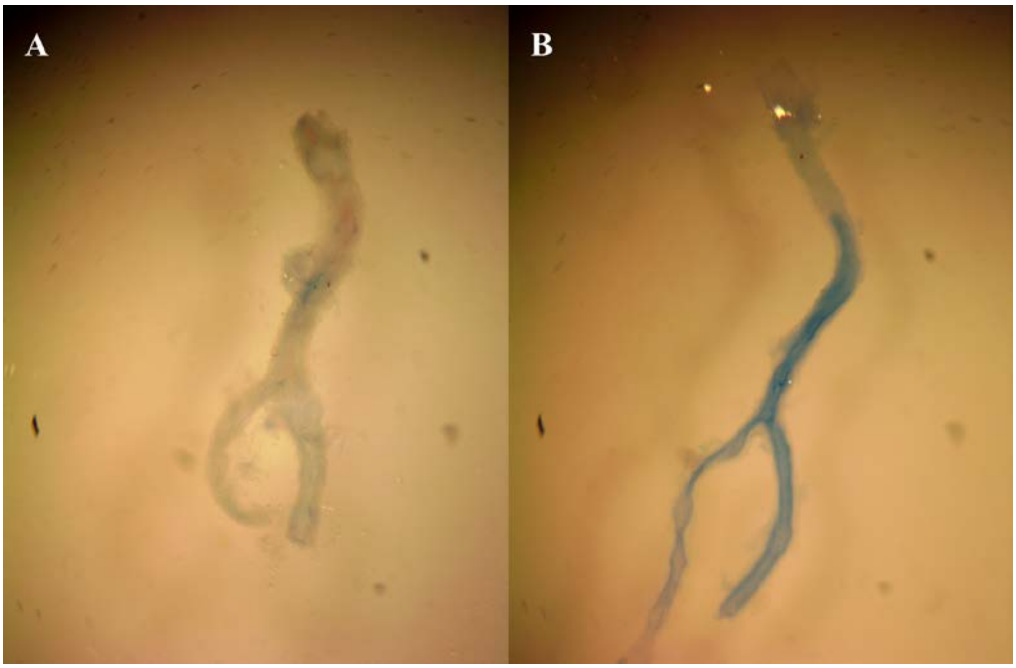

Figure 3.24 Permeability changes of femoral artery as determined by Evans blue staining. (A) The femoral artery is not treated with ultrasound. (B) Femoral artery is treated with ultrasound.

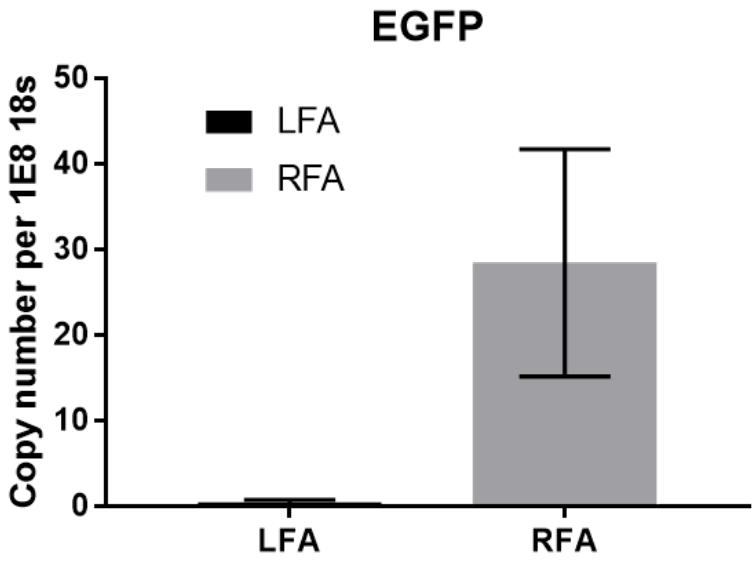

Figure 3.25 EGFP expression in femoral artery as determined with qPCR. EGFP expression in the femoral artery was checked 4 days post the ultrasound treatment and

AAV9-EGFP injection. The right femoral artery (RFA) is treated with ultrasound, while left femoral artery (LFA) is not treated. Data shown as mean ± s.e.m, n=4.

3.4 Summary

In this chapter, an ultrasound imaging-guided method for gene delivery to mouse was established. This method is based on the hypothesis that AAV can preferentially accumulate in the artery that are permeabilized by ultrasound in combination with microbubbles. Firstly, the position of the carotid artery can be localized with color Doppler ultrasound imaging and the area of interest can be selected by changing the sized and position of the color box in the ultrasound images. Then the ultrasound imaging is zoomed to the selected area so that ultrasound is only applied in the selected areas. After that, the microbubbles will be injected intravenously and the ultrasound used for ultrasound imaging can destroy microbubbles, resulting in the increased permeability of the artery. Following the ultrasound treatment, the AAV gene vector encoding genes of interest will be injected and the gene will be preferentially highly expressed in the ultrasound-treated area.

The power of ultrasound and dose of microbubbles were firstly optimized. With qPCR measurements, the gene expression in endothelial cells was found to be increased with the increasing of ultrasound power and microbubble dose. In addition, two important marker genes, ICAM1 and VCAM1, were also determined and no significant difference was detected, indicating the safety of the ultrasound treatment. Based on these results, the MI at 0.4 and microbubble dose at 1×10^8/mouse (~5×10^9/kg) were selected for further experiments.

Then, the time interval between microbubble and AAV injection was optimized. It was found that there was no significant difference in transgene expression if the time interval is shorter than 3 h, indicating that the permeability of artery could last for at least

3 h. The gene expression reduced significantly when the time interval was longer than 12 h, indicating that the permeability of artery was mostly recovered post 12 h.

The persistence of the gene expression in the carotid artery was also evaluated. The gene expression in arterial endothelium could last for at least 8 weeks (longer time is not determined). Interestingly, the gene was also expressed in media and adventitia layer but started at least 5 days later than endothelium. At the 4^{th} week, the gene expression of endothelium in the ultrasound-treated side was ~19 times higher than that in untreated side, while the gene expression of media and adventitia layer was increased by ~86 times after ultrasound treatment.

A mechanism study was conducted to determine why the ultrasound treatment could highly increase transgene expression in the carotid artery of mouse. With Evans blue staining, the ultrasound treatment was found to temporally increase the permeability of artery. By labelling AAV with fluorescent dyes, the distribution of AAV in artery wall was determined. Without ultrasound treatment, AAV could only temporally bind to arterial endothelium in big aggregates and was flushed away very soon. However, when the artery is permeabilized by ultrasound in combination with microbubbles, large amounts of AAV could be well dispersed in both intima and media layer and persist for a longer time. These results explained the reason why ultrasound in combination with microbubbles could highly increase transgene expression in arteries by AAV.

Finally the ultrasound-guided method was expanded for targeted gene delivery to arteries beyond carotid artery. This method was firstly applied for targeted gene delivery to abdominal aorta. Without ultrasound treatment, AAV alone cannot induce significant transgene expression in abdominal aorta. However, when ultrasound was applied to suprarenal abdominal aorta or infrarenal abdominal aorta, highly enhanced transgene expression could be detected in the ultrasound-treated area. As is the case for femoral artery.

Ultrasound treatment induced ~59 times higher transgene expression in femoral artery as compared with the untreated side. These results demonstrated the potential applications of this technology for diseases in abdominal aorta and femoral artery, such as AAA and PAD.

CHAPTER 4. TARGETED DELIVERY OF KLK10 TO INHIBIT ATHERASCLEROSIS

4.1 Introduction

In the previous chapter, the ultrasound-guided method was demonstrated to be a very efficient technology for transgene expression in arterial endothelium. In this chapter, this method will be used for targeted transgene expression of KLK10, a novel atheraprotective gene identified recently in our lab, to determine if this method can be used to inhibit atherosclerosis in the partial carotid ligation (PCL) model.

4.2 Methods

4.2.1 Package of KLK10-encoding AAV

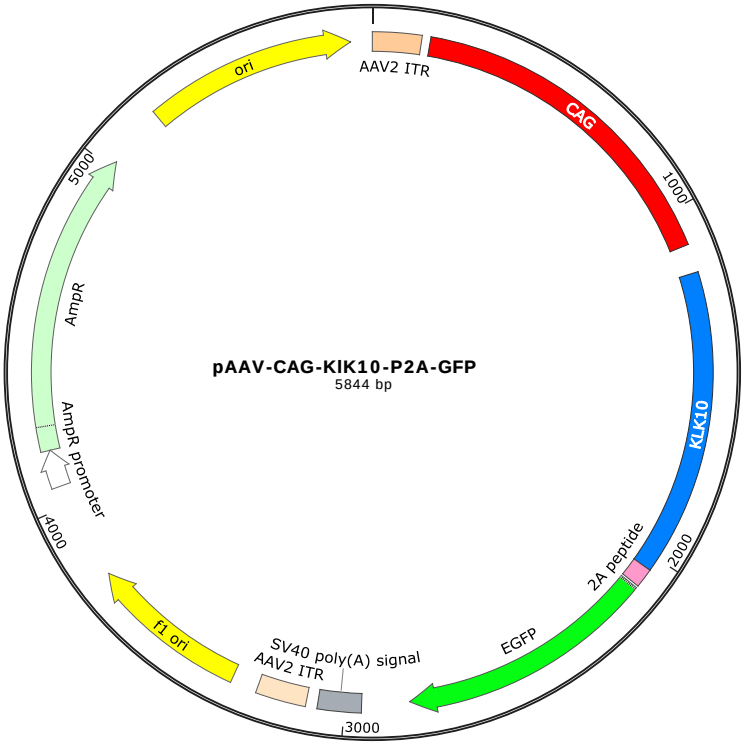

Figure 4.1 Map of plasmid encoding KLK10 for AAV packaging.

The KLK10-encoding plasmid was constructed by GENEWIZ (Suzhou, China) and confirmed with DNA sequencing (Figure 4.1). The encoding sequence is composed of a CAG promoter, KLK10 cDNA sequence, and EGFP sequence. The KLK10 is linked with

EGFP through a P2A peptide, which is a “self-cleaving” peptide, so KLK10 and EGFP can be separated after translation and their function are not affected. The plasmid was packed into AAV by Vigene Biosciences (Jinan, China).

4.2.2 Mouse partial carotid ligation surgery

All animal experiments were approved by the Animal Care and Use Committee at Peking University. The partial carotid ligation surgery was conducted as previously reported[17]. Male C57BL/6 and ApoE$^{-/-}$ mice (Charles River Laboratories, Beijing) were allowed ad libitum to standard chow diet and water until surgery at 8–9 weeks of age. Mice were anaesthetized with 3.5% isoflurane initially and then ~2% during the entire procedure. Before surgery, analgesic carprofen (5mg/kg) was administrated subcutaneously. The LCA bifurcation was exposed by blunt dissection and three caudal branches of LCA (left external carotid, internal carotid and occipital arteries) were ligated with 6-0 silk sutures while leaving the superior thyroid artery intact. For atherosclerotic studies, the ApoE$^{-/-}$ mice were fed with a Paigen’s high fat diet (Research diets) following the surgery until killed. C57BL/6 mice were continued with a chow diet.

4.2.3 En face staining of caratid artery

The carotid arteries are excised, fixed in 4% paraformaldehyde, penetrated with 0.025% Triton X-100 for 10 min, blocked with 10% goat serum for 1 h at room temperature, and incubated with primary anti-VCAM1 (Abcam, ab134047) or anti-KLK10 (Boster, BA3803-2) antibodies overnight at 4 ℃. To visualize primary antibodies, Alexa Fluor ® 594-conjugated goat anti-rabbit antibody (Abcam ab150080) was used for 1 h at room temperature. Nuclei were counterstained with DAPI. Samples were imaged using a Nikon confocal microscope.

4.2.4 Serum lipid analysis

Serum lipid analysis was performed by the department of laboratory animal science in Peking University Health Science Center for total cholesterol, triglycerides, HDL and LDL.

4.2.5 Plaque lesion analysis

Carotid arteries were isolated *en bloc* from ligated ApoE$^{-/-}$ mice fed with a high fat diet for 3 weeks. The artery trees were photographed using a dissection microscope and the opaque area covered by plaque and total area of LCA were quantified using NIH ImageJ software

4.2.6 Elisa

The serum KLK10 level was determined with a mouse KLK10 Elisa kit from Mybiosource following the manufacturer's instructions.

4.2.7 Immunohistochemistry

Arteries were embedded in optimal cutting temperature compound (Tissue-Tek), frozen on dry ice and stored at -80 ℃ until used. To visualize atherosclerosis development, Oil-red-O staining was carried out. Frozen sections were fixed in formalin for 10 min, rinsed with water and 60% propylene glycol, and then stained with Oil Red O staining solution (Solarbio). Slides were then differentiated in 60% propylene glycol, rinsed with distilled water, and counterstaining was done using Mayer's haematoxylin (Beijing Leagene Biotechnology Co., Ltd.) for 5 min.

For VCAM1 and CD45 staining, sections were fixed in a 1:1 mixture of methanol/acetone for 10 min at room temperature (RT) and then blocked using 10% (v/v) goat serum in TBS (2 h, at RT). Immunohistochemical staining was conducted anti-VCAM1 (Abcam ab134047) or anti-CD45-biotin (eBioscience) overnight at 4 ℃. Secondary staining for VCAM1 was performed using Alexa Fluor ® 594-conjugated goat

anti-rabbit antibody (Abcam ab150080) while Alexa Fluor ® 594-conjugated streptavidin (Bioss) was used for CD45. Nuclei were counterstained with DAPI. Samples were imaged using an Axio Scan.Z1 Slide Scanner (Zeiss).

4.3 Results and Discussion

4.3.1 Dose-dependent effect of AAV9-KLK10

To evaluate if the ultrasound-guided method can be used for targeted transgene expression, KLK10-encoding AAV9 was constructed. The coding sequence contains a CAG promoter, cDNA sequence of KLK10, and EGFP sequence. Between KLK10 and EGFP, a P2A peptide was added to make KLK10 and EGFP translated simultaneously. The P2A peptide is a "self-cleaving" peptide, which undergoes self-cleavage to generate mature viral proteins by a translational effect that is known as "stop-go" or "stop-carry"[106-108]. The cleavage site is located between the last glycine of its C-terminal and the first praline of the downstream protein. The incorporation of P2A makes the genes co-expressed while their function are not affected. Therefore, the level of EGFP expression should reflect how much KLK10 is the result of exogenous expression.

The expression of KLK10 is significantly reduced in the arterial endothelium that is affected by d-flow. In the PCL model, KLK10 expression of LCA is much reduced as compared with RCA. Therefore, this model was used to optimize the dose of AAV9-KLK10. Following microbubbles injection, the ultrasound was applied to LCA and then AAV9-KLK10 was injected intravenously at three different doses. Two days post the treatment, the PCL surgery was conducted. 3 days after the surgery, the mice were

sacrificed and the carotid endothelial cells were isolated for qPCR measurements (Figure 4.2).

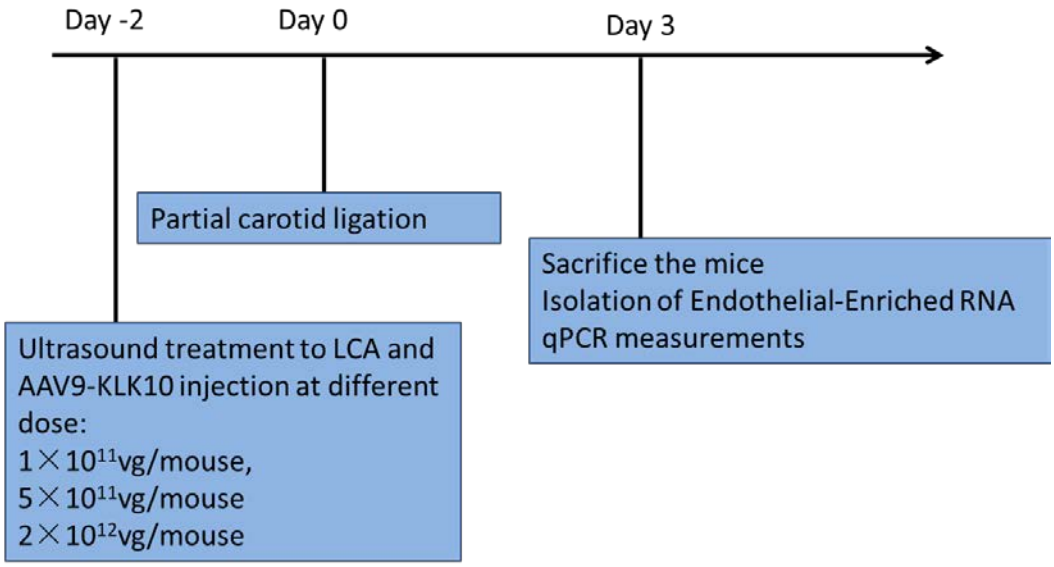

Figure 4.2. Experimental design for optimizing dose of AAV9-KLK10 in the PCL model.

As shown in Figure 4.3, the EGFP expression in LCA is dependent on the dose of AAV9-KLK10 while the expression in RCA remains very low, demonstrating that targeting ability of this ultrasound-guided method. Since EGFP is co-expressed with KLK10, a similar trend is also found in KLK10 expression of LCA. With partial carotid ligation surgery, the KLK10 expression in LCA is much reduced as compared with that in RCA. With a dose of AAV9-KLKL10 at 5×10^{11} vg/mouse, the KLK10 expression in LCA is recovered and not significantly different from that in RCA. Therefore, 5×10^{11} vg/mouse (~2.5×10^{13} vg/kg) is selected for further experiments.

Interestingly, with the increasing of dose of AAV9-KLK10, although the expression of EGFP in RCA is slightly increased, the KLK10 expression in RCA is reduced. This indicated that AAV9-KLK10 at high dose might have some side effects. Although AAV alone without ultrasound can induce a weak transgene expression in the endothelial cells as shown in the previous chapter, such a weak transgene expression in normal dose

cannot be used for therapeutic applications and high dose will induce adverse effects. This highlights the advantage of the ultrasound-guided method, inducing very high KLK10 expression with a relatively low dose of AAV9-KLK10.

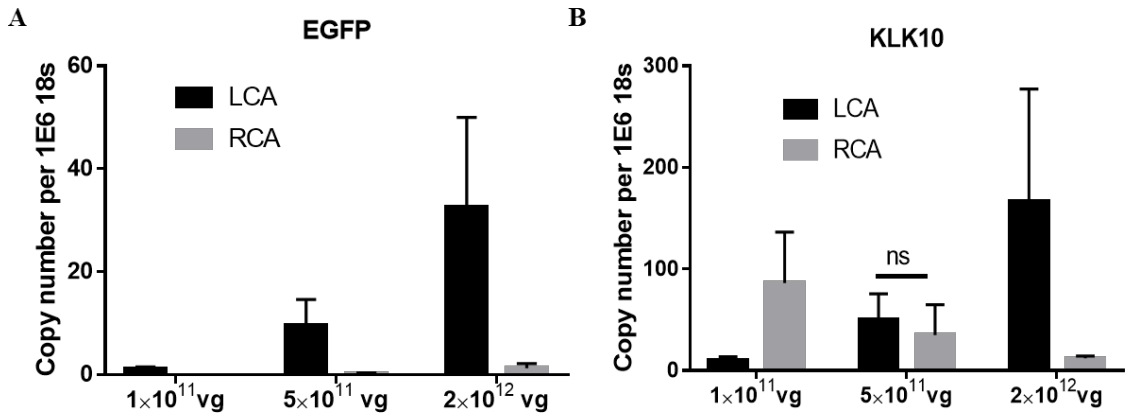

Figure 4.3 EGFP and KLK10 expression of carotid endothelium with different dose of AAV9-KLK10.

4.3.2 The role of US, MB, and AAV-KLK10

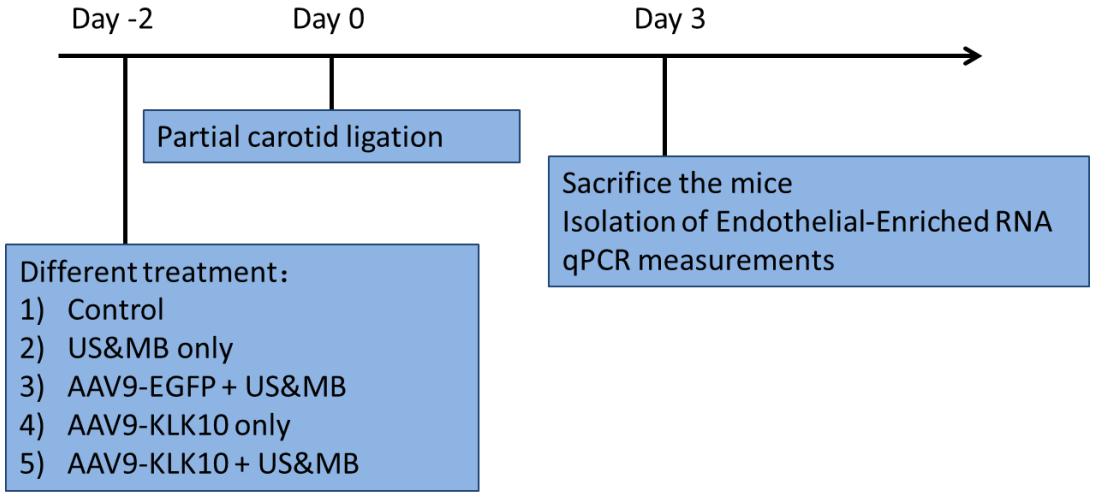

Figure 4.4 Experimental design for determining the role of US, MB, and AAV-KLK10.

To demonstrate the indispensable role of ultrasound, microbubbles and AAV9-KLK10, four additional groups was conducted: control (saline only), US&MB only, AAV9-EGFP + US&MB, and AAV9-KLK10 only (Figure 4.4). As expected, in the

control group, KLK10 expression in LCA is significantly downregulated, similar to our previous report (Figure 4.5)[42]. In addition, compared with the control group, US&MB only, AAV9-EGFP + US&MB, and AAV9-KLK10 only didn't induce any significant changes of KLK10 expression in both LCA and RCA. However, AAV9-KLK10 in combination with US&MB could recover the KLK10 expression in LCA to a level comparable to RCA, while the KLK10 expression in RCA was not significantly changed. These results demonstrate that AAV9-KLK10 in combination with US&MB could be used for targeted delivery of KLK10 gene and either of them are dispensable.

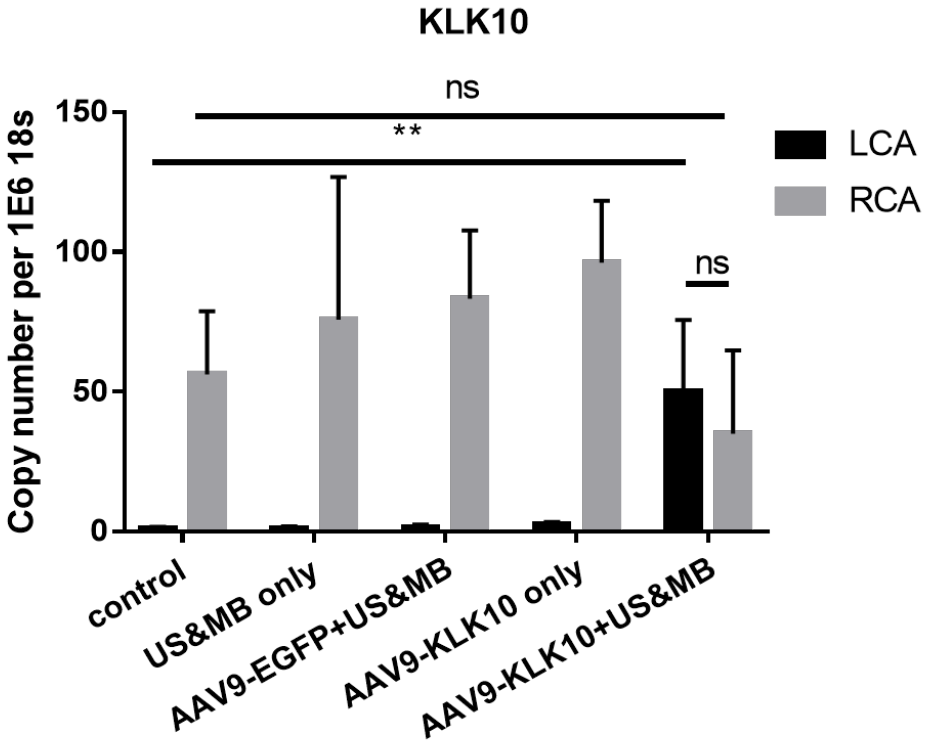

Figure 4.5 KLK10 expression of carotid endothelium with different treatments.

The targeted expression of KLK10 was further demonstrated with immunofluorescence staining. As shown Figure 4.6, the KLK10 expression of LCA in the control group is lower than that of RCA, which is correlated with the qPCR results. The AAV9-KLK10+US&MB treatment could significantly increase KLK10 expression in

LCA. Since KLK10 is a very important atheroprotective gene, the increased KLK10 expression is expected to attenuate inflammation in LCA. Therefore, the arteries were also stained with VCAM1 antibody. The VCAM1 expression of LCA in the control group was much increased and the AAV9-KLK10+US&MB treatment could reduce VCAM1 expression in LCA (Figure 4.7). These result demonstrated that ultrasound-guided method can be used for targeted delivery of KLK10 and inhibiting inflammation in areas affected by d-flow.

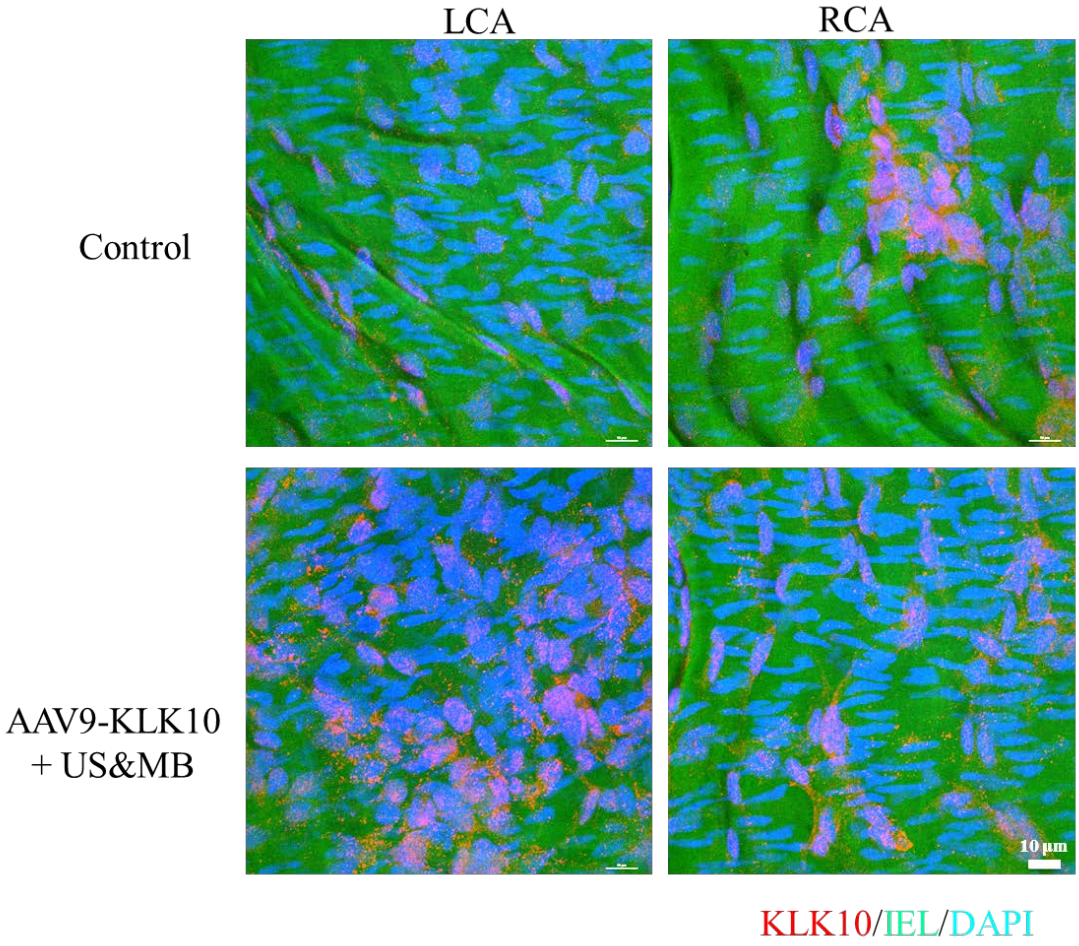

Figure 4.6 En face KLK10 staining of carotid artery. Two days before the PCL surgery, the mice were treated with AAV9-KLK10+US&MB, while the control mice were injected with saline only. The mice were sacrificed three days post PCL surgery. The carotid arteries were stained with KLK10 antibody and en face confocal imaged.

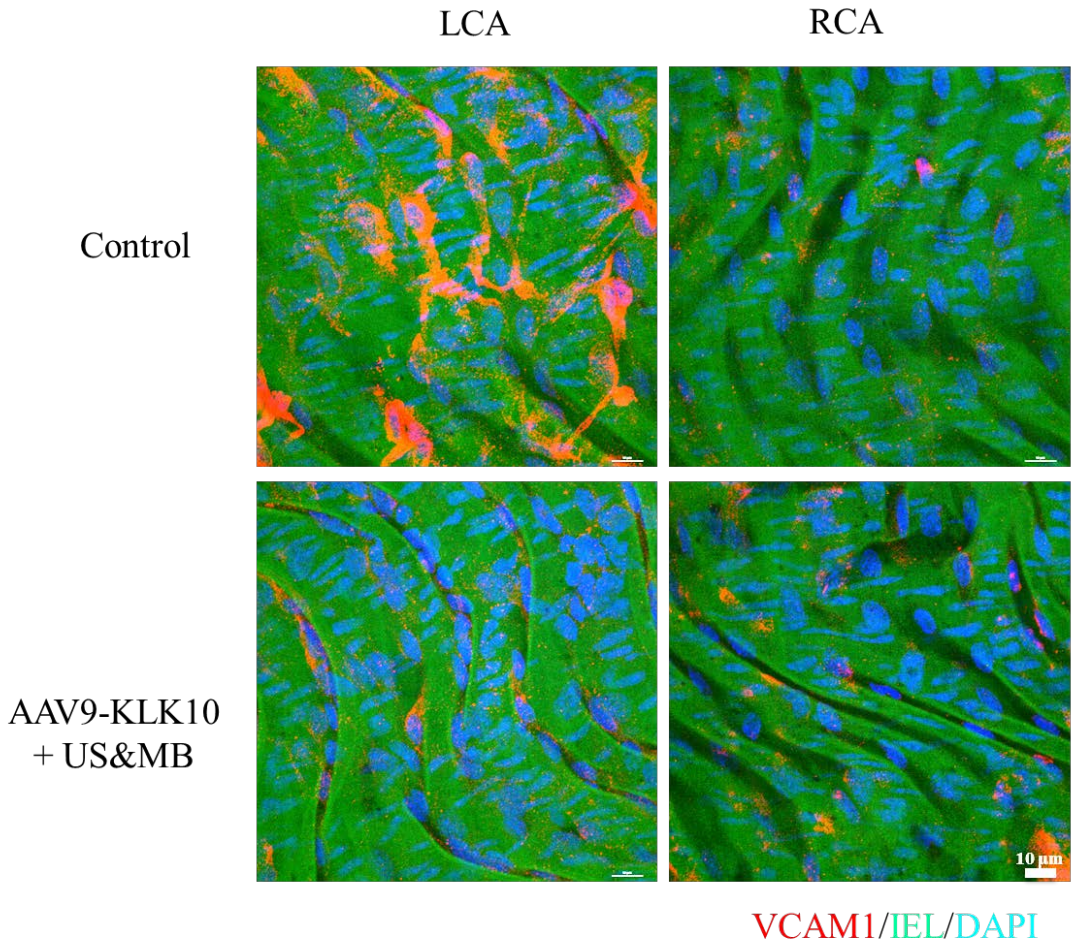

Figure 4.7 En face VCAM1 staining of carotid artery. Two days before the PCL surgery, the mice were treated with AAV9-KLK10+US&MB, while the control mice were injected with saline only. The mice were sacrificed three days post PCL surgery. The carotid arteries were stained with VCAM1 antibody and en face confocal imaged.

4.3.3 Atherosclerotic studies

The targeted delivery of KLK10 with the ultrasound-guided method was further characterized to see if atherosclerotic development could be inhibited in this way (Figure 4.8). After partial carotid ligation surgery and high fat diet for 3 weeks in ApoE$^{-/-}$ mice, the atherosclerotic plaques rapidly develop in LCA. Two days before the PCL surgery, the mice were treated with US&MB followed by AAV9-KLK10 injection (5×10^{11}vg/mouse), while the control mice were injected with saline only. After a high fat diet for 3 weeks, the mice were sacrificed for atherosclerotic analysis.

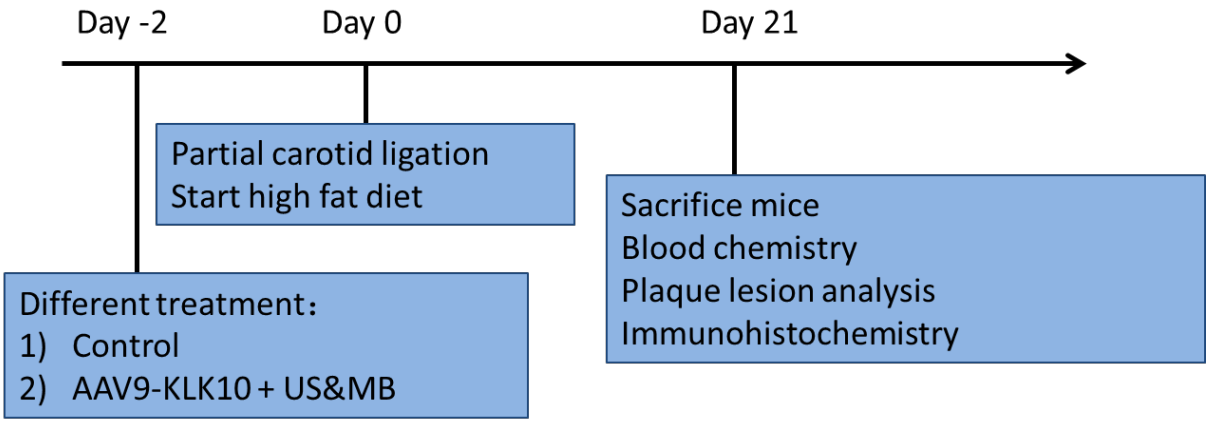

Figure 4.8 Experimental design of the atherosclerotic studies.

The carotid artery trees were dissected out and imaged under the bright field imaging. The opaque area covered by plaque can be visualized. The atherosclerotic lesion area is determined as the percent of opaque area divided by the total area of LCA. With targeted KLK10 delivery, the atherosclerotic lesion area was decreased from 70.1±6.0% to 32.2±4.9% (Figure 4.9) and the atherosclerotic lesion area was decreased by ~37.9%.

The frozen sectioning was then conducted from the middle part and then stained with Oil-Red-O. Oil-Red-O is a fat-soluble dye commonly used for staining of neutral triglycerides and lipids on the frozen sections. The Oil-Red-O staining can make fat more visible. The atherosclerotic plaque is characterized by accumulation of lipids in the artery wall, together with infiltration of immunocytes, such as macrophages, and the formation of a fibrous cap by vascular smooth muscle cells. As shown in Figure 4.10， the plaque size determined by Oil-Red-O staining was decreased by 89.8%.

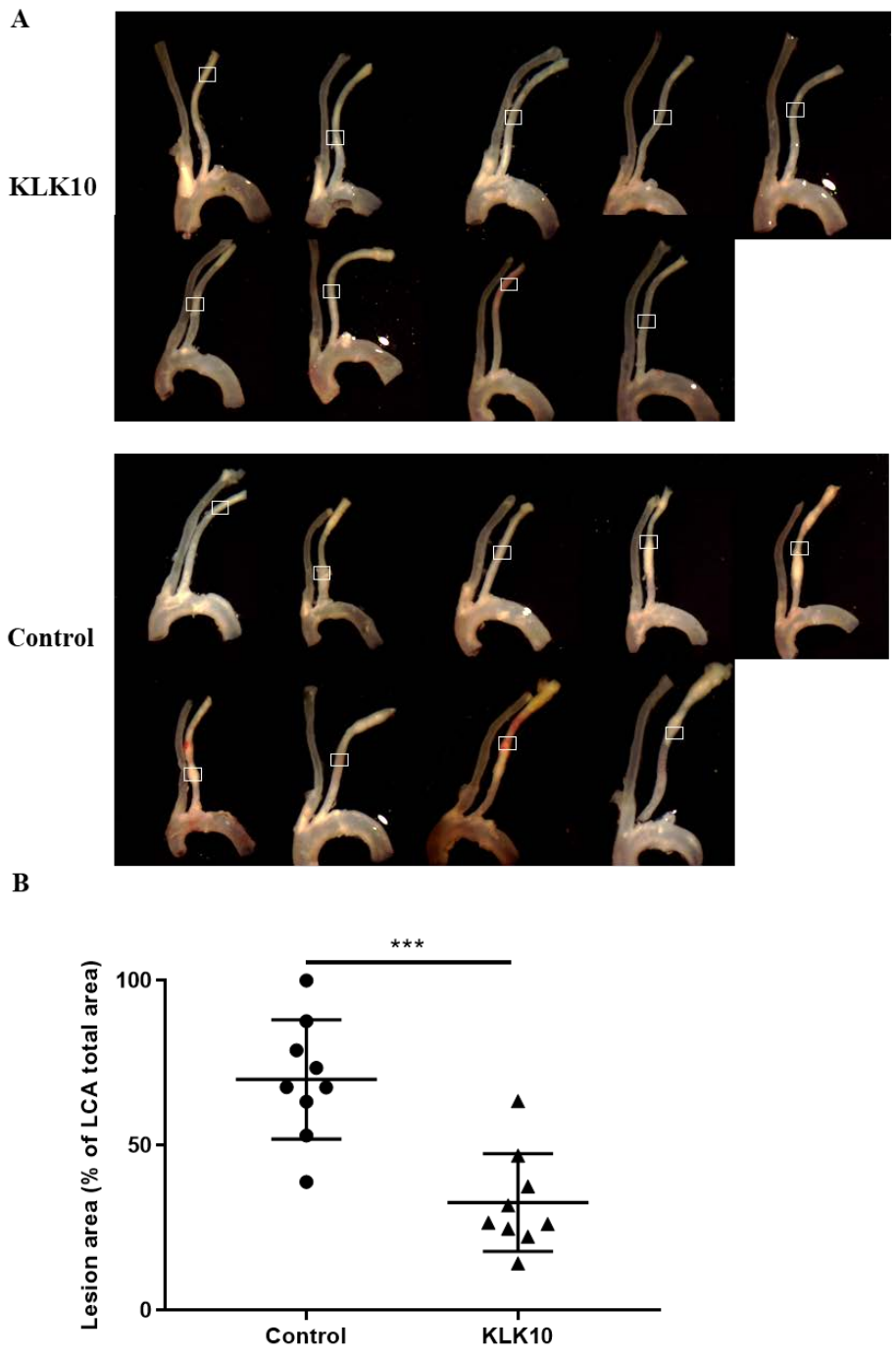

Figure 4.9. Atherosclerotic lesion analysis of carotid arteries. Two days before the PCL surgery, the mice were treated with AAV9-KLK10+US&MB (KLK10), while the control mice were injected with saline only. After PCL surgery, mice were fed with high fat diet for 3 weeks. The artery trees were dissected out and imaged with the bright field imaging (A). The lesion are quantified (B). n =9 each, data shown as mean ± s.e.m.; ***$p<0.001$ as determined by student's t-test. The while boxes in (A) indicated the sites where frozen sections is conducted.

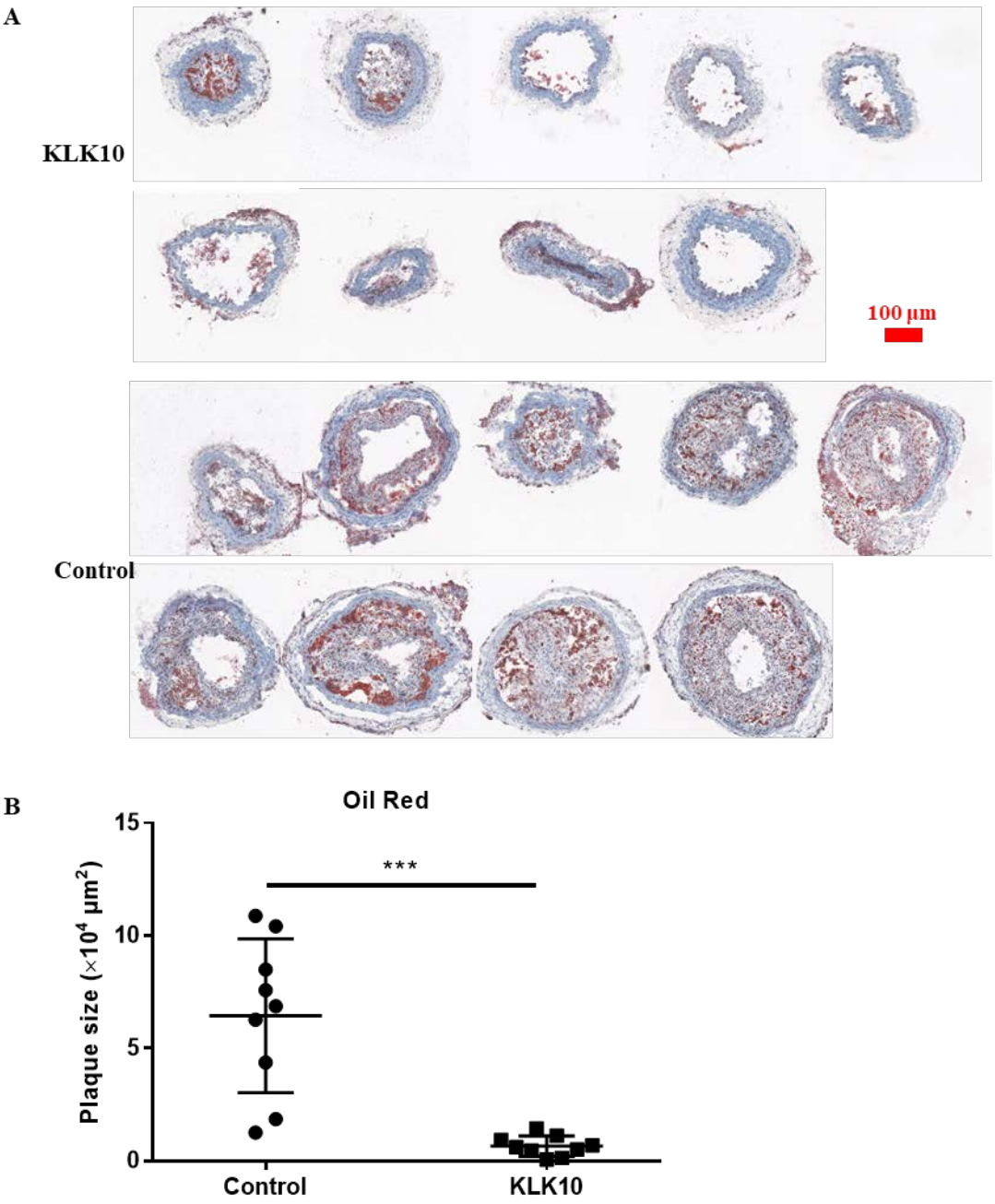

Figure 4.10 Oil-Red-O staining. The frozen sections are prepared from the middle parts of LCA and stained with Oil Red O. The images are collected with the bright field imaging (A). The plaque sized are quantified (B). n =9 each, data shown as mean ± s.e.m.; ***p<0.001 as determined by student's t-test.

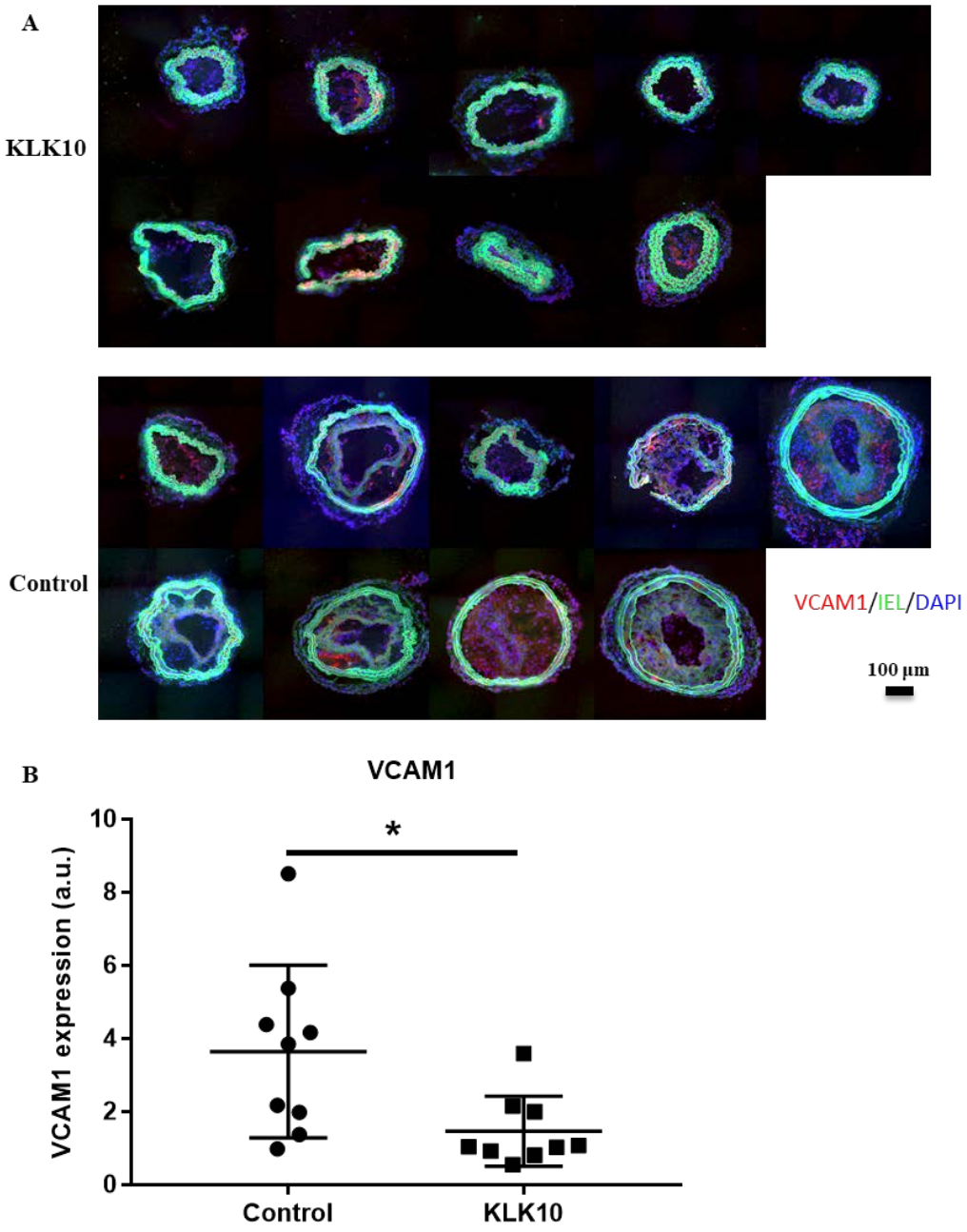

Figure 4.11 VCAM1 staining. The frozen sections are prepared from the middle parts of LCA and stained with CD45 antibody. The images are collected with the fluorescence imaging (A). The expression of CD45 are quantified (B). n =9 each, data shown as mean ± s.e.m.; *p<0.05 as determined by student's t-test.

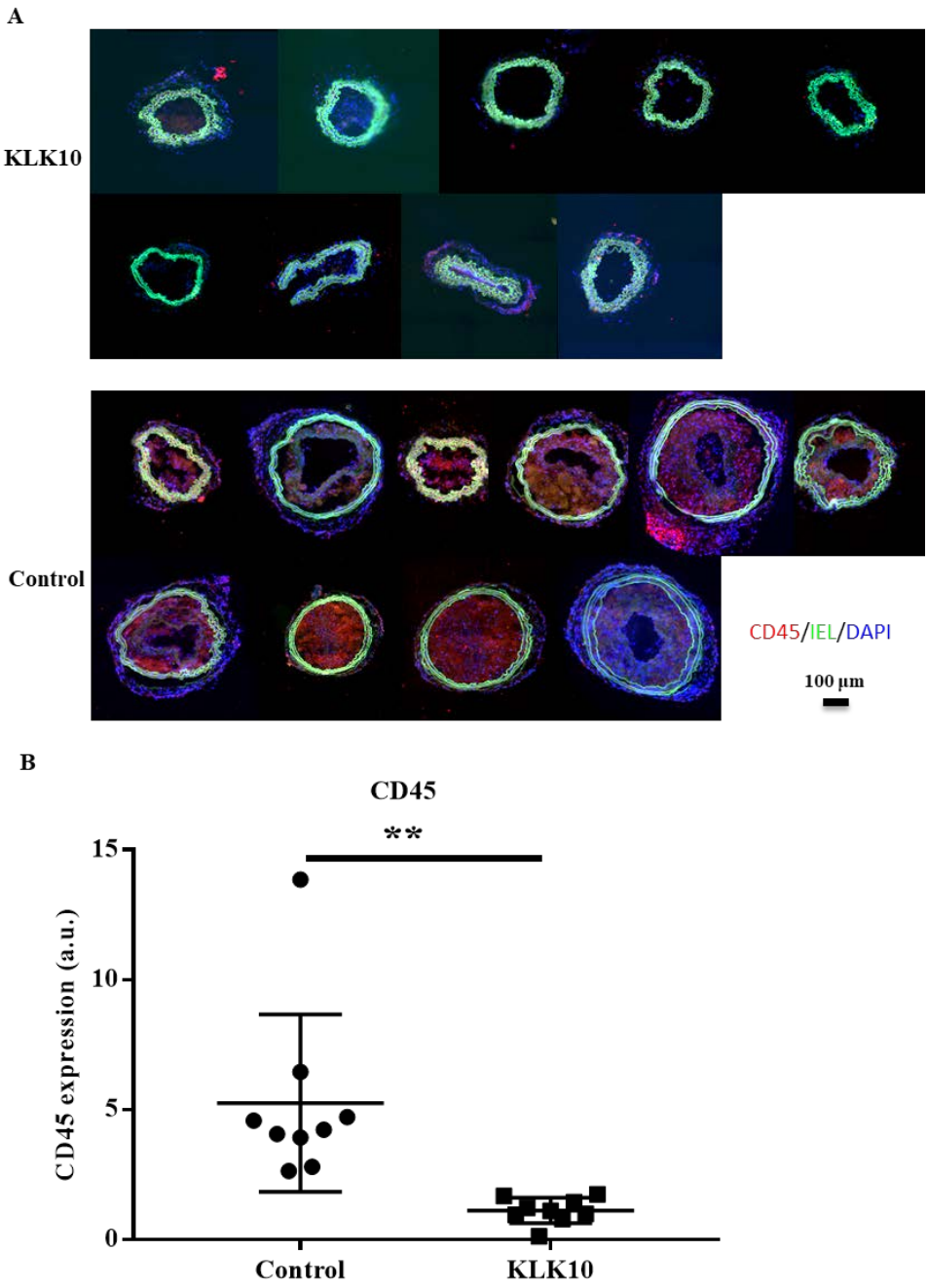

Figure 4.12 CD45 staining. The frozen sections are prepared from the middle parts of LCA and stained with CD45 antibody. The images are collected with the fluorescence imaging (A). The expression of CD45 are quantified (B). n =9 each, data shown as mean ± s.e.m.; **p<0.005 as determined by student's t-test.

The VAM1 protein is highly expressed in the inflamed arterial endothelium and mediates recruiting lymphocytes, monocytes, eosinophils, and basophils to vascular endothelium, which is important in the initialization and progressing of the atherosclerosis.

KLK10 is a atherprotective gene and the expression of KLK10 is expected to reduce the VCAM1 expression and inhibit atherosclerosis. Therefore, the frozen sections were also stained with VCAM1 antibody. As shown in Figure 4.11, the VCAM1 expression was decreased by 59.7% after the targeted delivery of KLK10

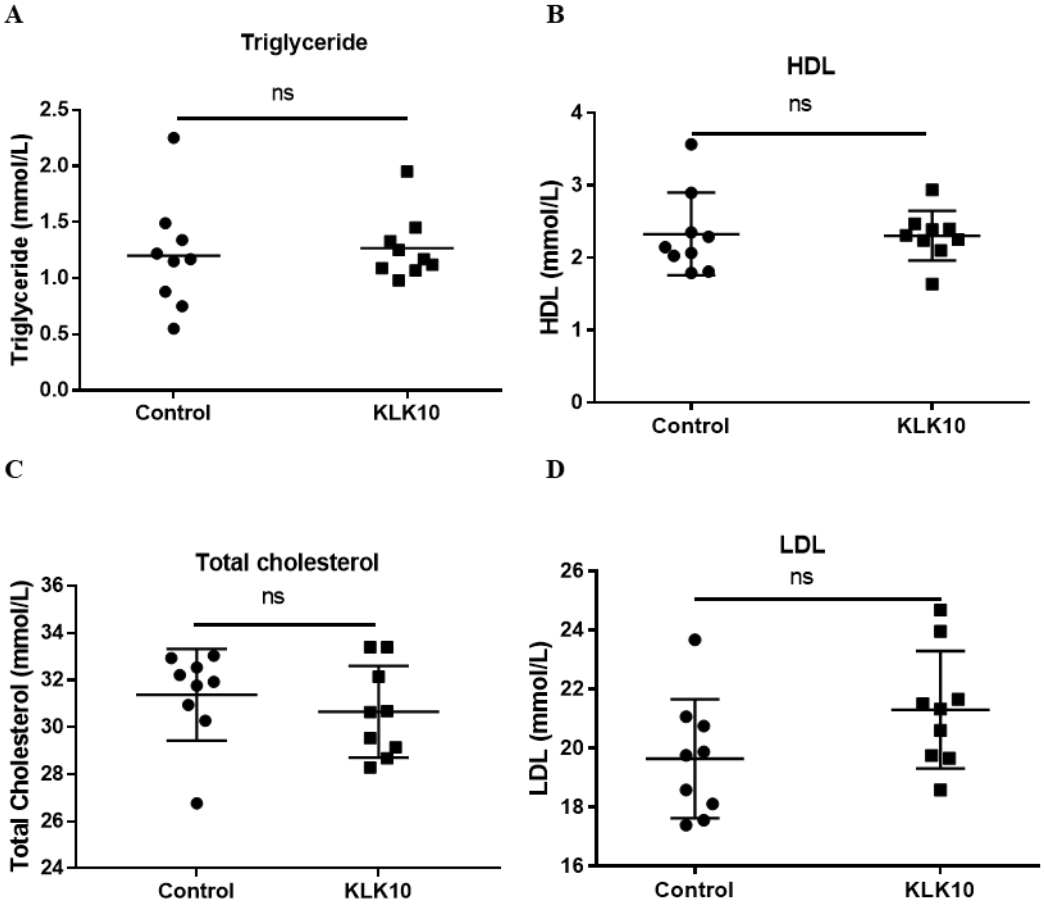

Figure 4.13 Plasma lipid profiles. Blood was collected immediately following sacrifice and the plasma was obtained then. The samples were then to measure triglycerides, high-density lipoprotein (HDL), total cholesterol, and low-density lipoprotein (LDL). n =9 each, data shown as mean ± s.e.m.; ns, p>0.05as determined by student's t-test.

Immunocytes, such as macrophages, play a pivotal role in the initialization and development of atherosclerosis. Macrophages can internalize cholesterol and become lipid-laden cells with a foamy appearance. The foamy macrophages contribute to all stages of atherosclerosis. The CD45 is one maker genes of immunocytes. Therefore, the CD45

expression can reflect the infiltration of immunocytes. As shown in Figure 4.12, the targeted delivery of KLK10 reduced the CD45 expression by 78.6%.

The hypercholesterolemia is the one of the major cause of atherosclerotic development by in ApoE$^{-/-}$ mice. To rule out the possibility that the reduction in atherosclerosis is the results of changes in plasma lipid profiles, the triglycerides, high-density lipoprotein (HDL), total cholesterol, and low-density lipoprotein (LDL) in both groups were determined. As shown in the Figure 4.13, no significant differences were found in the all the measurements.

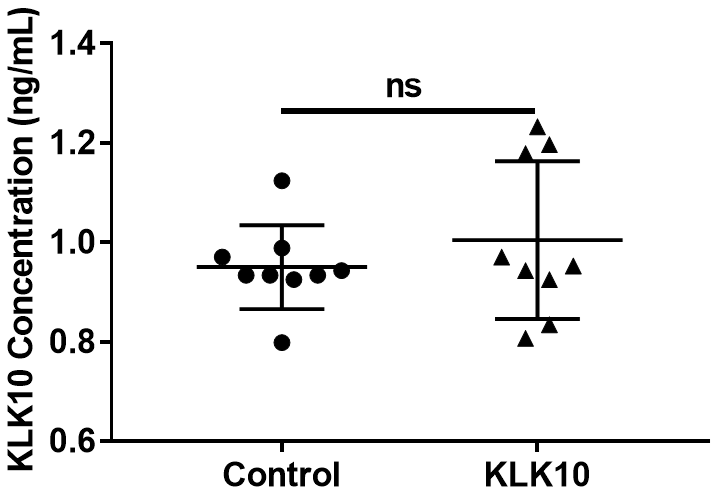

Figure 4.14 Plasma KLK10 level. The KLK10 level in the plasma was measured with a commercial ELISA Kit. n =9 each, data shown as mean ± s.e.m.; ns, $p>0.05$ as determined by student's t-test.

In our previous research, the elevation of KLK10 level in serum was demonstrated to be able to inhibit atherosclerotic development. Therefore, in this study, the plasma level of KLK10 was also measured with ELISA. NO significant difference was found in respect to plasma KLK10 concentration in both groups (Figure 47). This result demonstrated that the inhibited atherosclerotic development was a result of localized transgene expression of KLK10 in carotid artery.

Furthermore， after the sacrifice of the mice, the major organs including heart, liver, spleen, lung, kidney, and thymus in both groups were dissected, sectioned, and subjected to H&E staining. Compared with the control group, the microbubble, ultrasound, and AAV9-KLK10 treatment didn't induce any significant changes in these organs (Figure 4.15). This results demonstrated the safety of the targeted gene delivery KLK10 for the treatment of atherosclerosis

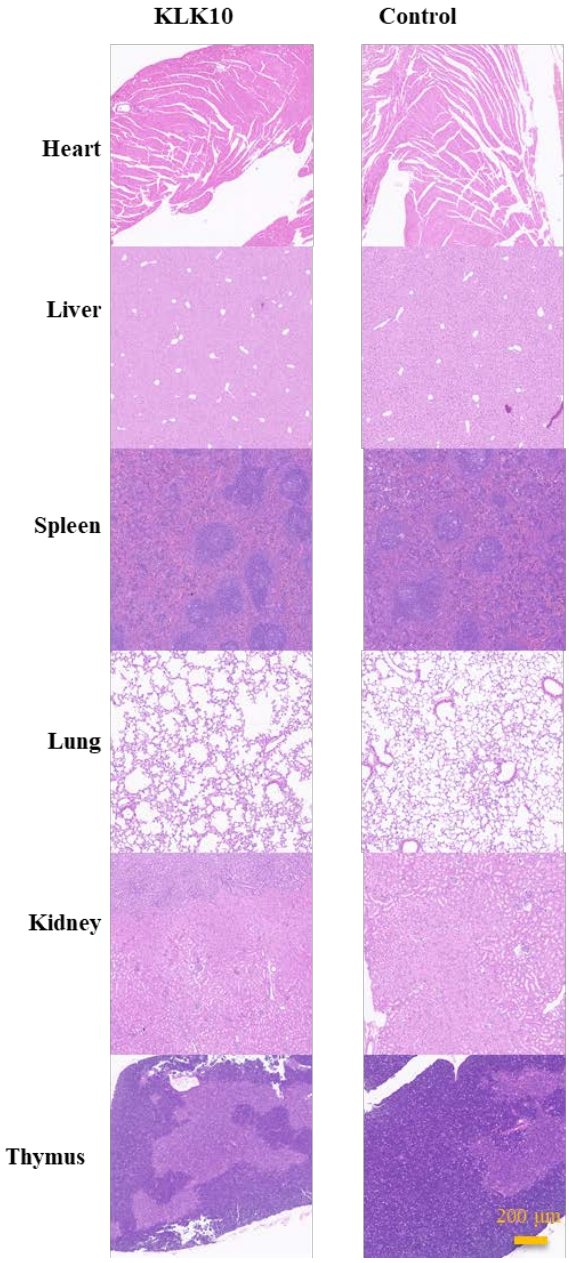

Figure 4.15 H&E staining of the major organs.

4.4 Summary

In this chapter, the ultrasound-guided method of gene delivery was investigated for the targeted delivery of KLK10 in the PCL model. After PCL surgery, the KLK10 expression in LCA is reduced compared with the RCA. After treating LCA with ultrasound combining with microbubbles, KLK10-encoding AAV9 at a dose of 2.5×10^{13}vg/kg could increase the expression of KLK10 in LCA to a level comparable to that in RCA. In the atherosclerotic studies, the targeted delivery of KLK10 gene with this technology could significantly reduce the plaque size, CD45, and VCAM1 expression. In addition, no significant difference in respect to plasm lipid profile, plasma KLK10, and H&E staining of major organs was found. These results demonstrate the atheroprotective role of KLK10 and highlight the potential of the ultrasound-guided method of gene delivery in respected to applications for therapy of artery diseases.

CHAPTER 5. CONCLUSIONS AND FUTURE DIRECTIONS

5.1 Conclusion

In this thesis, we established two technologies for ultrasound-enhance KLK10 delivery to inhibit atherosclerosis. In the first method, plasmid and microbubbles are intramuscularly injected in skeletal muscle. The ultrasound are then applied to injecting site to induce highly enhanced transgene expression in skeletal muscle. KLK10 expressed in the skeletal muscle can be secreted out and enter into the blood to act on the endothelial cells. In the second method, AAV gene vector, microbubbles and ultrasound imaging are combined for targeted gene delivery to mouse artery in a non-invasive and imaging-guided way. With color Doppler imaging, the anatomical structure of artery can be visualized and the area of interest can be selected so that ultrasound only irradiate the selected area. After microbubbles injection, the ultrasound can destroy the microbubbles only in the selected areas, resulting in increased permeability of the artery. Following system administration, AAV gene vector can preferentially accumulate in the ultrasound-treated area, leading to highly enhanced transgene expression. Both methods have been demonstrated to be able to deliver KLK10 in vivo and inhibit atherosclerosis development in the PCL model. Advantages and disadvantages of this technology are briefly listed below

5.1.1 Ultrasound-enhanced transgene expression in skeletal muscle

5.1.1.1 Advantages

(1) No-viral gene delivery

Gene transfer for gene therapy is a rapidly expanding field. However, most of the clinical trials for gene therapy are using virus gene vectors. Although the efficacy of virus is relatively higher in several applications, the immunogenicity and high price of virus are the major defects. Therefore, developing non-viral methods for gene delivery is continuously pursued by researchers. In this research, a non-viral method for transgene expression in skeletal muscle is established for the therapy of atherosclerosis. Utilizing the sonoporation effect of microbubble destruction, the efficacy of gene transfer by naked

plasmid can be enhanced. Since this kind of gene delivery is not immunogenicity, repeated administration is feasible

(2) Persistent transgene expression

Although systematic administration of recombinant KLK10 protein can inhibit atherosclerosis, repeated injection is needed owing to the short circulation time of recombinant protein. By the transgene expression of KLK10 in skeletal muscle, the KLK10 protein can be produced by the muscle cells and secreted into blood. With one injection, the gene expression can persist for over 3 weeks.

5.1.1.2 Disadvantages

(1) Potential adverse effects to normal tissues

Although the transgene expression of KLK10 in skeletal muscle can inhibit atherosclerosis, the expressed KLK10 proteins can act on the whole body, not the artery endothelium alone, which may cause some unexpected side effects to normal tissues.

(2) Inconsistent transfection efficacy

Although the average efficacy of gene transfer can be enhanced the sonoporation effect, the transfection efficacy is inconsistent and the gene transfer is not always successful. The variability of expression is probably due to non-uniform distribution of substances injected in the skeletal muscle[126]. Increasing the proficiency of operators might partly solve this issue.

5.1.2 Ultrasound-imaging-guided transgene expression in artery

5.1.2.1 Advantages

(1) No-invasive gene delivery

Targeted gene expression to arterial cells in vivo is a hard task before this research. One of the most common strategy is to temporally block the blood flow in artery and directly inject gene vector in the lumen [127]. However, this kind of methods require complicated surgery procedures and may cause very serious complications to the animals. With the technology established in this research, no surgical expertise is required and local delivery of high level of transgenic proteins comparable to that by surgery can be achieved in a non-invasive way.

(2) Image-guided gene delivery

With ultrasound imaging, the anatomical structure of arteries can be visualized and areas of interest can be selected so that the gene is only expressed in the selected areas. Since the ultrasound imaging is the most common imaging for artery disease, it's very promising to combine this technique with ultrasound imaging to achieve the theranostics of arterial diseases. With this technique, we can deliver the genes to any part of the arteries as we need.

(3) No complex chemical modification

One of the most common strategy for targeted delivery is to modify the vectors to targeting ligands. However, this strategy usually requires complex chemical procedures, which is not that attainable for regular biomedical researchers. With the ultrasound-guided method, both microbubbles and AAV are commercially available and most of the biomedical researchers can use it very easily.

(4) Universality

In this thesis, the ultrasound-guided method of gene delivery was tested for targeted delivery to carotid, abdominal aorta, and femoral artery. In theory, this technology may be further expanded for other part of arteries, veins, etc.

(5) High specificity

With the ultrasound-guided method, the transgene expression in the targeted area could be increased by as high as 85 fold, which is hard-to-achieve by any other methods.

5.1.2.2 Disadvantages

(1) Immunogenic

One of the biggest problems of virus gene vectors is that antibody will be generated after injection. Therefore, virus vector is only effective for the first administration. For multiple injections, the serotype of virus need to be changed

(2) Off-target effects

Although the ultrasound treatment could highly increase the accumulation of AAV in the targeted area, the retention of AAV in other organs especially liver is not affected. This issue might be solved by modifying the viral capsid or replacing the promoter to a cell-specific one.

5.2 Future Scientific Directions

Several future scientific directions are presented here regarding further development and applications of the technologies established in this thesis.

(1) The efficacy of gene transfer in skeletal muscle may be further increased.

After intramuscular injection, the plasmid and microbubbles are mostly located in the injecting sites. Therefore, the gene is mostly expressed in the cells close to the injecting sites. Therefore, if the microbubbles and plasmid can be dispersed in the muscle, the efficacy of gene transfer might be increased.

(2) The AAV gene vectors may be replaced with a non-viral gene vectors, such as liposome, polymer nanoparticles, etc.

Although AAV gene vector is very effective for gene delivery, it is immunogenic and very expensive, which may limit its further applications. Therefore, its's necessary to replace the AAV a non-viral gene vector, even though the efficacy might be compromised.

(3) The targeting specificity of ultrasound-imaging-based technology may be further improved by modifying the viral capsid or replacing the promoter to a cell-specific one.

With the ultrasound-imaging-based method for gene delivery, the external gene can be selectively delivered the selected artery. However, the endothelial cell is not the only cell type that is transfected. It is possible to achieve cell-specific gene delivery by modifying the viral capsid or replacing the promoter to a cell-specific one.

(4) The technologies might be used for therapy of other vascular diseases.

For the first technology, the protein expressed in skeletal muscle is secreted into blood and act on the whole body. Therefore, it is possible to apply this technology for the therapy of other artery diseases using secreted proteins.

The ultrasound-guided method of gene delivery was tested for targeted delivery to carotid, abdominal aorta, and femoral artery. In theory, this technology may be further expanded for other part of arteries, veins, etc.

5.3 Summary

In this chapter, advantages and disadvantages of the ultrasound-guided methods for transgene expression in vivo are summarized and some future scientific directions are proposed.

Targeted gene expression to arterial cells in vivo is a hard task before this research. This thesis introduced two simple but effective methods for non-invasive gene delivery to

inhibit atherosclerosis utilizing the sonoporation effect by ultrasound and microbubbles. In the first method, plasmid and microbubbles are intramuscularly injected in skeletal muscle. The ultrasound are then applied to injecting site to induce highly enhanced transgene expression in skeletal muscle. The ultrasound are then applied to injecting site to induce highly enhanced transgene expression in skeletal muscle. KLK10 expressed in the skeletal muscle can be secreted out and enter into the blood to act on the endothelial cells. This strategy might also be applicable for the gene delivery of other secreted protein. Although this method is effective in inhibiting atherosclerosis, the potential off-target effects and inconsistent efficiency might limit its further applications.

In the second method, AAV gene vector, microbubbles and ultrasound imaging are combined for targeted gene delivery to mouse artery in a non-invasive and imaging-guided way. With color Doppler imaging, the anatomical structure of artery can be visualized and the area of interest can be selected so that ultrasound only irradiate the selected area. After microbubbles injection, the ultrasound can destroy the microbubbles only in the selected areas, resulting increased permeability of the artery. Following system administration, AAV gene vector can preferentially accumulate in the ultrasound-treated area, resulting in highly enhanced transgene expression. The targeted delivery of KLK10 in this method could efficiently inhibit atherosclersosis. Although the targeting efficacy and specificity is extremely high, the potential immunogenicity and off-targets still need to further improvement.

In summary, this thesis established two technologies for transgene expression of KLK10 in vivo to inhibit atherosclerosis. This research not only highlights the potential of KLK10 for the gene therapy of atherosclerosis, but also provides two important methods of gene delivery, which may find their broad applications in fundamental studies and clinical translation in respect to artery diseases, such as atherosclerosis, AAA, and PAD.

However, these technologies are far from perfect and a lot of works still need to be done for further improvement.

APPENDIX A. PLASMID MAP

A.1 pCMV-Luc

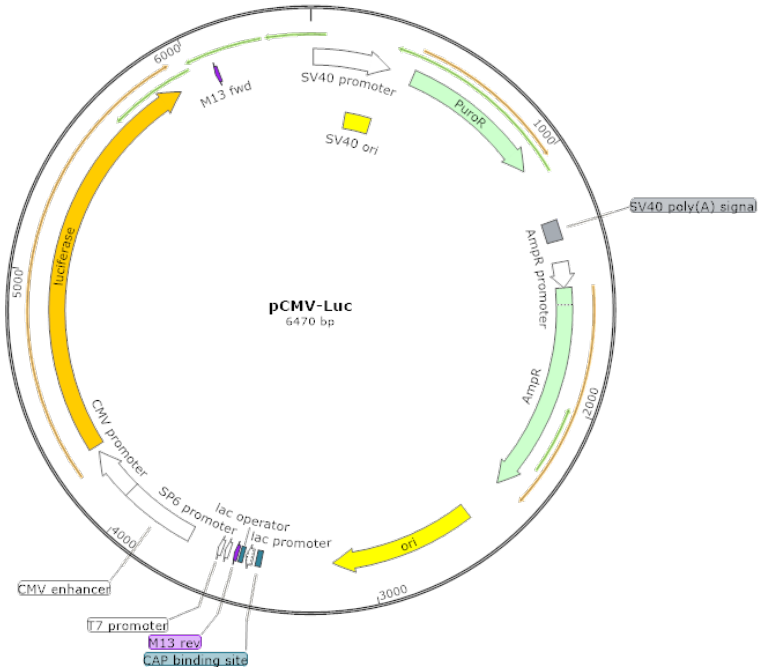

A.2 pCMV-Igκ-Luc

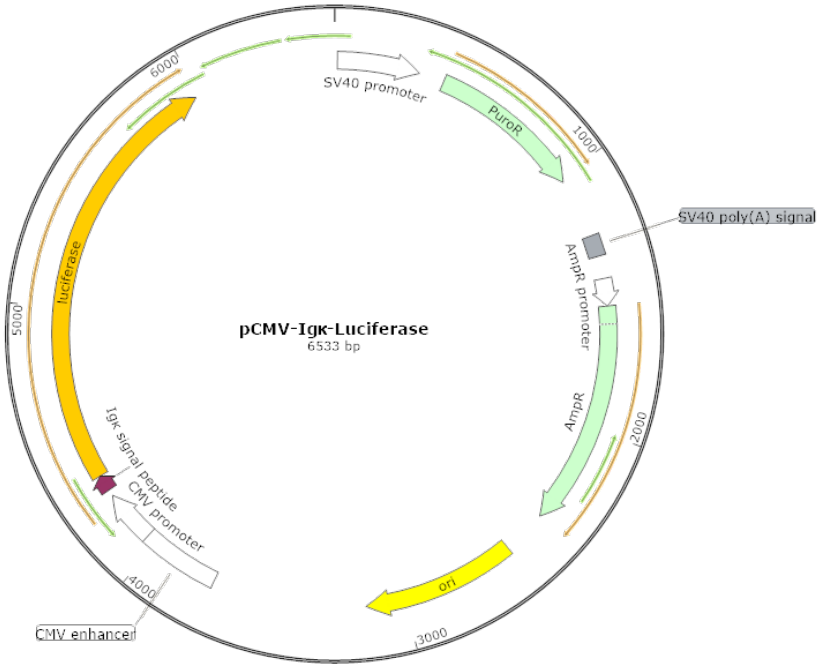

A.3 pCMV-KLK10-T2A-Luc

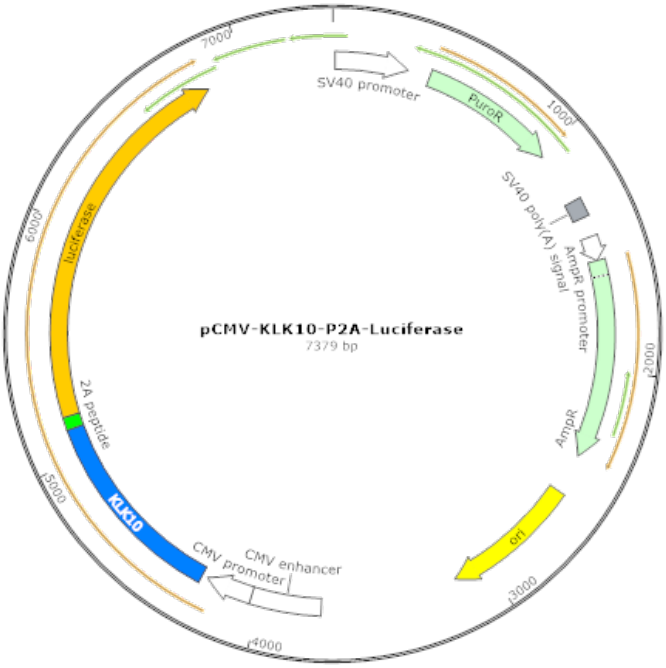

A.4 pCMV-Igκ-KLK10-T2A-Luc

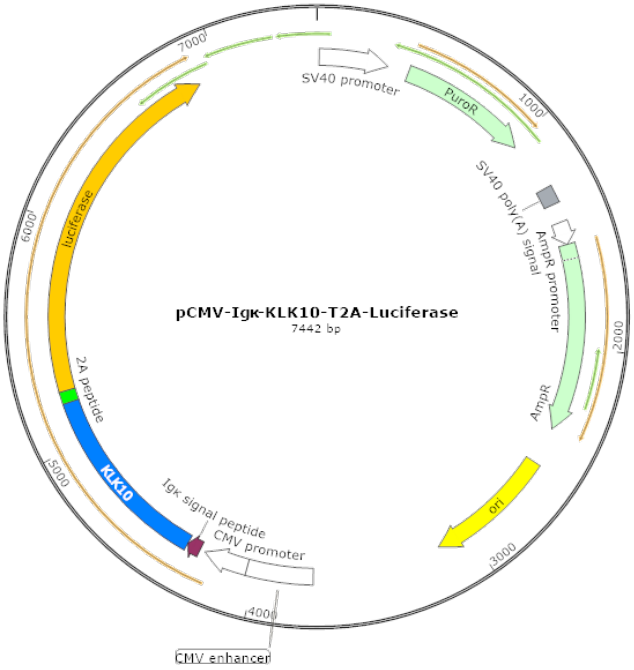

REFERENCES

[1] MEMBERS, W. G.; Benjamin, E. J.; Blaha, M. J.; Chiuve, S. E.; Cushman, M.; Das, S. R.; Deo, R.; de Ferranti, S. D.; Floyd, J.; Fornage, M., Heart disease and stroke statistics—2017 update: a report from the American Heart Association. Circulation 2017, 135 (10): e146.

[2] Aengevaeren, V. L.; Mosterd, A.; Braber, T. L.; Prakken, N. H.; Doevendans, P. A.; Grobbee, D. E.; Thompson, P. D.; Eijsvogels, T. M.; Velthuis, B. K., Relationship between lifelong exercise volume and coronary atherosclerosis in athletes. Circulation 2017, 136 (2): 138-148.

[3] Kaya, M.; Aydın, Ü.; Yeniterzi, M., Surgical treatment of extensive atherosclerosis of supraaortic arterial branches: Two case reports. Turkish Journal of Vascular Surgery 2017, 26 (3).

[4] Lee, S.-E.; Chang, H.-J.; Sung, J. M.; Park, H.-B.; Heo, R.; Rizvi, A.; Lin, F. Y.; Kumar, A.; Hadamitzky, M.; Kim, Y. J., Effects of statins on coronary atherosclerotic plaques: the PARADIGM study. JACC: Cardiovascular Imaging 2018, 11 (10): 1475-1484.

[5] Rodriguez, F.; Maron, D. J.; Knowles, J. W.; Virani, S. S.; Lin, S.; Heidenreich, P. A., Association between intensity of statin therapy and mortality in patients with atherosclerotic cardiovascular disease. JAMA cardiology 2017, 2 (1): 47-54.

[6] Nilsson, J., Atherosclerotic plaque vulnerability in the statin era. European heart journal 2017, 38 (21): 1638-1644.

[7] Shah, R. V.; Murthy, V. L.; Allison, M. A.; Ding, J.; Budoff, M.; Frazier-Wood, A. C.; Lima, J. A.; Steffen, L.; Siscovick, D.; Tucker, K., Diet and adipose tissue distributions: the multi-ethnic study of atherosclerosis. Nutrition, Metabolism and Cardiovascular Diseases 2016, 26 (3): 185-193.

[8] Chen, J.; Guo, Y.; Gui, Y.; Xu, D., Physical exercise, gut, gut microbiota, and atherosclerotic cardiovascular diseases. Lipids in health and disease 2018, 17 (1): 17.

[9] Weber, C.; Noels, H., Atherosclerosis: current pathogenesis and therapeutic options. Nature medicine 2011, 17 (11): 1410.

[10] Gimbrone Jr, M. A.; García-Cardeña, G., Endothelial cell dysfunction and the pathobiology of atherosclerosis. Circulation research 2016, 118 (4): 620-636.

[11] Bennett, M. R.; Sinha, S.; Owens, G. K., Vascular smooth muscle cells in atherosclerosis. Circulation research 2016, 118 (4): 692-702.

[12] Tabas, I.; García-Cardeña, G.; Owens, G. K., Recent insights into the cellular biology of atherosclerosis. J cell Biol 2015, 209 (1): 13-22.

[13] Chinetti-Gbaguidi, G.; Colin, S.; Staels, B., Macrophage subsets in atherosclerosis. Nature Reviews Cardiology 2015, 12 (1): 10.

[14] Feinberg, M. W.; Moore, K. J., MicroRNA regulation of atherosclerosis. Circulation research 2016, 118 (4): 703-720.

[15] Gisterå, A.; Hansson, G. K., The immunology of atherosclerosis. Nature Reviews Nephrology 2017, 13 (6): 368.

[16] Bäck, M.; Hansson, G. K., Anti-inflammatory therapies for atherosclerosis. Nature Reviews Cardiology 2015, 12 (4): 199.

[17] Nam, D.; Ni, C.-W.; Rezvan, A.; Suo, J.; Budzyn, K.; Llanos, A.; Harrison, D.; Giddens, D.; Jo, H., Partial carotid ligation is a model of acutely induced disturbed flow, leading to rapid endothelial dysfunction and atherosclerosis. American Journal of Physiology-Heart and Circulatory Physiology 2009, 297 (4): H1535-H1543.

[18] Son, D. J.; Kumar, S.; Takabe, W.; Kim, C. W.; Ni, C.-W.; Alberts-Grill, N.; Jang, I.-H.; Kim, S.; Kim, W.; Kang, S. W., The atypical mechanosensitive microRNA-712 derived from pre-ribosomal RNA induces endothelial inflammation and atherosclerosis. Nature communications 2013, 4.

[19] Chatzizisis, Y. S.; Coskun, A. U.; Jonas, M.; Edelman, E. R.; Feldman, C. L.; Stone, P. H., Role of endothelial shear stress in the natural history of coronary atherosclerosis and vascular remodeling: molecular, cellular, and vascular behavior. Journal of the American College of Cardiology 2007, 49 (25): 2379-2393.

[20] Hansson, G. K.; Hermansson, A., The immune system in atherosclerosis. Nature immunology 2011, 12 (3): 204.

[21] Libby, P.; Ridker, P. M.; Hansson, G. K., Progress and challenges in translating the biology of atherosclerosis. Nature 2011, 473 (7347): 317.

[22] Jo, H.; Song, H.; Mowbray, A., Role of NADPH oxidases in disturbed flow-and BMP4-induced inflammation and atherosclerosis. Antioxidants & redox signaling 2006, 8 (9-10): 1609-1619.

[23] Chien, S., Effects of disturbed flow on endothelial cells. Annals of biomedical engineering 2008, 36 (4): 554-562.

[24] Zhao, Y.; Chen, B. P.; Miao, H.; Yuan, S.; Li, Y.-S.; Hu, Y.; Rocke, D. M.; Chien, S., Improved significance test for DNA microarray data: temporal effects of shear stress on endothelial genes. Physiological genomics 2002, 12 (1): 1-11.

[25] Chen, B. P.; LI, Y.-S.; Zhao, Y.; CHEN, K.-D.; Li, S.; Lao, J.; Yuan, S.; SHYY, J. Y.-J.; Chien, S., DNA microarray analysis of gene expression in endothelial cells in response to 24-h shear stress. Physiological genomics 2001, 7 (1): 55-63.

[26] McCormick, S. M.; Eskin, S. G.; McIntire, L. V.; Teng, C. L.; Lu, C.-M.; Russell, C. G.; Chittur, K. K., DNA microarray reveals changes in gene expression of shear stressed human umbilical vein endothelial cells. Proceedings of the National Academy of Sciences 2001, 98 (16): 8955-8960.

[27] Dekker, R. J.; Van Soest, S.; Fontijn, R. D.; Salamanca, S.; De Groot, P. G.; VanBavel, E.; Pannekoek, H.; Horrevoets, A. J., Prolonged fluid shear stress induces a distinct set of endothelial cell genes, most specifically lung Krüppel-like factor (KLF2). Blood 2002, 100 (5): 1689-1698.

[28] Conway, D. E.; Williams, M. R.; Eskin, S. G.; McIntire, L. V., Endothelial cell responses to atheroprone flow are driven by two separate flow components: low time-average shear stress and fluid flow reversal. American Journal of Physiology-Heart and Circulatory Physiology 2009, 298 (2): H367-H374.

[29] Himburg, H. A.; Dowd, S. E.; Friedman, M. H., Frequency-dependent response of the vascular endothelium to pulsatile shear stress. American Journal of Physiology-Heart and Circulatory Physiology 2007, 293 (1): H645-H653.

[30] Dai, G.; Kaazempur-Mofrad, M. R.; Natarajan, S.; Zhang, Y.; Vaughn, S.; Blackman, B. R.; Kamm, R. D.; García-Cardeña, G.; Gimbrone, M. A., Distinct endothelial phenotypes evoked by arterial waveforms derived from atherosclerosis-susceptible and-resistant regions of human vasculature. Proceedings of the National Academy of Sciences 2004, 101 (41): 14871-14876.

[31] Chu, T. J.; Peters, D. G., Serial analysis of the vascular endothelial transcriptome under static and shear stress conditions. Physiological genomics 2008, 34 (2): 185-192.

[32] Sorescu, G. P.; Sykes, M.; Weiss, D.; Platt, M. O.; Saha, A.; Hwang, J.; Boyd, N.; Boo, Y. C.; Vega, J. D.; Taylor, W. R., Bone morphogenic protein 4 produced in endothelial cells by oscillatory shear stress stimulates an inflammatory response. Journal of Biological Chemistry 2003, 278 (33): 31128-31135.

[33] SenBanerjee, S.; Lin, Z.; Atkins, G. B.; Greif, D. M.; Rao, R. M.; Kumar, A.; Feinberg, M. W.; Chen, Z.; Simon, D. I.; Luscinskas, F. W., KLF2 Is a novel transcriptional regulator of endothelial proinflammatory activation. Journal of Experimental Medicine 2004, 199 (10): 1305-1315.

[34] Tressel, S. L.; Kim, H.; Ni, C.-W.; Chang, K.; Velasquez-Castano, J. C.; Taylor, W. R.; Yoon, Y.-s.; Jo, H., Angiopoietin-2 stimulates blood flow recovery after femoral artery occlusion by inducing inflammation and arteriogenesis. Arteriosclerosis, thrombosis, and vascular biology 2008, 28 (11): 1989-1995.

[35] Tressel, S. L.; Huang, R.-P.; Tomsen, N.; Jo, H., Laminar shear inhibits tubule formation and migration of endothelial cells by an angiopoietin-2–dependent mechanism. Arteriosclerosis, thrombosis, and vascular biology 2007, 27 (10): 2150-2156.

[36] Atkins, G. B.; Wang, Y.; Mahabeleshwar, G. H.; Shi, H.; Gao, H.; Kawanami, D.; Natesan, V.; Lin, Z.; Simon, D. I.; Jain, M. K., Hemizygous deficiency of Kruppel-like factor 2 augments experimental atherosclerosis. Circulation research 2008, 103 (7): 690-693.

[37] Kawanami, D.; Mahabeleshwar, G. H.; Lin, Z.; Atkins, G. B.; Hamik, A.; Haldar, S. M.; Maemura, K.; LaManna, J. C.; Jain, M. K., Kruppel-like factor 2 inhibits hypoxia-inducible factor 1α expression and function in the endothelium. Journal of Biological Chemistry 2009, 284 (31): 20522-20530.

[38] Sorescu, G. P.; Song, H.; Tressel, S. L.; Hwang, J.; Dikalov, S.; Smith, D. A.; Boyd, N. L.; Platt, M. O.; Lassegue, B.; Griendling, K. K., Bone morphogenic protein 4 produced in endothelial cells by oscillatory shear stress induces monocyte adhesion by stimulating reactive oxygen species production from a nox1-based NADPH oxidase. Circulation research 2004, 95 (8): 773-779.

[39] Hamik, A.; Lin, Z.; Kumar, A.; Balcells, M.; Sinha, S.; Katz, J.; Feinberg, M. W.; Gerszten, R. E.; Edelman, E. R.; Jain, M. K., Kruppel-like factor 4 regulates endothelial inflammation. Journal of Biological Chemistry 2007, 282 (18): 13769-13779.

[40] Ni, C.-W.; Qiu, H.; Rezvan, A.; Kwon, K.; Nam, D.; Son, D. J.; Visvader, J. E.; Jo, H., Discovery of novel mechanosensitive genes in vivo using mouse carotid artery endothelium exposed to disturbed flow. Blood 2010, 116 (15): e66-e73.

[41] Ni, C.-W.; Qiu, H.; Rezvan, A.; Kwon, K.; Nam, D.; Son, D. J.; Visvader, J. E.; Jo, H., Discovery of novel mechanosensitive genes in vivo using mouse carotid artery endothelium exposed to disturbed flow. Blood 2010: blood-2010-04-278192.

[42] Kioulafa, M.; Kaklamanis, L.; Stathopoulos, E.; Mavroudis, D.; Georgoulias, V.; Lianidou, E., Kallikrein 10 (KLK10) methylation as a novel prognostic biomarker in early breast cancer. Annals of oncology 2009, 20 (6): 1020-1025.

[43] Sidiropoulos, M.; Pampalakis, G.; Sotiropoulou, G.; Katsaros, D.; Diamandis, E. P., Downregulation of human kallikrein 10 (KLK10/NES1) by CpG island

hypermethylation in breast, ovarian and prostate cancers. Tumor Biology 2005, 26 (6): 324-336.

[44] Talieri, M.; Alexopoulou, D. K.; Scorilas, A.; Kypraios, D.; Arnogiannaki, N.; Devetzi, M.; Patsavela, M.; Xynopoulos, D., Expression analysis and clinical evaluation of kallikrein-related peptidase 10 (KLK10) in colorectal cancer. Tumor Biology 2011, 32 (4): 737-744.

[45] Cormode, D. P.; Jarzyna, P. A.; Mulder, W. J.; Fayad, Z. A., Modified natural nanoparticles as contrast agents for medical imaging. Advanced drug delivery reviews 2010, 62 (3): 329-338.

[46] Duivenvoorden, R.; Tang, J.; Cormode, D. P.; Mieszawska, A. J.; Izquierdo-Garcia, D.; Ozcan, C.; Otten, M. J.; Zaidi, N.; Lobatto, M. E.; Van Rijs, S. M., A statin-loaded reconstituted high-density lipoprotein nanoparticle inhibits atherosclerotic plaque inflammation. Nature communications 2014, 5: 3065.

[47] Tang, J.; Lobatto, M. E.; Hassing, L.; van der Staay, S.; van Rijs, S. M.; Calcagno, C.; Braza, M. S.; Baxter, S.; Fay, F.; Sanchez-Gaytan, B. L., Inhibiting macrophage proliferation suppresses atherosclerotic plaque inflammation. Science advances 2015, 1 (3): e1400223.

[48] Rui, K.; Li, D.; Chen, Y. E.; Moon, J. J.; Schwendeman, A., High-Density Lipoproteins: Nature's Multifunctional Nanoparticles. Acs Nano 2016, 10 (3): 3015.

[49] Gao, W.; Sun, Y.; Cai, M.; Zhao, Y.; Cao, W.; Liu, Z.; Cui, G.; Tang, B., Copper sulfide nanoparticles as a photothermal switch for TRPV1 signaling to attenuate atherosclerosis. Nature communications 2018, 9 (1): 231.

[50] Kheirolomoom, A.; Kim, C. W.; Seo, J. W.; Kumar, S.; Son, D. J.; Gagnon, M. K. J.; Ingham, E. S.; Ferrara, K. W.; Jo, H., Multifunctional nanoparticles facilitate molecular targeting and miRNA delivery to inhibit atherosclerosis in ApoE–/–mice. ACS nano 2015, 9 (9): 8885-8897.

[51] DiStasio, N.; Lehoux, S.; Khademhosseini, A.; Tabrizian, M., The Multifaceted Uses and Therapeutic Advantages of Nanoparticles for Atherosclerosis Research. Materials 2018, 11 (5): 754.

[52] Park, Y.; Kitahara, T.; Takagi, R.; Kato, R., Current status of therapy for breast cancer worldwide and in Japan. World journal of clinical oncology 2011, 2 (2): 125.

[53] Chen, Y.; Chen, H.; Shi, J., Nanobiotechnology Promotes Noninvasive High‐Intensity Focused Ultrasound Cancer Surgery. Advanced healthcare materials 2015, 4 (1): 158-165.

[54] Meng, Y.; Volpini, M.; Black, S.; Lozano, A. M.; Hynynen, K.; Lipsman, N., Focused ultrasound as a novel strategy for Alzheimer disease therapeutics. Annals of neurology 2017, 81 (5): 611-617.

[55] Leinenga, G.; Götz, J., Scanning ultrasound removes amyloid-β and restores memory in an Alzheimer's disease mouse model. Science translational medicine 2015, 7 (278): 278ra33-278ra33.

[56] Li, Z.; Sun, X.; Guo, S.; Wang, L.; Wang, T.; Peng, C.; Wang, W.; Tian, Z.; Zhao, R.; Cao, W., Rapid stabilisation of atherosclerotic plaque with 5-aminolevulinic acid-mediated sonodynamic therapy. Thrombosis and haemostasis 2015, 114 (04): 793-803.

[57] Schinkel, A. F.; Kaspar, M.; Staub, D., Contrast-enhanced ultrasound: clinical applications in patients with atherosclerosis. The international journal of cardiovascular imaging 2016, 32 (1): 35-48.

[58] Steinl, D.; Kaufmann, B., Ultrasound imaging for risk assessment in atherosclerosis. International journal of molecular sciences 2015, 16 (5): 9749-9769.

[59] López-Melgar, B.; Fernández-Friera, L.; Oliva, B.; García-Ruiz, J. M.; Peñalvo, J. L.; Gómez-Talavera, S.; Sánchez-González, J.; Mendiguren, J. M.; Ibáñez, B.; Fernández-Ortiz, A., Subclinical atherosclerosis burden by 3D ultrasound in mid-life: the PESA study. Journal of the American College of Cardiology 2017, 70 (3): 301-313.

[60] Mitchell, C. C.; Korcarz, C. E.; Tattersall, M. C.; Gepner, A. D.; Young, R. L.; Post, W. S.; Kaufman, J. D.; McClelland, R. L.; Stein, J. H., Carotid artery ultrasound texture, cardiovascular risk factors, and subclinical arterial disease: the Multi-Ethnic Study of Atherosclerosis (MESA). The British journal of radiology 2018, 91 (1084): 20170637.

[61] Gardener, H.; Caunca, M. R.; Dong, C.; Cheung, Y. K.; Elkind, M. S.; Sacco, R. L.; Rundek, T.; Wright, C. B., Ultrasound markers of carotid atherosclerosis and cognition: the Northern Manhattan Study. Stroke 2017, 48 (7): 1855-1861.

[62] Ikeda, N.; Gupta, A.; Dey, N.; Bose, S.; Shafique, S.; Arak, T.; Godia, E. C.; Saba, L.; Laird, J. R.; Nicolaides, A., Improved correlation between carotid and coronary atherosclerosis SYNTAX score using automated ultrasound carotid bulb plaque IMT measurement. Ultrasound in medicine & biology 2015, 41 (5): 1247-1262.

[63] O'leary, D. H.; Polak, J. F.; Kronmal, R. A.; Manolio, T. A.; Burke, G. L.; Wolfson Jr, S. K., Carotid-artery intima and media thickness as a risk factor for myocardial infarction and stroke in older adults. New England Journal of Medicine 1999, 340 (1): 14-22.

[64] Crouse, J. R.; Raichlen, J. S.; Riley, W. A.; Evans, G. W.; Palmer, M. K.; O'Leary, D. H.; Grobbee, D. E.; Bots, M. L.; Group, M. S., Effect of rosuvastatin on progression of carotid intima-media thickness in low-risk individuals with subclinical atherosclerosis: the METEOR Trial. Jama 2007, 297 (12): 1344-1353.

[65] Polak, J. F.; Pencina, M. J.; Pencina, K. M.; O'donnell, C. J.; Wolf, P. A.; D'Agostino Sr, R. B., Carotid-wall intima–media thickness and cardiovascular events. New England Journal of Medicine 2011, 365 (3): 213-221.

[66] Ho, S. S. Y., Current status of carotid ultrasound in atherosclerosis. Quantitative imaging in medicine and surgery 2016, 6 (3): 285.

[67] Gray-Weale, A.; Graham, J.; Burnett, J.; Byrne, K.; Lusby, R., Carotid artery atheroma: comparison of preoperative B-mode ultrasound appearance with carotid endarterectomy specimen pathology. The Journal of cardiovascular surgery 1988, 29 (6): 676-681.

[68] Brinjikji, W.; Rabinstein, A. A.; Lanzino, G.; Murad, M. H.; Williamson, E. E.; DeMarco, J. K.; Huston III, J., Ultrasound characteristics of symptomatic carotid plaques: a systematic review and meta-analysis. Cerebrovascular Diseases 2015, 40 (3-4): 165-174.

[69] Steinl, D. C.; Kaufmann, B. A., Ultrasound imaging for risk assessment in atherosclerosis. International journal of molecular sciences 2015, 16 (5): 9749-9769.

[70] Xiong, L.; Deng, Y.-B.; Zhu, Y.; Liu, Y.-N.; Bi, X.-J., Correlation of carotid plaque neovascularization detected by using contrast-enhanced US with clinical symptoms. Radiology 2009, 251 (2): 583-589.

[71] Gerrit, L.; van Dijk, A. C.; van den Oord, S. C.; Hussain, B.; Verhagen, H. J.; Sijbrands, E. J.; van der Steen, A. F.; van der Lugt, A.; Schinkel, A. F., Usefulness of contrast-enhanced ultrasound for detection of carotid plaque ulceration in patients with symptomatic carotid atherosclerosis. The American journal of cardiology 2013, 112 (2): 292-298.

[72] Villanueva, F. S.; Jankowski, R. J.; Klibanov, S.; Pina, M. L.; Alber, S. M.; Watkins, S. C.; Brandenburger, G. H.; Wagner, W. R., Microbubbles targeted to intercellular adhesion molecule-1 bind to activated coronary artery endothelial cells. Circulation 1998, 98 (1): 1-5.

[73] Wu, J.; Leong-Poi, H.; Bin, J.; Yang, L.; Liao, Y.; Liu, Y.; Cai, J.; Xie, J.; Liu, Y., Efficacy of contrast-enhanced US and magnetic microbubbles targeted to vascular cell adhesion molecule–1 for molecular imaging of atherosclerosis. Radiology 2011, 260 (2): 463-471.

[74] Wang, S.; Unnikrishnan, S.; Herbst, E. B.; Klibanov, A. L.; Mauldin Jr, F. W.; Hossack, J. A., Ultrasound molecular imaging of inflammation in mouse abdominal aorta. Investigative radiology 2017, 52 (9): 499-506.

[75] Wang, S.; Unnikrishnan, S.; Herbst, E. B.; Klibanov, A. L.; Jr, M. F.; Hossack, J. A., Ultrasound Molecular Imaging of Inflammation in Mouse Abdominal Aorta. Investigative Radiology 2017, 52 (9): 1.

[76] Taniyama, Y.; Tachibana, K.; Hiraoka, K.; Namba, T.; Yamasaki, K.; Hashiya, N.; Aoki, M.; Ogihara, T.; Yasufumi, K.; Morishita, R., Local delivery of plasmid DNA into rat carotid artery using ultrasound. Circulation 2002, 105 (10): 1233-1239.

[77] Wang, X.; Searle, A. K.; Hohmann, J. D.; Liu, A. L.; Abraham, M.-K.; Palasubramaniam, J.; Lim, B.; Yao, Y.; Wallert, M.; Yu, E., Dual-targeted theranostic delivery of miRs arrests abdominal aortic aneurysm development. Molecular Therapy 2018, 26 (4): 1056-1065.

[78] Jin, H.; Li, D. Y.; Chernogubova, E.; Sun, C.; Busch, A.; Eken, S. M.; Saliba-Gustafsson, P.; Winter, H.; Winski, G.; Raaz, U., Local Delivery of miR-21 Stabilizes Fibrous Caps in Vulnerable Atherosclerotic Lesions. Molecular Therapy 2018, 26 (4): 1040-1055.

[79] Sun, X.; Guo, S.; Yao, J.; Wang, H.; Peng, C.; Li, B.; Wang, Y.; Jiang, Y.; Wang, T.; Yang, Y., Rapid Inhibition of Atherosclerotic Plaque Progression by Sonodynamic Therapy. Cardiovascular research 2018.

[80] Szablowski, J. O.; Lee-Gosselin, A.; Lue, B.; Malounda, D.; Shapiro, M. G., Acoustically targeted chemogenetics for the non-invasive control of neural circuits. Nature Biomedical Engineering 2018, 2 (7): 475-484.

[81] Kumar, S.; Kang, D. W.; Rezvan, A.; Jo, H., Accelerated atherosclerosis development in C57Bl6 mice by overexpressing AAV-mediated PCSK9 and partial carotid ligation. Lab Invest 2017, 97 (8): 935-945.

[82] Chertok, B.; Langer, R.; Anderson, D. G., Spatial control of gene expression by nanocarriers using heparin masking and ultrasound-targeted microbubble destruction. ACS nano 2016, 10 (8): 7267-7278.

[83] Kessler, P. D.; Podsakoff, G. M.; Chen, X.; McQuiston, S. A.; Colosi, P. C.; Matelis, L. A.; Kurtzman, G. J.; Byrne, B. J., Gene delivery to skeletal muscle results in sustained expression and systemic delivery of a therapeutic protein. Proceedings of the National Academy of Sciences 1996, 93 (24): 14082-14087.

[84] Mir, L. M.; Bureau, M. F.; Gehl, J.; Rangara, R.; Rouy, D.; Caillaud, J.-M.; Delaere, P.; Branellec, D.; Schwartz, B.; Scherman, D., High-efficiency gene transfer into

skeletal muscle mediated by electric pulses. Proceedings of the National Academy of Sciences 1999, 96 (8): 4262-4267.

[85] Guiraud, S.; Chen, H.; Burns, D. T.; Davies, K. E., Advances in genetic therapeutic strategies for Duchenne muscular dystrophy. Experimental physiology 2015, 100 (12): 1458-1467.

[86] Schnyder, S.; Handschin, C., Skeletal muscle as an endocrine organ: PGC-1α, myokines and exercise. Bone 2015, 80: 115-125.

[87] Isaka, Y.; Brees, D. K.; Ikegaya, K.; Kaneda, Y.; Imai, E.; Noble, N. A.; Border, W. A., Gene therapy by skeletal muscle expression of decorin prevents fibrotic disease in rat kidney. Nature medicine 1996, 2 (4): 418.

[88] Athanasopoulos, T.; Owen, J. S.; Hassall, D.; Dunckley, M. G.; Drew, J.; Goodman, J.; Tagalakis, A. D.; Riddell, D. R.; Dickson, G., Intramuscular injection of a plasmid vector expressing human apolipoprotein E limits progression of xanthoma and aortic atheroma in apoE-deficient mice. Human Molecular Genetics 2000, 9 (17): 2545-2551.

[89] Signori, E.; Rinaldi, M.; Fioretti, D.; Iurescia, S.; Seripa, D.; Perrone, G.; Norata, G. D.; Catapano, A. L.; Fazio, V. M., ApoE gene delivery inhibits severe hypercholesterolemia in newborn ApoE-KO mice. Biochemical and biophysical research communications 2007, 361 (2): 543-548.

[90] Shapiro, G.; Wong, A. W.; Bez, M.; Yang, F.; Tam, S.; Even, L.; Sheyn, D.; Ben-David, S.; Tawackoli, W.; Pelled, G., Multiparameter evaluation of in vivo gene delivery using ultrasound-guided, microbubble-enhanced sonoporation. Journal of Controlled Release 2016, 223: 157-164.

[91] Bez, M.; Sheyn, D.; Tawackoli, W.; Avalos, P.; Shapiro, G.; Giaconi, J. C.; Da, X.; David, S. B.; Gavrity, J.; Awad, H. A., In situ bone tissue engineering via ultrasound-mediated gene delivery to endogenous progenitor cells in mini-pigs. Science translational medicine 2017, 9 (390): eaal3128.

[92] http://www.abedia.com/wiley/vectors.php, "Vectors used in Gene Therapy Clinical Trials". Journal of Gene Medicine. August 2019.

[93] Lehrke, M.; Lebherz, C., AAV-Mediated Gene Therapy for Atherosclerosis. Curr Atheroscler Rep 2014, 16 (9).

[94] Naso, M. F.; Tomkowicz, B.; Perry, W. L.; Strohl, W. R., Adeno-Associated Virus (AAV) as a Vector for Gene Therapy. Biodrugs 2017, 31 (4): 317-334.

[95] Seymour, L. W.; Thrasher, A. J., Gene therapy matures in the clinic. Nature Biotechnology 2012, 30 (7): 588-593.

[96] Crudele, J. M.; Finn, J. D.; Siner, J. I.; Martin, N. B.; Niemeyer, G. P.; Zhou, S.; Mingozzi, F.; Lothrop, C. D.; Arruda, V. R., AAV liver expression of FIX-Padua prevents and eradicates FIX inhibitor without increasing thrombogenicity in hemophilia B dogs and mice. Blood 2015, 125 (10): 1553-1561.

[97] Yang, Y.; Wang, L.; Bell, P.; McMenamin, D.; He, Z.; White, J.; Yu, H.; Xu, C.; Morizono, H.; Musunuru, K., A dual AAV system enables the Cas9-mediated correction of a metabolic liver disease in newborn mice. Nature biotechnology 2016, 34 (3): 334.

[98] Colella, P.; Puzzo, F.; Biferi, M.; Bali, D.; Paulk, N.; Vidal, P.; Collaud, F.; Simon-Sola, M.; Charles, S.; Hardet, R., Whole-body rescue of Pompe disease with AAV liver delivery of engineered secretable GAA transgenes. Neuromuscular Disorders 2017, 27: S246.

[99] Rezvani, M.; Español-Suñer, R.; Malato, Y.; Dumont, L.; Grimm, A. A.; Kienle, E.; Bindman, J. G.; Wiedtke, E.; Hsu, B. Y.; Naqvi, S. J., In vivo hepatic reprogramming of myofibroblasts with AAV vectors as a therapeutic strategy for liver fibrosis. Cell Stem Cell 2016, 18 (6): 809-816.

[100] Puzzo, F.; Colella, P.; Biferi, M. G.; Bali, D.; Paulk, N. K.; Vidal, P.; Collaud, F.; Simon-Sola, M.; Charles, S.; Hardet, R., Rescue of Pompe disease in mice by AAV-mediated liver delivery of secretable acid α-glucosidase. Science translational medicine 2017, 9 (418): eaam6375.

[101] Lloyd-Jones, D.; Adams, R. J.; Brown, T. M.; Carnethon, M.; Dai, S.; De Simone, G.; Ferguson, T. B.; Ford, E.; Furie, K.; Gillespie, C., Heart disease and stroke statistics—2010 update. Circulation 2010, 121 (7): e46-e215.

[102] Gruchała, M.; Bhardwaj, S.; Pajusola, K.; Roy, H.; Rissanen, T. T.; Kokina, I.; Kholová, I.; Markkanen, J. E.; Rutanen, J.; Heikura, T., Gene transfer into rabbit arteries with adeno‐associated virus and adenovirus vectors. The Journal of Gene Medicine: A cross‐disciplinary journal for research on the science of gene transfer and its clinical applications 2004, 6 (5): 545-554.

[103] Turunen, M.; Hiltunen, M.; Ruponen, M.; Virkamäki, L.; Szoka Jr, F.; Urtti, A.; Ylä-Herttuala, S., Efficient adventitial gene delivery to rabbit carotid artery with cationic polymer–plasmid complexes. Gene therapy 1999, 6 (1): 6.

[104] Wacker, B.; Bi, L.; Dichek, D., In Vivo Gene Transfer to the Rabbit Common Carotid Artery Endothelium. Journal of visualized experiments: JoVE 2018, (135).

[105] Namiki, M.; Kawashima, S.; Yamashita, T.; Ozaki, M.; Sakoda, T.; Inoue, N.; Hirata, K.-I.; Morishita, R.; Kaneda, Y.; Yokoyama, M., Intramuscular gene

transfer of interleukin-10 cDNA reduces atherosclerosis in apolipoprotein E-knockout mice. Atherosclerosis 2004, 172 (1): 21-29.